

UNCLASSIFIED

AD 400 746

*Reproduced
by the*

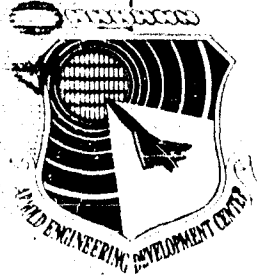
**ARMED SERVICES TECHNICAL INFORMATION AGENCY
ARLINGTON HALL STATION
ARLINGTON 12, VIRGINIA**



UNCLASSIFIED

NOTICE: When government or other drawings, specifications or other data are used for any purpose other than in connection with a definitely related government procurement operation, the U. S. Government thereby incurs no responsibility, nor any obligation whatsoever; and the fact that the Government may have formulated, furnished, or in any way supplied the said drawings, specifications, or other data is not to be regarded by implication or otherwise as in any manner licensing the holder or any other person or corporation, or conveying any rights or permission to manufacture, use or sell any patented invention that may in any way be related thereto.

400 746



AD No. 1

ASTIA FILE COPY

AEDC-TDR-63-58

400 746

63-3-1

(10)

466 26

ANALYTICAL STUDIES ON NOZZLE THROAT COOLING

By

P. F. Pasqua, P. N. Stevens, J. E. Mott,

H. C. Roland, and J. C. Robinson

Nuclear Engineering Department

The University of Tennessee

Knoxville, Tennessee

APR 9 1963

TISIA

A

TECHNICAL DOCUMENTARY REPORT NO. AEDC-TDR-63-58

April 1963

AFSC Program Area 750E, Project 6951, Task 695101

(Prepared under Contract No. AF 49(600)-981 by The University
of Tennessee, Knoxville, Tennessee.)

ARNOLD ENGINEERING DEVELOPMENT CENTER
AIR FORCE SYSTEMS COMMAND
UNITED STATES AIR FORCE

NOTICES

Qualified requesters may obtain copies of this report from ASTIA. Orders will be expedited if placed through the librarian or other staff member designated to request and receive documents from ASTIA.

When Government drawings, specifications or other data are used for any purpose other than in connection with a definitely related Government procurement operation, the United States Government thereby incurs no responsibility nor any obligation whatsoever; and the fact that the Government may have formulated, furnished, or in any way supplied the said drawings, specifications, or other data, is not to be regarded by implication or otherwise as in any manner licensing the holder or any other person or corporation, or conveying any rights or permission to manufacture, use, or sell any patented invention that may in any way be related thereto.

ANALYTICAL STUDIES ON
NOZZLE THROAT COOLING

By

P. F. Pasqua, P. N. Stevens, J. E. Mott,
H. C. Roland, and J. C. Robinson

Nuclear Engineering Department

The University of Tennessee

Knoxville, Tennessee

(The reproducibles used in the reproduction
of this report were supplied by the authors.)

April 1963



ABSTRACT

Analytical studies have been made concerning many of the problems associated with the expansion of extremely high temperature and pressure plasmas through the converging section of a hypersonic wind tunnel nozzle. The problems in this study relate to the establishment of heat fluxes to the nozzle wall; methods of removing the heat load or protecting the nozzle wall; determining the stress levels in the nozzle liner; analysing various materials for strength and thermal properties.

In all cases parametric studies have been made resulting in design criteria which can be used for specific conditions. The conditions are established from the performance envelope for a typical low density hypersonic wind tunnel. Throughout the report the performance envelope is plotted on stagnation pressure and temperature coordinates which correspond to free stream velocities and altitudes up to 25 kilofeet/sec and 350 kilofeet respectively. Ultimate use of the information will depend upon the reliability of the assumptions made which in many cases must be determined by new experiments.

PUBLICATION REVIEW

This report has been reviewed and publication is approved.

	
Donald R. Eastman, Jr. DCS/Research	Jean A. Jack Colonel, USAF DCS/Test

CONTENTS

	<u>Page</u>
ABSTRACT	iii
I. INTRODUCTION	1
II. HEAT FLUX FOR LAMINAR AND TURBULENT BOUNDARY LAYERS	1
III. THERMAL RADIATION	17
IV. TRANSPIRATION AND FILM COOLING OF HYPERSONIC NOZZLES	27
V. NOZZLE LINER STRESS ANALYSIS	46
VI. MATERIAL STUDY	80
VII. SHARP EDGED NOZZLE.	86
VIII. BACKSIDE COOLING	93
BIBLIOGRAPHY	107
APPENDIX A. Fortran Programs for Nozzle and Rib Stresses	109
B. Fortran Programs for Backside Cooling Calculations.	129

ILLUSTRATIONS

Figure

1. Comparison of Laminar Heat Transfer in a Convergent Nozzle	11
2. Heat Flux to Wall at 700°K, Laminar Boundary Layer, $x_{ref} = 3''$	12
3. Convective Heat Load (Throat); Turbulent Boundary Layer; $T_{wall} = 700^{\circ}K$ $D^* = 0.042''$	14
4. Convective Heat Load (Throat); Turbulent Boundary Layer; $T_{wall} = 700^{\circ}K$ $D^* = 0.272''$	15
5. Convective Heat Load (Throat); Turbulent Boundary Layer; $T_{wall} = 700^{\circ}K$ $D^* = 0.784''$	16
6. Model for Gas Thermal Radiation Study	17
7. Integration of Equations (19) and (20)	22
8. Mean Absorption Coefficient for Air	23
9. Equation (20) versus Temperature.	24

<u>Figure</u>	<u>Page</u>
10. Radiation Heat Flux for Spheres of 1.91 and 1.0 cm Radii	25
11. Radiation Heat Flux	26
12. Combined Radiation and Laminar Boundary Layer Heat Flux	28
13. Sketch of Film Cooling.	29
14. Sketch of Transpiration Cooling.	29
15. Energy Balance on Coolant Film	31
16. Flow Ratios for Transpiration Cooling; Blocking Factor = 1.0; $D^* = 0.784''$	33
17. Flow Ratios for Transpiration Cooling; Blocking Factor = 0.5; $D^* = 0.784''$	34
18. Flow Ratios for Transpiration Cooling; Blocking Factor = 0.1; $D^* = 0.784''$	35
19. Blocking Factors for Transpiration Cooling; $M(\text{coolant})/M(\text{gas}) = 0.1$; $D^* = 0.784''$	36
20. Flow Ratios for Transpiration Cooling; Blocking Factor = 1.0; $D^* = 0.272''$	37
21. Flow Ratios for Transpiration Cooling; Blocking Factor = 0.5; $D^* = 0.272''$	38
22. Flow Ratios for Transpiration Cooling; Blocking Factor = 0.1; $D^* = 0.272''$	39
23. Blocking Factors for Transpiration Cooling; $M(\text{coolant})/M(\text{gas}) = 0.1$; $D^* = 0.272''$	40
24. Flow Ratios for Transpiration Cooling; Blocking Factor = 1.0; $D^* = 0.042''$	41
25. Flow Ratios for Transpiration Cooling; Blocking Factor = 0.5; $D^* = 0.042''$	42
26. Flow Ratios for Transpiration Cooling; Blocking Factor = 0.1; $D^* = 0.042''$	43
27. Blocking Factors for Transpiration Cooling; $M(\text{coolant})/M(\text{gas}) = 0.1$; $D^* = 0.042''$	44
28. Sketch of Liner, Rib, and Sleeve	48
29. Sketch of Nozzle with Ribs Perpendicular to Flow of Gas	66

<u>Figure</u>	<u>Page</u>
30. Stress versus Liner Thickness; Diameter = 1.5"	75
31. Stress versus Liner Thickness; Diameter = 0.78"	76
32. Stress versus Liner Thickness; Diameter = 0.27"	77
33. Stress versus Liner Thickness; Diameter = 0.042"	78
34. Strength versus Temperature for Mo-Ti-Zr.	79
35. Sketch of Typical Nozzle Design	81
36. Temperature Effect on the Stress Parameter of Various Nozzle Liner Materials	83
37. Sketch of Sharp Edged Nozzle (Not to Scale)	88
38. Nomenclature Used Near Throat of Sharp Edged Nozzle	89
39. Comparison of Burnout Heat Flux Equations.	100
40. Burnout Heat Flux versus Pressure Ratio.	101
41. Comparison of Burnout Heat Flux Equations.	102
42. Plot of Equation (212); Pressure = 100 psia	103
43. Plot of Equation (212); Pressure = 300 psia	104
44. Viscosity of Water	134
45. Prandtl Number for Water.	135
46. Pressure-Temperature Relationships for Water.	137

I. INTRODUCTION

Analytical studies have been made concerning many of the problems associated with the expansion of extremely high temperature and pressure plasmas through the converging section of a hypersonic wind tunnel nozzle. The problems in this study relate to the establishment of heat fluxes to the nozzle wall; methods of removing the heat load or protecting the nozzle wall; determining the stress levels in the nozzle liner; analysing various materials for strength and thermal properties.

In all cases parametric studies have been made resulting in design criteria which can be used for specific conditions. The conditions are established from the performance envelope for a typical low density hypersonic wind tunnel. Throughout the report the performance envelope is plotted on stagnation pressure and temperature coordinates which correspond to free stream velocities and altitudes up to 25 kilofeet/sec and 350 kilofeet respectively. Ultimate use of the information will depend upon the reliability of the assumptions made which in many cases must be determined by new experiments. For example, curves of heat flux for a laminar boundary layer and for a turbulent boundary layer are shown - each excluding a portion of the phase envelope. If it is assumed, and further verified experimentally, that the boundary layer is laminar, the heat flux from a large percentage of the phase envelope can be handled. However, there is no known published experimental information on the transition in converging sections to assist in checking the reliability of an assumed boundary layer. Thus, the heat flux from both types of boundary layers is included in the report.

The problems in this report have been investigated and reported by various investigators associated with the contract. Specifically, Dr. Stevens has made the analysis on film and transpiration cooling, and on heat flux for laminar and turbulent boundary layers; Mr. Roland has made the analysis on structural design, materials, and backside coolant flow conditions; Professor Mott is investigating the problems of transition from laminar to turbulent boundary layer; Dr. Pasqua has studied the radiation heat flux exchange between the plasma and the nozzle walls; Mr. Robinson has made the analysis on a new configuration - a sharp edged nozzle.

II. HEAT FLUX FOR LAMINAR AND TURBULENT BOUNDARY LAYERS

When backside cooling of the nozzle liner is considered, the amount of energy that can be removed by the coolant is limited by the backside heat transfer coefficient. The limiting energy removed by backside cooling is approximately $50 \text{ Btu/in}^2\text{sec}$. Therefore, in order to maintain the integrity of the nozzle liner, the heat flux into the liner must not exceed some critical value. The energy addition to the liner depends upon many factors and is controlled by the type of boundary layer between the plasma and the wall. A laminar boundary layer is preferred over the turbulent boundary layer as a lower heat flux exists for the former when the same

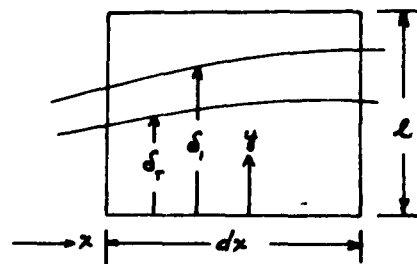
free stream and wall conditions exist.

Several analyses have been made for heat transfer assuming a laminar boundary layer (1, 14, 15)*. However, they do not include all of the effects encountered in the present investigation. The following analysis is made to establish the heat transfer coefficient for a laminar boundary layer on a flat plate considering the effects of compressibility, high temperatures, and variable fluid properties in the boundary layer. This flat plate model will provide a good estimate of the average heat flux in the converging section if evaluated using flow conditions that exist at the throat of the nozzle. The flat plate model also serves as the basis for an incremental calculation of the laminar heat transfer coefficients along the converging section of the nozzle. Briefly, the nozzle is divided into a series of flat plates each subjected to the local fluid properties of the nozzle. The flat plate equation adjusted for variable free-stream conditions is used to calculate the variation of the heat transfer coefficient across each of the intervals.

Flat Plate Model

Consider the following sketch and definitions:

ρ = density
 u = velocity
 T = temperature
 i = specific enthalpy
 c_p = specific heat
 μ = viscosity
 k = thermal conductivity
 δ = hydrodynamic boundary layer thickness
 δ_T = thermal boundary layer thickness ($\delta_T < \delta$)



Subscripts:

w = wall
 aw = adiabatic wall
 s = free stream

The integral momentum equation for a flat plate with constant free stream velocity is:

$$\frac{d}{dx} \int_0^l (u_s - u) u \rho dy - \frac{d}{dx} \int_0^l \rho u dy = \tau_w + l \frac{dp}{dx}$$

*Underlined numbers in parentheses refer to similar numbers in the bibliography.

which can be reduced to

$$\rho_s u_s^2 \frac{d}{dx} \left[\int_0^{\delta_1} \left(1 - \frac{u}{u_s}\right) \frac{u}{u_s} \frac{\rho}{\rho_s} dy \right] = \mu_w \left(\frac{du}{dy} \right)_w$$

Define a new variable η such that

$$d\eta = \frac{\rho}{\rho_s} dy$$

$$\eta = \int_0^y \frac{\rho}{\rho_s} dy$$

$$\delta_1 = \int_0^{\delta_1} \frac{\rho}{\rho_s} dy \quad \therefore \eta = \delta_1 \text{ at } y = \delta_1$$

$$\frac{du}{dy} = \frac{du}{d\eta} \frac{d\eta}{dy} ; \left(\frac{du}{dy} \right)_w = \left(\frac{du}{d\eta} \right)_w \frac{\rho_w}{\rho_s}$$

Therefore, the integral momentum equation becomes

$$\rho_s u_s^2 \frac{d}{dx} \left[\int_0^{\delta_1} \left(1 - \frac{u}{u_s}\right) \frac{u}{u_s} d\eta \right] = \frac{\rho_w}{\rho_s} \mu_w \left(\frac{du}{d\eta} \right)_w \quad (1)$$

Assume a velocity profile of the form

$$\frac{u}{u_s} = a + b\eta + c\eta^2 + e\eta^3$$

$$\text{at } \eta = 0, u = 0 = \frac{du}{d\eta} \therefore a = c = 0$$

$$\text{at } \eta = \delta_1, \frac{u}{u_s} = 1 = b\delta_1 + e\delta_1^3 \therefore 1 = b\delta_1 + e\delta_1^3$$

$$\frac{1}{u_s} \frac{du}{d\eta} = 0 = b + 3e\eta^2 \therefore 0 = b + 3e\delta_1^2$$

$$\text{thus } b = \frac{3}{2\delta_1} ; e = -\frac{1}{2\delta_1^3}$$

The velocity profile becomes

$$\frac{u}{U_s} = \frac{3}{2} \left(\frac{\eta}{\delta_i} \right) - \frac{1}{2} \left(\frac{\eta}{\delta_i} \right)^3 \quad (2)$$

$$\text{and} \quad \int_0^{\delta_i} \left(1 - \frac{u}{U_s} \right) \frac{u}{U_s} d\eta = \frac{39}{280} \delta_i \quad (3)$$

$$\text{and} \quad \left(\frac{du}{d\eta} \right)_w = \frac{3}{2} \frac{U_s}{\delta_i}$$

Substituting equations (2) and (3) into (1) gives

$$\begin{aligned} \text{or} \quad \frac{39}{280} \rho_s U_s^2 \frac{d\delta_i}{dx} &= \frac{3}{2} \left(\frac{\rho_w}{\rho_s} \right) \mu_w \frac{U_s}{\delta_i} \\ \delta_i d\delta_i &= \frac{140}{13} \frac{\mu_w}{U_s} \frac{\rho_w}{\rho_s^2} dx \\ \delta_i &= 4.64 \left(\frac{\rho_w}{\rho_s} \right)^{1/2} \left(\frac{\mu_w x}{\rho_s U_s} \right)^{1/2} \end{aligned} \quad (4)$$

The integral energy equation for the same model is

$$\rho_s U_s \frac{d}{dx} \int_0^{\delta_i} i_s \frac{u}{U_s} \frac{\rho}{\rho_s} dy - \rho_s U_s \frac{d}{dx} \int_0^{\delta_i} i \frac{u}{U_s} \frac{\rho}{\rho_s} dy = q_w$$

Introduce the variable η and express

$$q_w = k_w \left(\frac{dT}{dy} \right)_w = k_w \left(\frac{dT}{d\eta} \right)_w \left(\frac{d\eta}{dy} \right)_w$$

Also for reasonably low wall temperatures

$$i \approx c_p T \quad \text{and} \quad \left(\frac{dT}{d\eta} \right)_w = \frac{1}{c_{p_w}} \left(\frac{di}{d\eta} \right)_w$$

Then

$$\rho_s U_s \frac{d}{dx} \int_0^{\delta_i} i_s \frac{u}{U_s} d\eta - \rho_s U_s \frac{d}{dx} \int_0^{\delta_i} i \frac{u}{U_s} d\eta = \frac{k_w}{c_{p_w}} \left(\frac{\rho_w}{\rho_s} \right) \left(\frac{di}{d\eta} \right)_w$$

where

$$\Delta \equiv \int_0^{\delta_r} \frac{\rho}{\rho_s} d\eta \quad (\Delta < \delta_i \text{ if } \delta_r < \delta_i)$$

Rearranging

$$(i_s - i_w) \rho_s u_s \frac{d}{dx} \int_0^{\Delta} \left[1 - \frac{i - i_w}{i_s - i_w} \right] \frac{u}{u_s} d\eta = \frac{k_w}{c_{pw}} \left(\frac{\rho_w}{\rho_s} \right) \frac{di}{d\eta}_w \quad (5)$$

Assume an enthalpy profile as

$$\frac{i - i_w}{i_s - i_w} = a' + b'\eta + c'\eta^2 + e'\eta^3$$

at

$$\eta = 0, \frac{di}{d\eta} = 0 \text{ and } i = i_w; \therefore c' = a' = 0$$

also

$$\text{at } i = \Delta, i = i_s \text{ and } \frac{di}{d\eta} = 0 \therefore \eta = \Delta \text{ at } y = \delta_r$$

which leads to

$$\frac{i - i_w}{i_s - i_w} = \frac{3}{2} \frac{\eta}{\Delta} - \frac{1}{2} \left(\frac{\eta}{\Delta} \right)^3 \quad (6)$$

$$\text{where } \frac{di}{d\eta} \bigg|_{\eta=0} = \frac{3}{2} \frac{(i_s - i_w)}{\Delta} = \frac{3}{2} \frac{(i_s - i_w)}{\xi \delta_i}$$

$$\xi = \frac{\Delta}{\delta_i}$$

Thus, using equations (2) and (6)

$$\int_0^{\Delta} \left[1 - \frac{i - i_w}{i_s - i_w} \right] \frac{u}{u_s} d\eta \approx \frac{3}{20} \delta_i \xi^2$$

The integral energy equation becomes

$$(i_s - i_w) \rho_s u_s \frac{3}{20} \frac{d}{dx} (\delta_i \xi^2) = \frac{3}{2} \frac{k_w}{c_{pw}} \left(\frac{\rho_w}{\rho_s} \right) \frac{i_s - i_w}{\xi \delta_i}$$

and can be reduced to

$$\frac{U_1}{10} \left(\xi^3 \delta_1 \frac{d\delta_1}{dx} + 2 \xi^2 \delta_1^2 \frac{d\xi}{dx} \right) = \frac{3}{2} \frac{k_w}{c_{pw}} \left(\frac{\rho_w}{\rho_s} \right) \frac{i_s - i_w}{\xi \delta_1} \quad (7)$$

Substituting equation (4) for δ_1 into equation (7) gives

$$\frac{14}{13} (P_r)_w \left[\xi^3 + 4 \xi^2 \frac{d\xi}{dx} \right] = 1$$

where

$$(P_r)_w \equiv \frac{c_p \mu}{k} \Big|_w$$

then

$$\xi = \frac{1}{1.026 (P_r)_w^{1/3}} \left[1 - \left(\frac{x_0}{x} \right)^{3/4} \right]^{1/3} \quad (8)$$

x_0 = unheated starting section

Define a heat transfer coefficient such that

$$q_w = h_i (i_s - i_w) = \frac{k_w}{c_{pw}} \left(\frac{\rho_w}{\rho_s} \right) \frac{di}{d\xi} \Big|_w$$

or

$$h_i = \frac{3}{2} \frac{k_w}{\xi \delta_1} \left(\frac{\rho_w}{\rho_s} \right) \quad (9)$$

Substitute equations (4) and (8) into equation (9), assuming $x_0 = 0$, gives

$$h_i = 0.332 \frac{k_w}{c_{pw}} (P_r)_w^{1/3} (Re)_w^{1/2} x^{-1} \quad (10)$$

where

$$Re)_w = \frac{\rho_w U_\infty x}{\mu_w}$$

$$Pr)_w = \frac{c_{pw} \mu_w}{k_w}$$

The heat transfer coefficient from equation (10) is used to determine the heat flux for low free stream velocities by

$$q_w = h_i (i_s - i_w) \quad (11)$$

however, at high free stream velocities, it can be shown that

$$q_w = h_i (i_{aw} - i_w) \quad (12)$$

where

$$i_{aw} = i_s + r_i \frac{U_\infty^2}{2g_j} ; \quad r_i = (Pr)^{1/2} \quad (13)$$

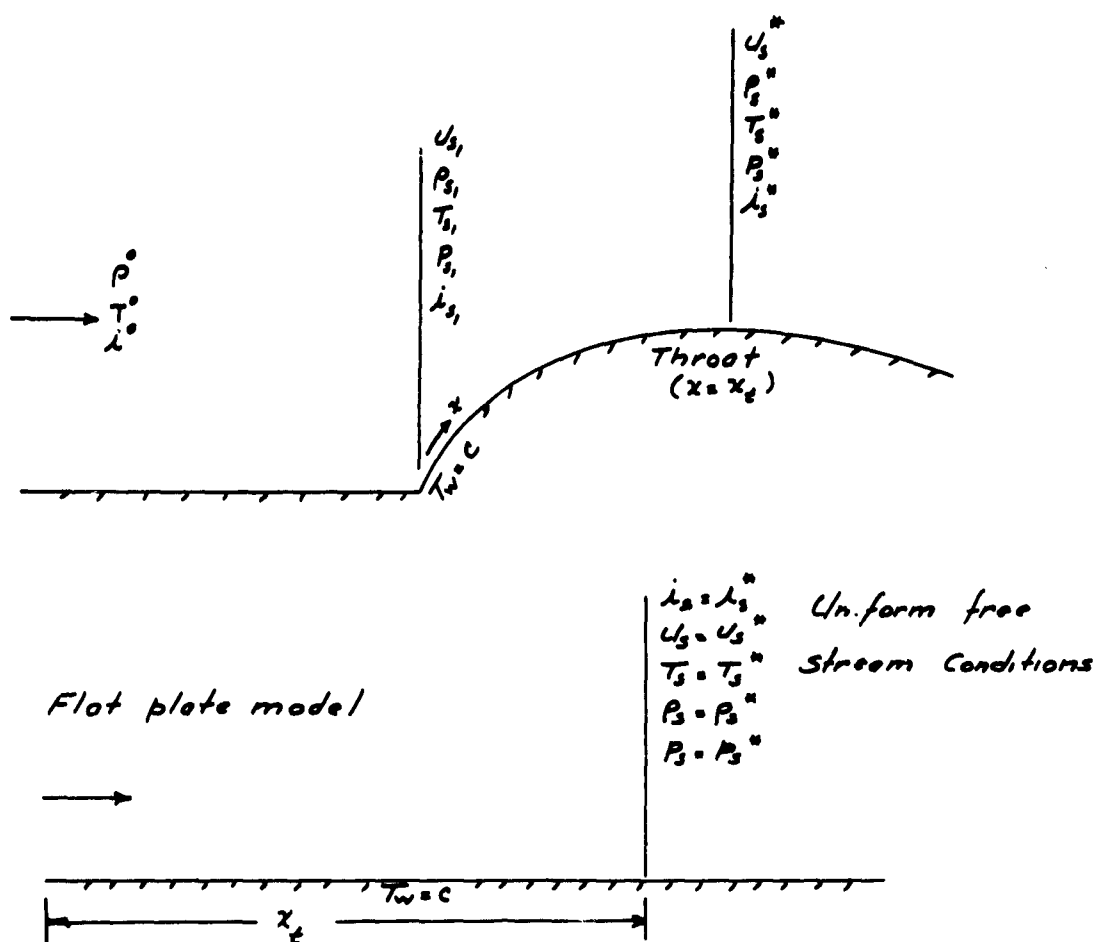
Eckert suggests that better correlation with experimental data is obtained if the fluid properties are evaluated at a reference enthalpy

$$i^{\oplus} = 0.5(i_s + i_w) + 0.22(i_{aw} - i_s) \quad (14)$$

Equation (10) was developed assuming the following conditions or restrictions for the flat plate:

- 1) laminar boundary layer
- 2) constant free stream conditions
- 3) variable fluid properties in the boundary layer
- 4) constant wall temperature along the flat plate.

This model may be translated to a nozzle in order to calculate an average heat transfer coefficient for the convergent section by assuming that the free stream conditions of the flat plate model are equivalent to the nozzle throat conditions. The converging section of the nozzle in the following sketch and the flat plate model at $x = x_t$ are assumed equivalent.

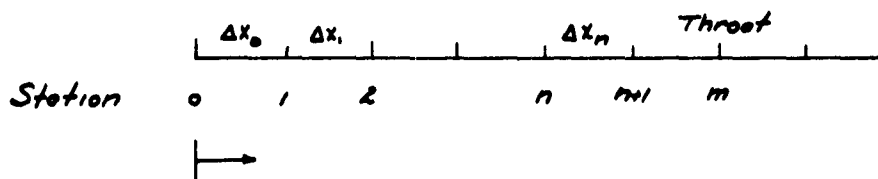


It will be shown later (by comparison with an incremental calculation) that this flat plate model yields an average heat transfer coefficient suitable for parametric analyses.

Incremental Technique

The determination of the local heat transfer coefficient in a nozzle of the type considered in this report is most difficult if approached by the usual techniques. In contrast, the incremental technique presented here is basically simple. Many difficult problems (theoretical and calculational) are circumvented by a direct utilization of accepted flat plate results.

The nozzle is represented as a series of m incremental flat plates each of length Δx_n . The nozzle free stream conditions are superimposed on this flat plate model.



Let us then assume that the variation in heat transfer coefficient across an incremental flat plate Δx_n can be represented as

$$h_{n+1} \approx h_n + \Delta h_n$$

where Δh_n represents the total change in the flat plate heat transfer coefficient across the Δx_n interval. For the general problem, it must be assumed that variations in the free stream flow parameters u_s and ρ_s over Δx_n will affect Δh_n . It follows that Δh_n can be written as

$$\Delta h_n = \left(\frac{\partial h}{\partial x} \right)_{\rho_s} \Delta x_n + \left(\frac{\partial h}{\partial u_s} \right)_x \Delta u_{s,n} + \left(\frac{\partial h}{\partial \rho_s} \right)_x \Delta \rho_{s,n}$$

Let h for an incompressible laminar boundary layer (small temperature differences) be represented by

$$h = 0.332 \frac{k}{x} (Pr)^{1/3} (Re)^{1/2}$$

Thus

$$\left(\frac{\partial h}{\partial x} \right)_{\rho_s} = - \left[\frac{0.332}{x^2} (Pr)^{1/3} k \right]_n (Re)_n^{1/2} x_n^{-2}$$

$$\left(\frac{\partial h}{\partial \rho_s} \right)_x = \left[\frac{0.332}{x} (Pr)^{1/3} k \right]_n (Re)_n^{1/2} (\rho_n x_n)^{-1}$$

$$\left(\frac{\partial h}{\partial u_s} \right)_x = \left[\frac{0.332}{x} (Pr)^{1/3} k \right]_n (Re)_n^{1/2} (u_n x_n)^{-1}$$

The fluid properties of the boundary layer could be assumed as constant over the entire heat transfer surface (evaluated at some reference temperature T^*) or as constant over each particular interval Δx_n and evaluated at some local reference temperature T_m^* .

This technique requires that the heat transfer coefficient be known at some position x_0 as an initial condition, i.e., the stagnation point or a sharp edge consideration.

A nozzle subject to the following conditions

$$\begin{aligned} T^* &= 4000 \text{ K}, T_w = 800 \text{ K}, P^* = 34 \text{ atm.} \\ \gamma &= 1.3, \text{ isentropic expansion} \end{aligned}$$

was selected for an example problem. Calculations of the local heat transfer coefficient were made using the incremental technique. Also, estimates of the average heat transfer coefficient were obtained for several variations of the flat plate model. Figure 1 shows a comparison of the results of these calculations with the predictions of Cohen and Reshotko (1) - the solution to this problem is given in considerable detail in the Cohen and Reshotko report.

A good correlation between calculation techniques was achieved for the sample problem. It is proposed that nozzle heat transfer coefficients be calculated by incremental techniques when accurate local values are required. The precise nozzle geometry and flow conditions are necessary input data for this calculation. Further, the extremely simple-to-use flat plate model should provide a good estimate of the average coefficient over the entire converging section. This calculation is independent of the throat size so that results can be applied (with some caution) to any of the considered nozzles for a given flow condition if the result is modified by the simple $(x_{ref}/x_t)^{1/2}$ ratio. A parametric analysis of heat flux for a $x_{ref} = 3''$ based on the flat plate model is shown in Figure 2 in relation to the performance envelop.

The magnitude of heat transfer from the plasma main-stream to the nozzle walls is strongly influenced by the nature of the boundary layer which develops along the nozzle wall. A laminar boundary layer will in effect insulate the nozzle wall from the hot plasma. In contrast, the transverse fluid motions characteristic of a turbulent boundary layer promotes extreme rates of heat transfer. It is felt that an accurate estimate of the heat transfer under turbulent conditions be known since the nature of the boundary layer cannot be predicated with confidence for all nozzle configurations. Following usual practice, the rates of turbulent heat transfer were calculated according to the approximate method of Bartz (2).

The usual approximate method of solution for a turbulent boundary layer involve considerable calculation complexity - usually requiring an elaborate computer program. The Bartz (2) approximation equation for the heat transfer coefficient was obtained by effecting a numerical fit of a simple dimensionless equation containing the characteristic parameters of the system with the results of the usual approximate boundary layer calculations

$$T_o = 4000^{\circ}\text{R} \quad P_o = 500 \text{ psi}$$

$$T_w = 800^{\circ}\text{R} \quad \gamma = 1.3$$

Key

- Cohen and Reshotko, NACA 1289, 1956
 --- Incremental Technique (Stagnation Point Entrance)
 - - - Incremental Technique (Sharp Edge Entrance)
 X $q_w = h(T_o - T_w)$
 □ $q_w = h(T_{aw} - T_w)$

$$h = 0.332 \frac{K_w^3}{x} \sqrt{\text{Pr}_w} \frac{1_w u_s x_t}{\mu_w}$$

$$T_{aw} = T_s + 0.88 \frac{u_s^2}{2qJC_p}$$

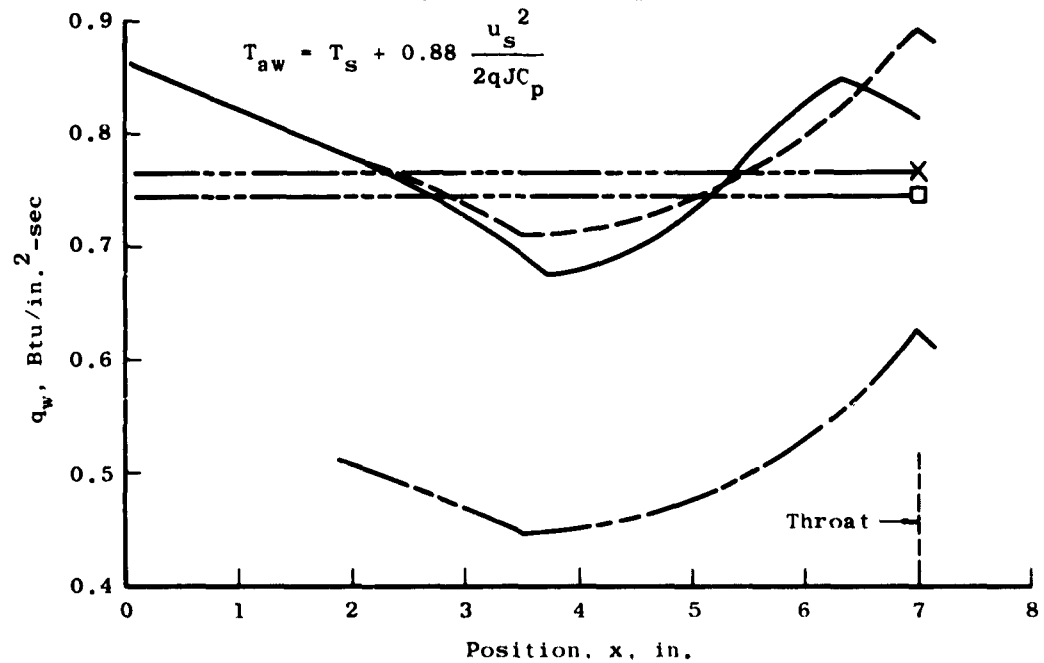


Fig. 1 Comparison of Laminar Heat Transfer in a Convergent Nozzle

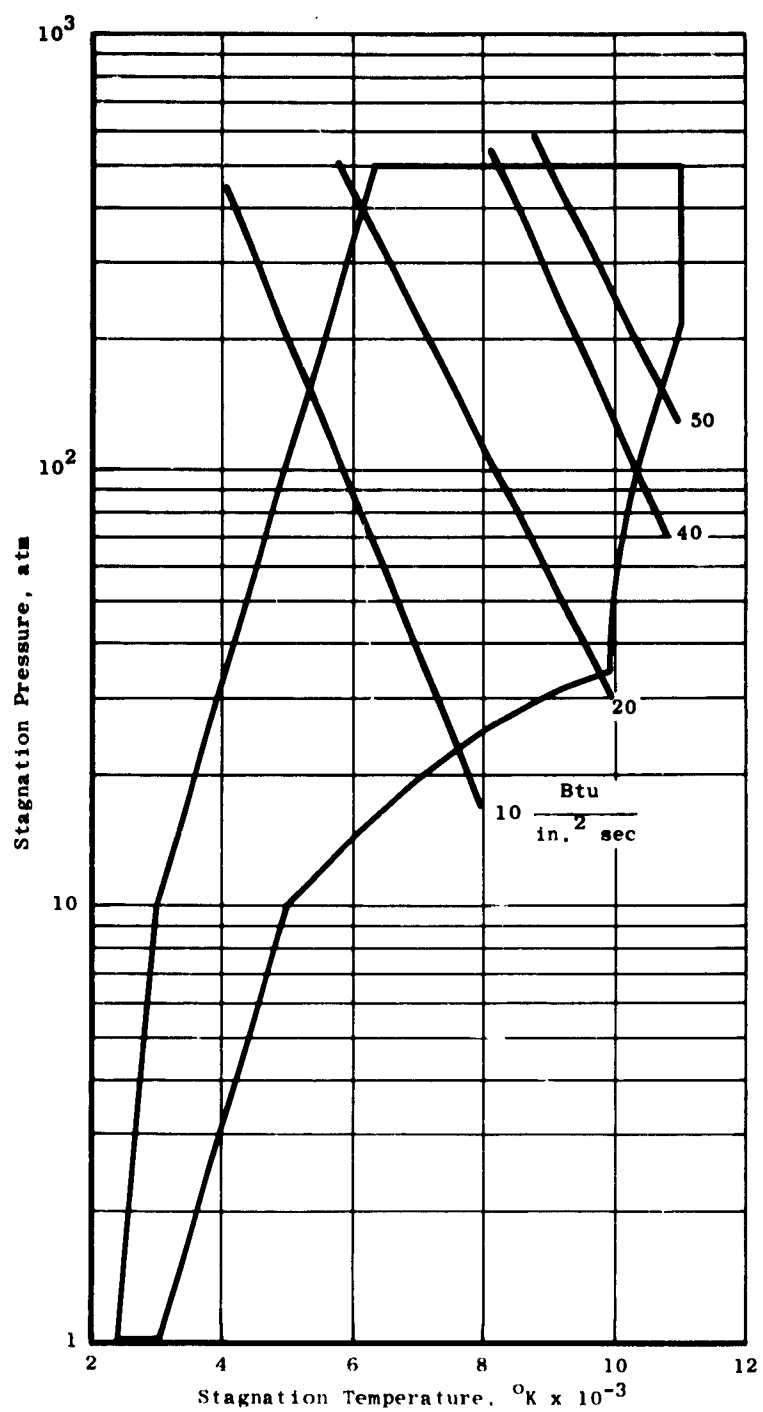


Fig. 2 Heat Flux to Wall at 700°K, Laminar Boundary Layer, $x_{ref} = 3''$

$$h = \left[\frac{0.026}{D^{0.2}} \left(\frac{\mu^{0.2} c_p}{Pr} \right)_o \left(\frac{A g}{c^*} \right)^{0.8} \left(\frac{D}{c} \right)^{0.17} \right] \left(\frac{A}{A^*} \right)^{0.9} \sigma \quad (15)$$

where σ is a correction factor.

The heat transfer coefficient obtained from equation (15) is based on a temperature difference, i.e., $q_w = h (T_{aw} - T_w)$. The temperature difference seriously underestimates the energy available for heat transfer from the disassociated gas. Experience has shown (3) that a heat transfer coefficient based on an enthalpy difference (otherwise evaluated in the usual manner) provides a reasonable estimate of the heat transfer from a gas with disassociation effects present. Following this procedure, the turbulent heat transfer was calculated by

$$q = h_i (i_{ow} - i_w) \quad (16)$$

$$\text{where } h_i = \frac{h}{c_p} \text{ from Equation (15)} \quad (17)$$

i = local plasma enthalpy

The calculation of the turbulent heat transfer was included as a sub-routine to the parametric analysis of transpiration and film cooling, Chapter IV. The results are shown in graphical form for the three nozzle sizes under consideration, Figures 3, 4, and 5. It should be noted that the practical limit of 50 B/in²sec excludes most of the desired performance envelope if the boundary layer is turbulent.

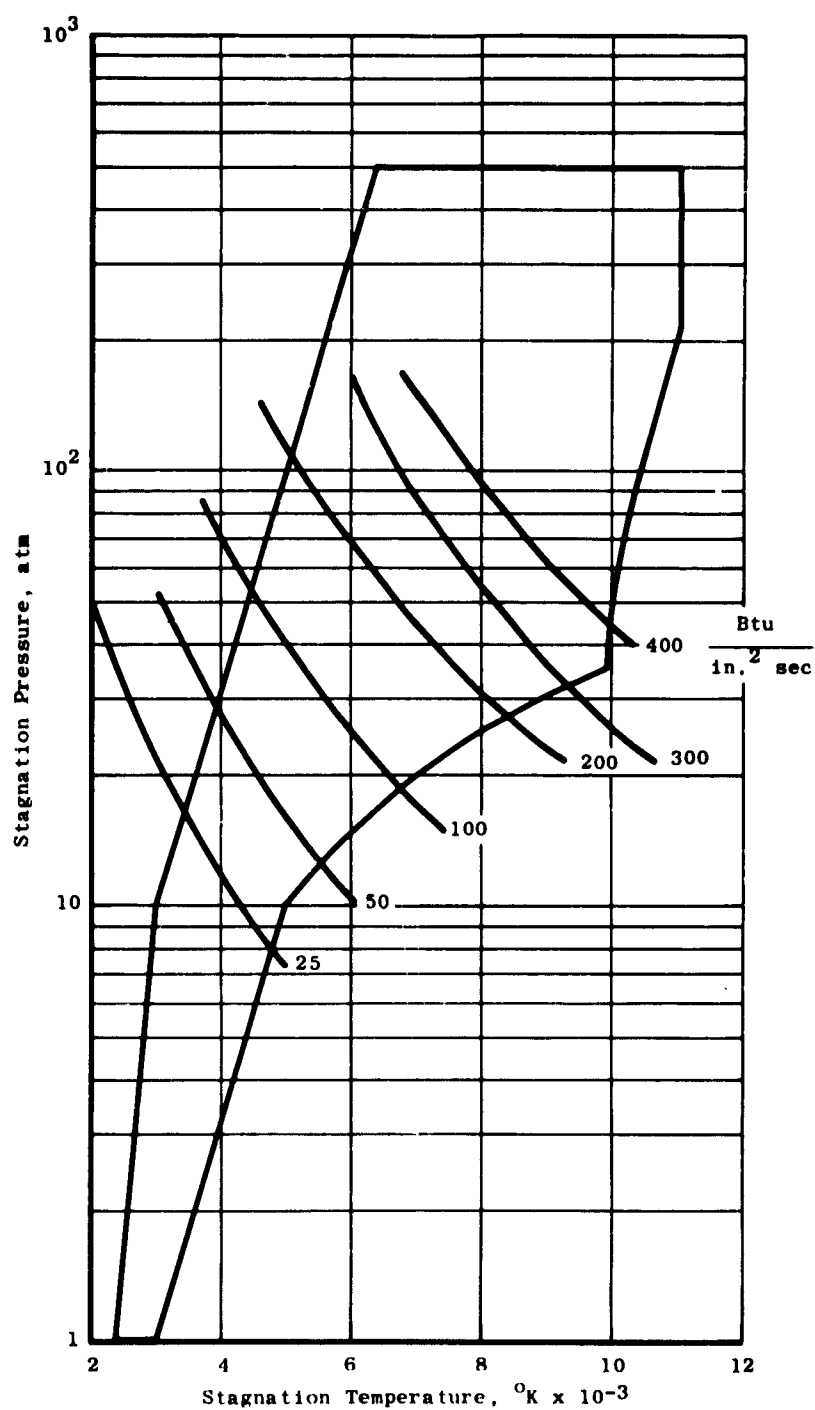


Fig. 3 Convective Heat Load (Throat); Turbulent Boundary Layer;
 $T_{wall} = 700^{\circ}\text{K}$ $D^* = 0.042''$

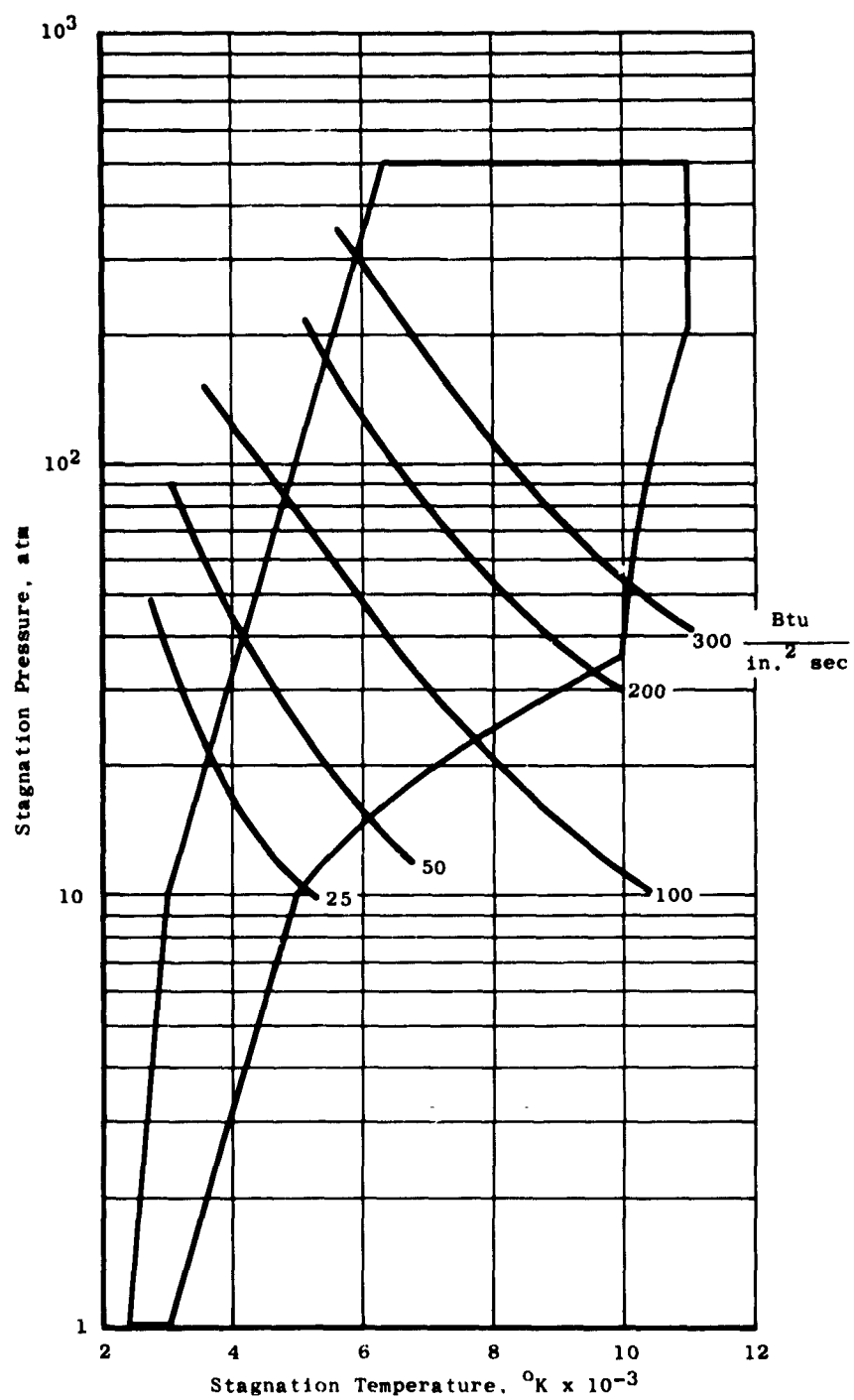


Fig. 4 Convective Heat Load (Throat); Turbulent Boundary Layer;
 $T_{\text{wall}} = 700^\circ\text{K}$ $D^* = 0.272''$

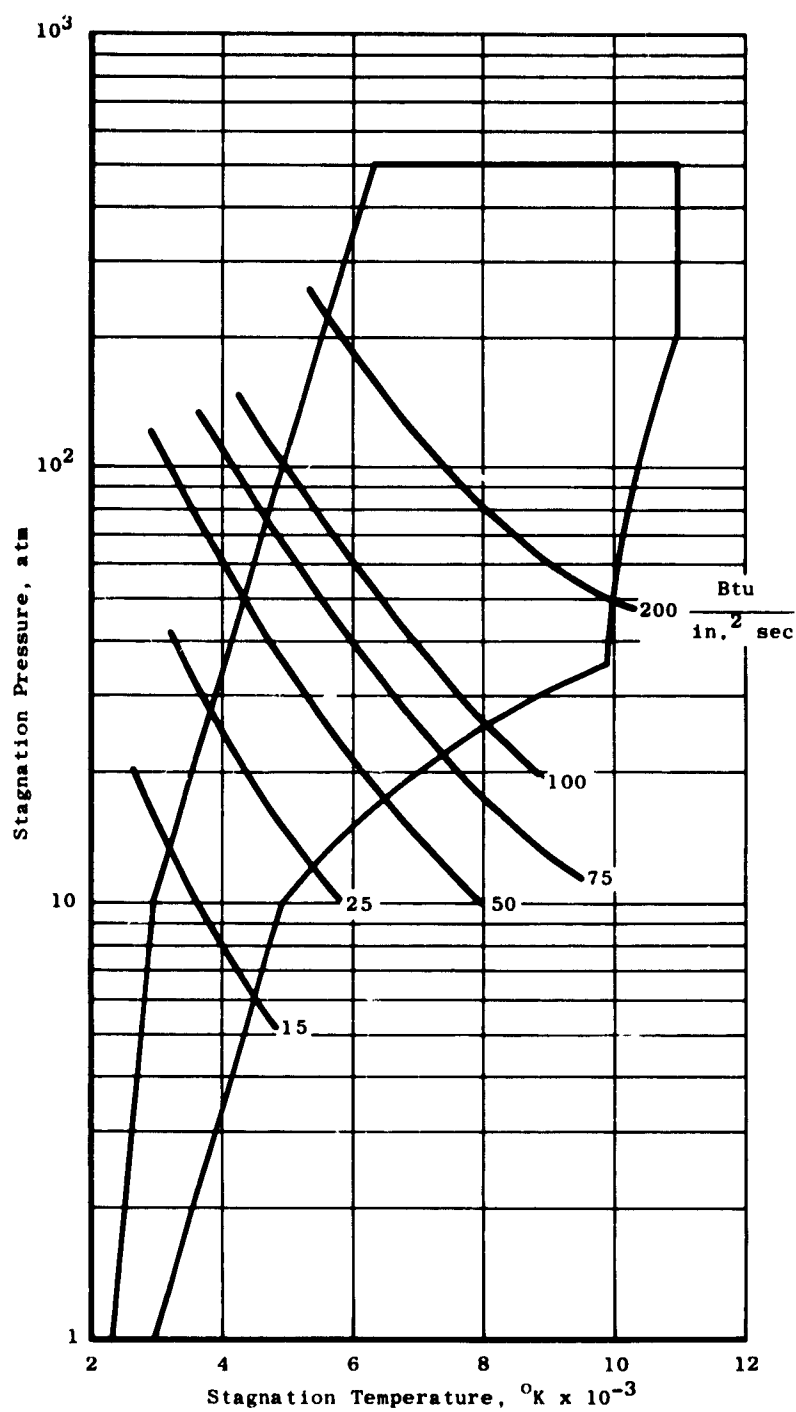


Fig. 5 Convective Heat Load (Throat); Turbulent Boundary Layer;
 $T_{wall} = 700^{\circ}\text{K}$ $D^* = 0.784''$

III. THERMAL RADIATION

The problems of thermal radiation are more pronounced in the entrance to the nozzle than in the throat because of higher temperatures and larger volumes of gases. The analysis for radiation heat flux assumes a particular model involving an emitting and absorbing gas enclosed by black, non-radiating walls. The assumption of black walls is conservative as there could be a reduction in absorbed energy at the walls if the reflectivity was high and gas velocity high. However, it is doubtful whether a reflective surface could be maintained because of contamination. The walls have been assumed non-radiating because of their relatively low temperatures.

The assumed configuration for the entrance and the converging walls of the nozzle is one of a sphere as shown in Figure 6.

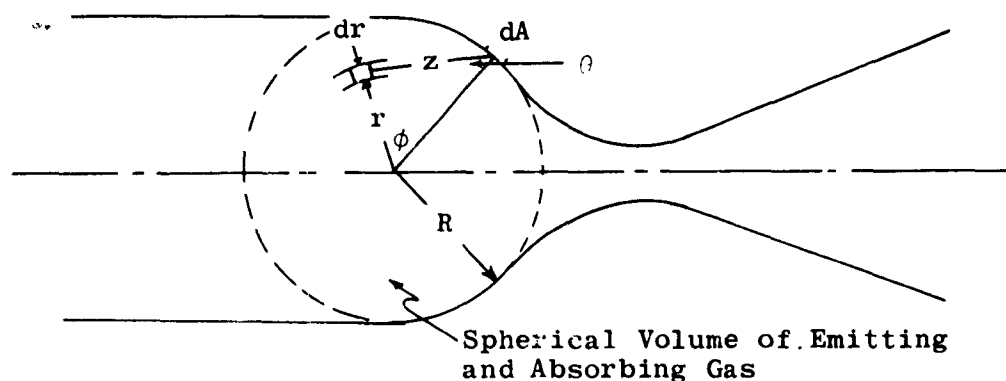


Fig. 6 Model for Gas Thermal Radiation Study

The emission of a gray gas of volume V to $V + dV$, radiating uniformly in all directions is

$$dq_r = 4\bar{\mu}\sigma T^4 dV \frac{d\omega}{4\pi}$$

where $\bar{\mu}$ is the mean absorption coefficient. The volume element is expressed as

$$dV = 2\pi r^2 \sin\phi d\phi dr$$

Assuming exponential absorption of emitted energy, the amount of energy per unit solid angle absorbed on the black walls becomes

$$q_{\lambda} = \int_0^R \int_0^{\pi} 2\bar{\mu}\sigma T^* r^2 e^{-\bar{\mu}z} \sin\phi d\phi dr d\omega$$

Noting that

$$z^2 = R^2 + r^2 - 2rR \cos\phi$$

$$d\omega = \frac{dA}{2} \cos\phi$$

$$\cos\phi = \frac{R-r\cos\phi}{z}$$

the energy absorbed per unit wall area becomes

$$q = \int_0^R \int_0^{\pi} \frac{2\bar{\mu}\sigma T^* (R-r\cos\phi) r \sin\phi e^{-\bar{\mu}(R^2+r^2-2rR\cos\phi)^{1/2}}}{(R^2+r^2-2rR\cos\phi)^{3/2}} dr d\phi \quad (18)$$

In order to integrate equation (18) define

$$\lambda^2 \equiv \bar{\mu}^2 (R^2 + r^2 - 2rR \cos\phi)$$

$$\beta \equiv \frac{r}{R}$$

thus

$$2\lambda d\lambda = 2\bar{\mu}^2 r R \sin\phi d\phi$$

$$\sin\phi d\phi = \frac{\lambda d\lambda}{\bar{\mu}^2 r R}$$

then

$$q = \int_0^1 d\beta \int_{\bar{\mu}R(1-\beta)}^{\bar{\mu}R(1+\beta)} \frac{2\bar{\mu}\sigma T^* (R-r\cos\phi) R\beta e^{-\lambda^2}}{\lambda^2} d\lambda$$

and

$$(R - r \cos \phi) = \frac{R}{2} + \frac{\lambda^2}{2R\bar{\mu}^2} - \frac{r^2}{2R}$$

resulting in

$$g = \int_0^1 d\beta \int_{\bar{\mu}R(1-\beta)}^{\bar{\mu}R(1+\beta)} 2\bar{\mu}\sigma_T^* \beta R \frac{e^{-\lambda}}{\lambda^2} \left(\frac{R}{2} + \frac{\lambda^2}{2R\bar{\mu}^2} - \frac{r^2}{2R} \right) d\lambda$$

or

$$\frac{g}{\sigma_T^*} = \int_0^1 d\beta \left\{ \int_{\bar{\mu}R(1-\beta)}^{\bar{\mu}R(1+\beta)} \beta e^{-\lambda} d\lambda + \int_{\bar{\mu}R(1-\beta)}^{\bar{\mu}R(1+\beta)} (\bar{\mu}^2 \beta R^2 - \bar{\mu}^2 \beta^3 R^2) \frac{e^{-\lambda}}{\lambda^2} d\lambda \right\}$$

Integrating the λ variable gives

$$\begin{aligned} \frac{g}{\sigma_T^*} = \bar{\mu}R \int_0^1 d\beta \left\{ \left[\frac{\beta}{\bar{\mu}R} + \beta(1+\beta) \right] e^{-\bar{\mu}R(1-\beta)} - \left[\frac{\beta}{\bar{\mu}R} + \beta(1-\beta) \right] e^{-\bar{\mu}R(1+\beta)} \right. \\ \left. - \bar{\mu}R(\beta-\beta^3) \int_{\bar{\mu}R(1-\beta)}^{\bar{\mu}R(1+\beta)} \frac{e^{-\lambda}}{\lambda^2} d\lambda \right\} \end{aligned} \quad (19)$$

or

$$\frac{g}{\bar{\mu}R\sigma_T^*} = \int_0^1 \gamma d\beta \quad (20)$$

Equation (20) is evaluated for a particular value of $\bar{\mu}^R$ by graphically integrating a Y versus β curve. The results of such integrations give Figure 7.

In order to determine the mean absorption coefficient, information from Kivel and Bailey (4) is used. They have expressed the intensity of radiation in wave length ν to $\nu+d\nu$ as

$$I_\nu d\nu = 2\mu L \sigma T^4 \left(\frac{15}{\pi^4} \right) u^3 e^{-u} du$$

where

$$u \equiv \frac{h\nu}{KT} \quad ; \quad \text{or} \quad \frac{du}{d\nu} = \frac{h}{KT}$$

and I_ν = intensity per unit wave length.

Thus

$$I_\nu = 2\mu L \sigma T^4 \left(\frac{15}{\pi^4} \right) u^3 e^{-u} \frac{h}{KT}$$

or

$$I = 2L \sigma T^4 \left(\frac{15}{\pi^4} \right) \left(\frac{h}{KT} \right) \int_0^\infty \mu \nu^3 e^{-\frac{h}{KT} \nu} d\nu$$

define

$$\bar{\mu} \equiv \frac{\int_0^\infty \mu \nu^3 e^{-\frac{h}{KT} \nu} d\nu}{\int_0^\infty \nu^3 e^{-\frac{h}{KT} \nu} d\nu}$$

Then

$$I = 2\bar{\mu} L \sigma T^4 \left(\frac{15}{\pi^4} \right) \left(\frac{h}{KT} \right) \int_0^\infty \nu^3 e^{-\frac{h}{KT} \nu} d\nu$$

Integrating

$$I = 2\bar{\mu} L \sigma T^* \left(\frac{15}{\pi^*} \right) \left(\frac{h}{\kappa T} \right)^* \frac{3!}{\left(\frac{h}{\kappa T} \right)^*}$$

$$I = 1.84 \bar{\mu} L \sigma T^*$$

Using

$$I = \epsilon \sigma T^*$$

the mean absorption coefficient becomes.

$$\bar{\mu} = \frac{\epsilon}{1.84 L}$$

Values of total emissivity per cm, $\frac{\epsilon}{L}$, are taken from the report (2) and the resulting values of mean absorption coefficient $\bar{\mu}$ are shown in Figure 8 as related to temperature.

Using the information from Figures 7 and 8, and choosing a radius of 1.91 cm (0.75 in), enables one to plot $\bar{\mu} R \int \gamma d\beta$ as a function of temperature and this is shown in Figure 9. The heat flux per unit area

$$q = \sigma T^* \bar{\mu} R \int_0^\pi \gamma d\beta$$

can now be calculated and the results are shown in Figure 10. The heat flux information is also shown in Figure 11.

A limiting value of heat flux from this analysis exists when the gas does not absorb any of the emitted radiation. This situation occurs when $e^{-\bar{\mu} z}$ in equation (18) is one, i.e., $\bar{\mu} z = 0$ (note that $\bar{\mu}$ is not considered zero in the emission process). Using the condition that $e^{-\bar{\mu} z}$ is one, equation (18) reduces to

$$q = \frac{4}{3} \bar{\mu} R \sigma T^* \quad (21)$$

which is the heat flux per unit area of an emitting and non-absorbing gas. Results from equation (21) are shown in Figure 10 which shows that the heat flux is increased for the non-absorbing gas.

The analysis for thermal radiation heat flux assumes that the convergent walls of the nozzle see a spherical volume of emitting and absorbing gas; the gas exhibits an exponential absorption characteristic; the amount of energy emitted by the gas is proportional to the mean absorption

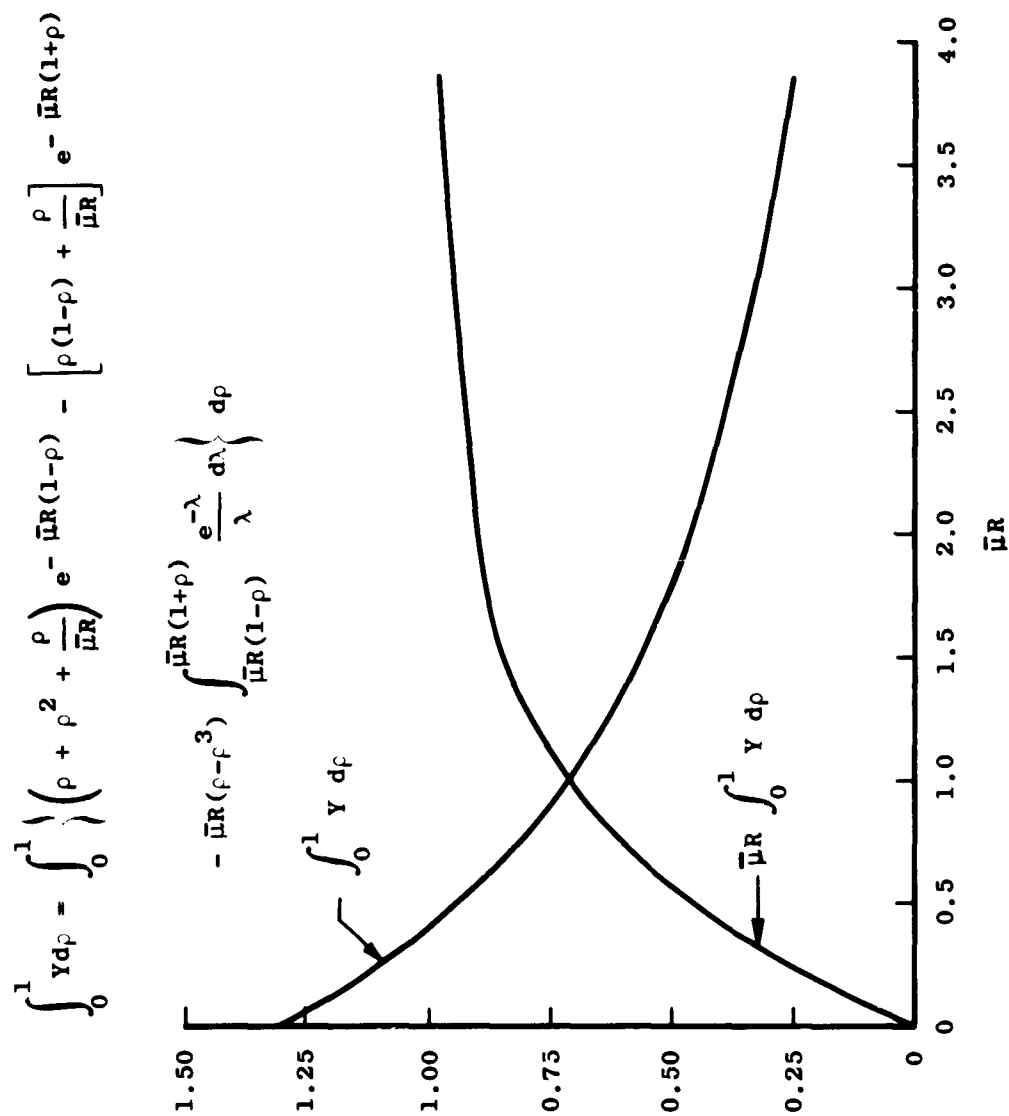


Fig. 7 Integration of Equations (19) and (20)

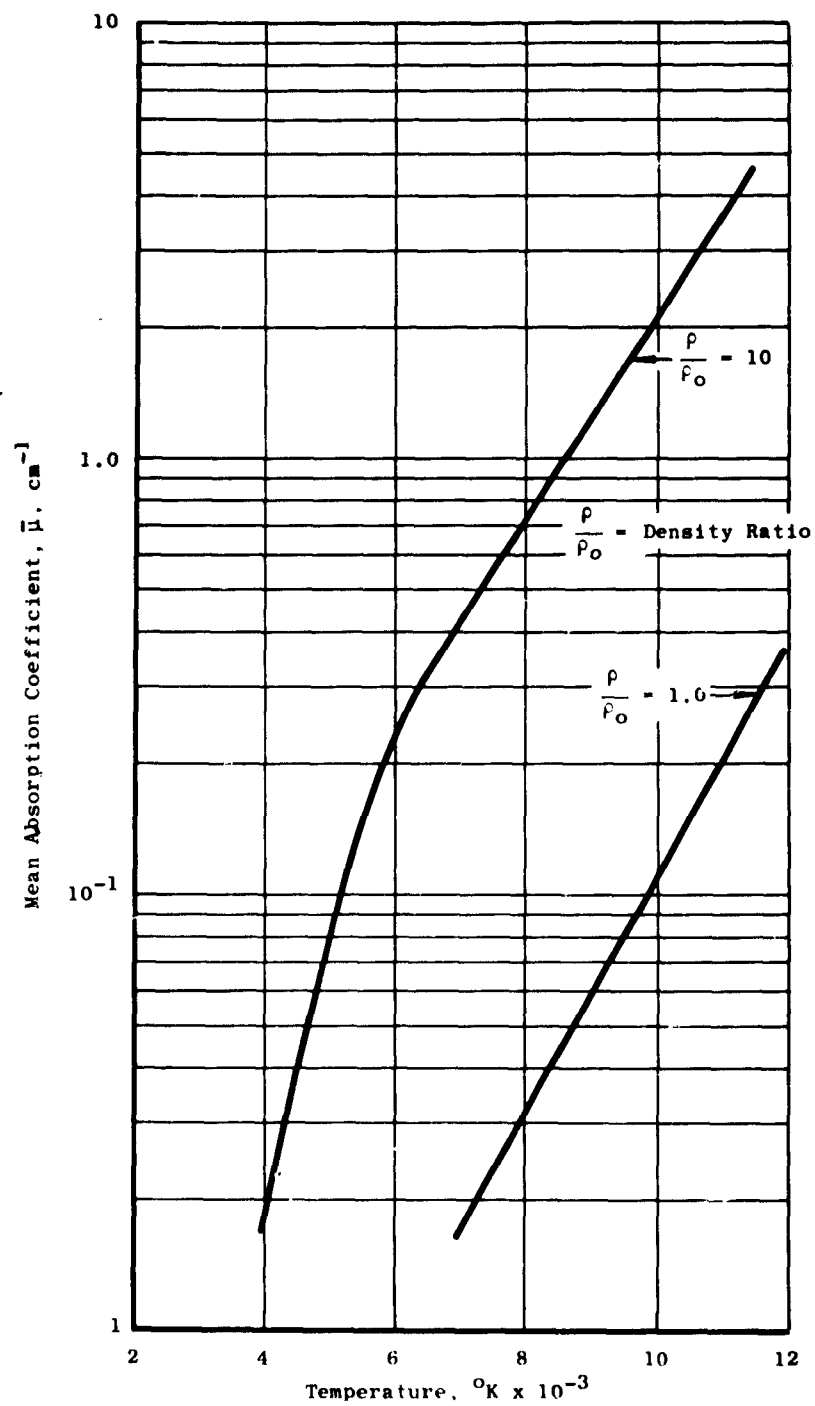


Fig. 8 Mean Absorption Coefficient for Air

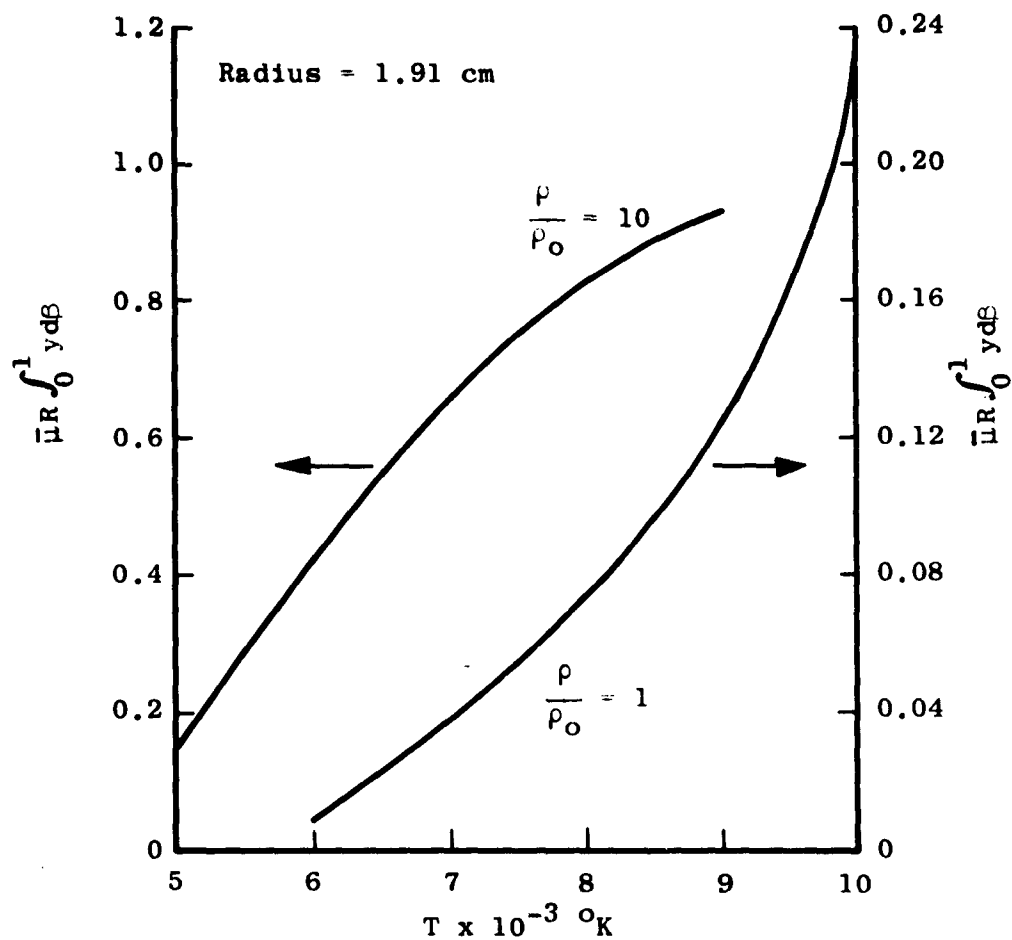


Fig. 9 Equation (20) versus Temperature

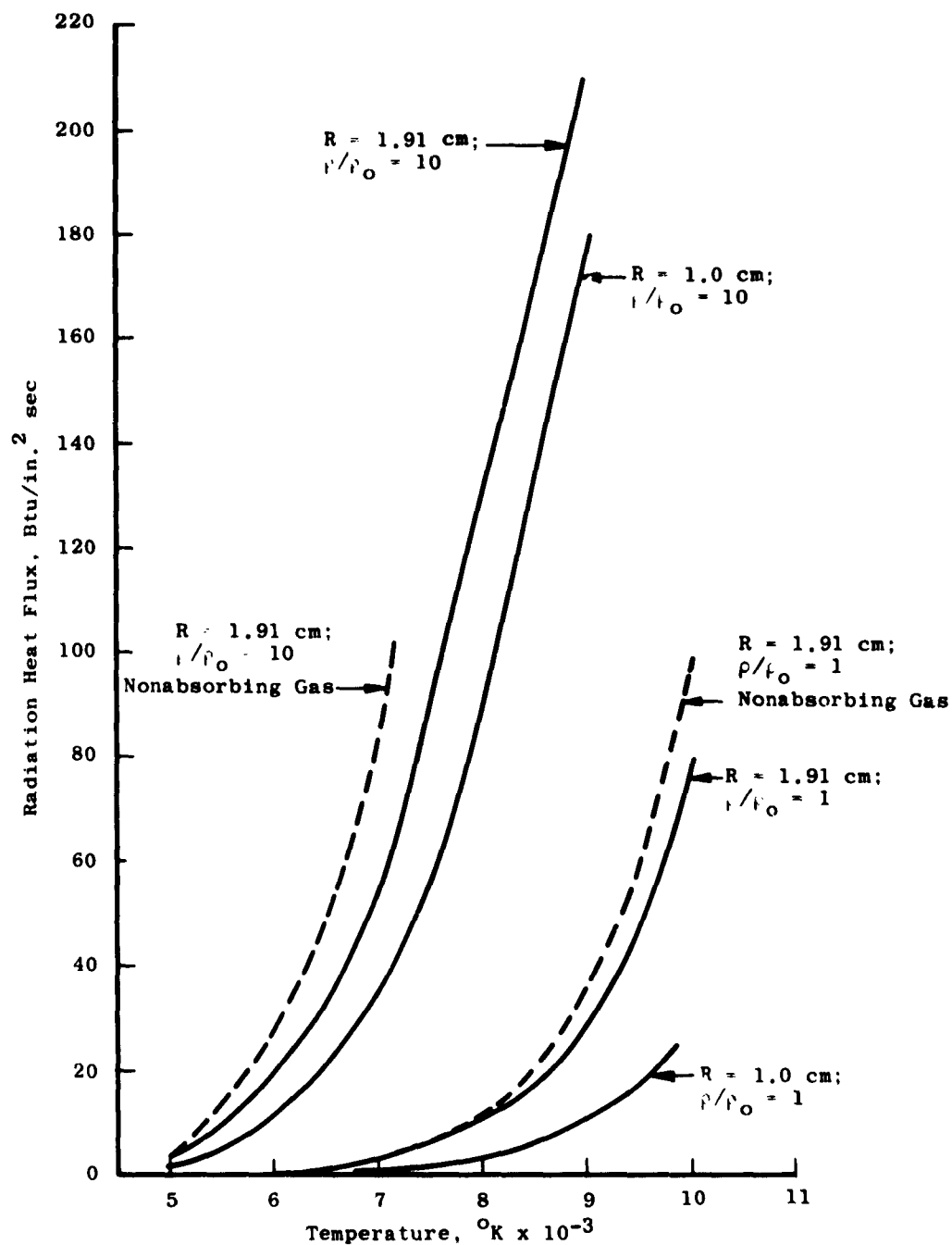


Fig. 10 Radiation Heat Flux for Spheres of 1.91 and 1.0 cm Radii

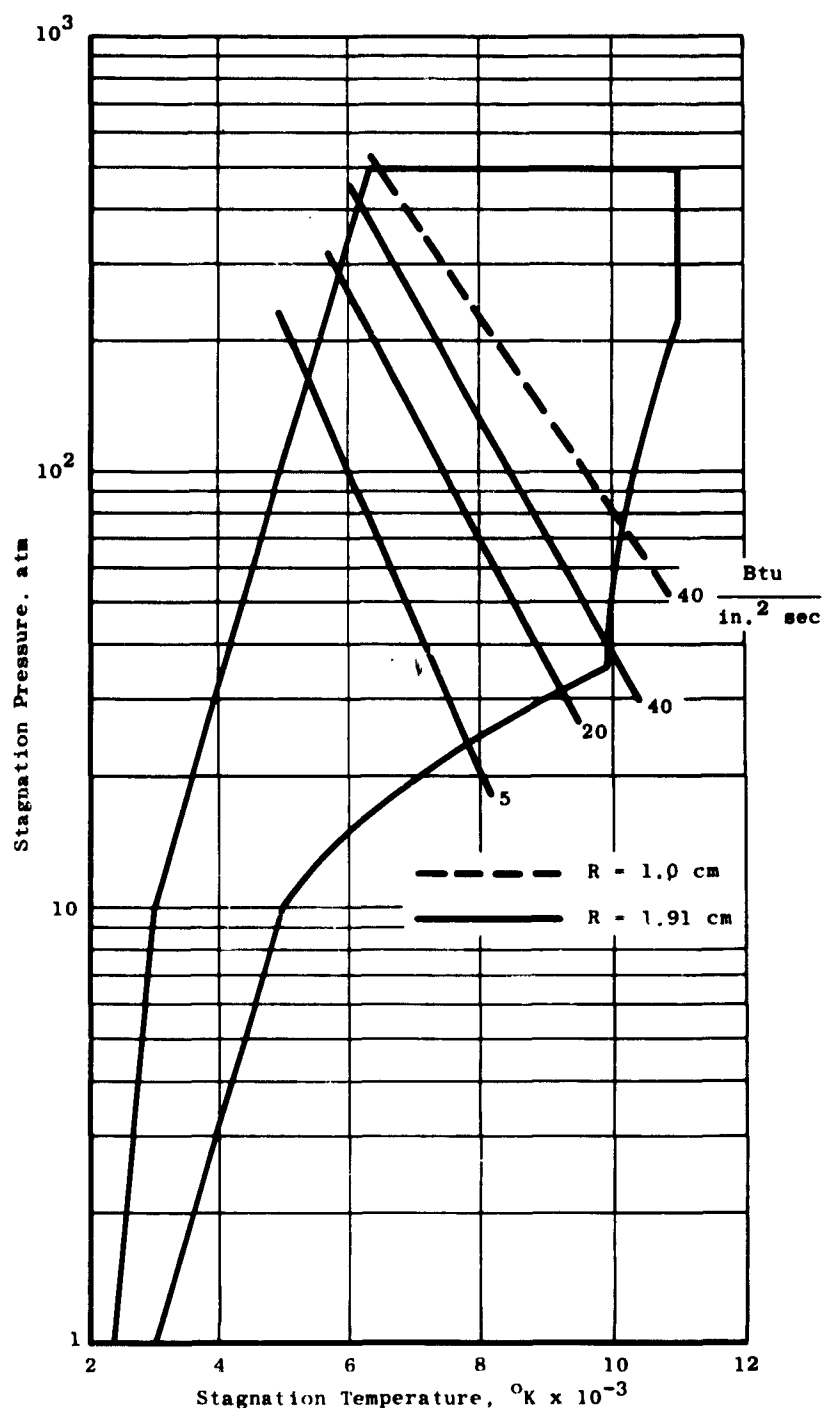


Fig. 11 Radiation Heat Flux

coefficient of the gas; and that the mean absorption coefficient of the gas can be determined by integrating the intensity per unit wave length over all wave lengths. The final results shown in Figure 12 indicate that radiation contributes an important part to the total heat flux as the pressure or density increases. The effects of thermal radiation can be reduced significantly by decreasing the radius of the plenum or stagnation region. Since thermal radiation would be the major contributor to the heat flux in the plenum region it becomes a necessity to decrease the radius of this section to as small a value as possible without effecting other parameters.

IV. TRANSPIRATION AND FILM COOLING OF HYPERSONIC NOZZLES

Laminar boundary layer stability considerations may restrict the use of pure 'backside' cooling techniques to a small portion of the desired performance envelope. Other cooling techniques - 'transpiration' and 'film' - may allow nozzle operation over a considerably larger portion of the envelope.

Film cooling is accomplished by introducing the coolant at some point upstream of the critical heat transfer areas. The joint actions of the system pressure gradient and the shear stress of the plasma boundary layer establishes a coolant film over the surface to be protected. A schematic illustrating the basic features of film cooling is shown in Figure 13. The magnitude of the 'apparent' heat flux may be decreased or increased over that with backside cooling alone because of the interactions of the coolant with the plasma boundary layer. The influence of this effect upon the heat load imposed on the coolant film will be described by a suitably defined 'blockage factor.' The blockage factor is defined as the ratio of the convective heat transfer to the film to that transferred to the wall when there is no film. It may be necessary to augment film cooling with backside cooling to ensure stability of the film and to achieve a maximum cooling effect.

Transpiration cooling is similar in concept to film cooling except that the coolant is introduced as required along the entire cooled surface, Figure 14. The energy is first transferred from the plasma to the porous nozzle wall and then to the coolant as it flows through the porous wall. The diffusion out from the wall of the coolant vapor acts to reduce the magnitude of the heat flux. Again a blockage factor will be used to quantitatively describe this effect. The nature of the transpiration process should ensure a large and dependable reduction in heat flux. Backside cooling will not in general be compatible with transpiration cooling.

The basic mechanisms of film and transpiration cooling can be represented by a single generalized model. The magnitudes of a suitably defined blockage factor Ψ and a backside cooling heat flux q_w can be adjusted to provide a representation of either film or transpiration cooling adequate for parametric analyses. The results of the parametric analyses indicate that both transpiration and film cooling appear to offer promise of extend-

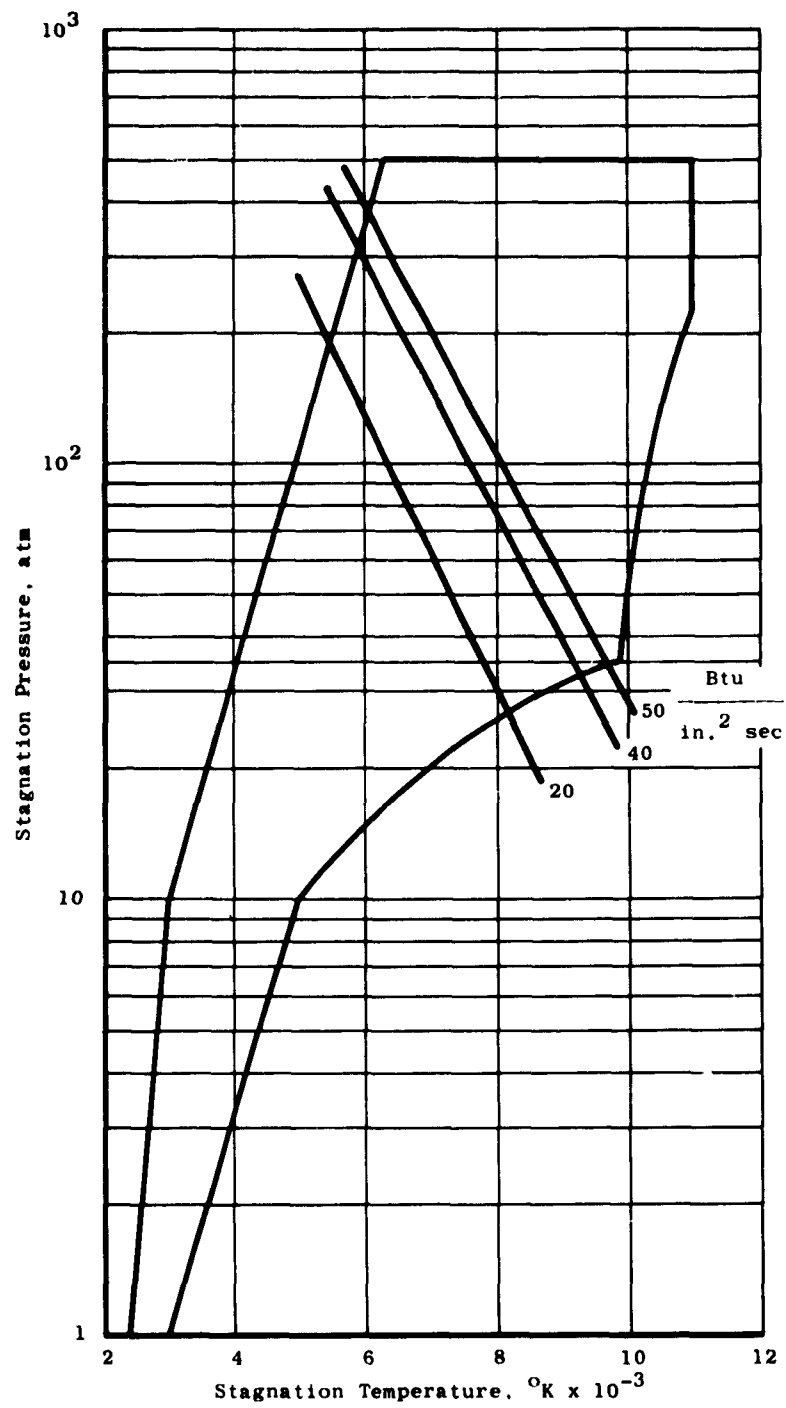


Fig. 12 Combined Radiation and Laminar Boundary Layer Heat Flux

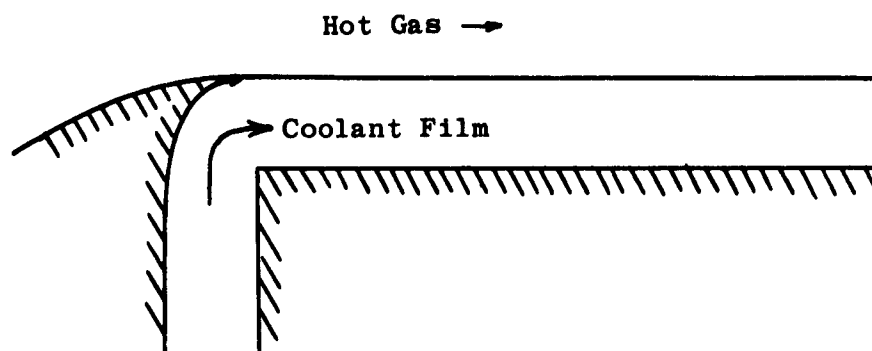


Fig. 13 Sketch of Film Cooling

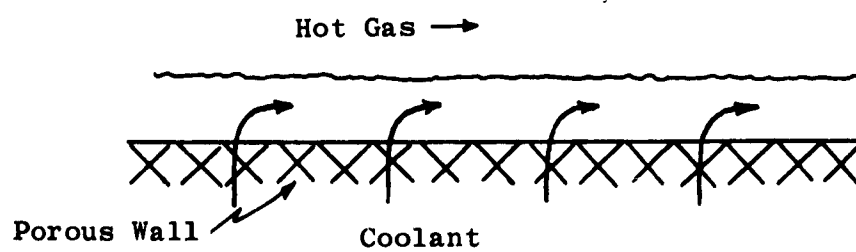


Fig. 14 Sketch of Transpiration Cooling

ing the envelope of nozzle operation. It should be noted that an actual design would require a more precise calculation for its basis.

PARAMETRIC ANALYSES

The flow schematic shown in Figure 15 represents a generalized energy balance for a differential section of the boundary layer region - either transpiration or film cooling. The net energy transferred to the coolant in the differential element is carried off by a dm amount of coolant which experiences both an enthalpy increase and a change in state. The blockage factor ψ is so defined that changes in heat transfer due to coolant diffusion into the plasma and increased coolant requirements because of coolant loss (directly into plasma stream before experiencing a complete enthalpy increase as a film coolant) are properly accounted for. Consider an energy balance on the element of coolant film shown in Figure 15.

$$dm = \left[\psi h_i (i_g - i_{sat}) + q_r - q_w \right] \frac{dA}{h_g - h_{fc}} \quad (22)$$

$$q_w = q_{wc} + \phi q_r \quad (23)$$

where

- dA = differential nozzle-surface area
- dm = differential coolant requirement
- h_i = local turbulent heat transfer coefficient based on an enthalpy (plasma) difference
- h_g = local enthalpy of coolant vapor evaluated at the local saturation temperature
- h_{fc} = initial coolant enthalpy
- i_g = local stagnation enthalpy (plasma)
- i_{sat} = enthalpy (plasma) corresponding to the local saturation temperature of the coolant
- q_c = local turbulent convective heat flux (without film)
- q_r = local radiative heat flux
- q_w = local heat flux removed by backside cooling
- q_{wc} = local heat flux from the film to the wall
- ϕ = transmissivity of the water film
- ψ = $\frac{\text{"apparent" local convective heat flux to the film}}{\text{local turbulent convective heat flux to the wall (without film)}}$

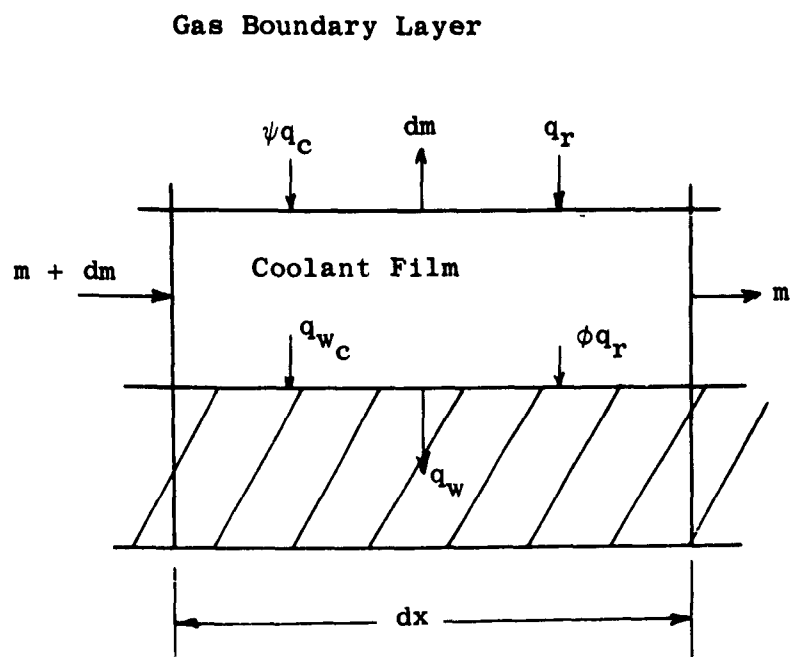


Fig. 15 Energy Balance on Coolant Film

The total coolant requirement is obtained by integrating equation (22) over the entire nozzle area

$$m_T = \int_A \left[\psi h_i (i_g - i_{sat}) + g_r - g_w \right] \frac{dA}{h_g - h_{fc}} \quad (24)$$

Equation (24) was evaluated for various combinations of stagnation temperatures (T°) and stagnation pressures (P°) for the three nozzle sizes under consideration ($D = 0.042, 0.272, 0.784$ in.) by use of an IBM 1620 digital computer. The program includes the calculation of the plasma flow which is uniquely determined by a T°, P°, D combination for the assumed isentropic (frozen) expansion through the nozzle. The coolant requirements were calculated as a coolant-flow to plasma-flow ratio. These results are presented in parametric form in Figures 16 through 27. It should be noted that results are not shown for system stagnation pressures in excess of 150 atmospheres. Thermodynamic plasma properties at higher pressures could not be found in the literature. The calculations can easily be extended to the higher pressures when the data becomes available. The data contained in these figures should be regarded as intermediate data which require careful interpretation in their use.

The parametric results for pure transpiration cooling ($q_r = 0$) can be extended to include radiation heat loads and to predict film cooling requirements by addition of the value of the second integral of equation (24) to

$$m = m_{trans} + \int \frac{g_r - g_w}{h_g - h_{fc}} dA$$

Again let us simplify the integration (conservatively) by replacing the local values of q_w and h_g by their nozzle throat values and q_r by $q_r(T^\circ P^\circ D^\circ)$

$q_r(T^\circ P^\circ D^\circ)$ = upstream radiation load corresponding to the stagnation temperature T° , stagnation pressure P° , and entrance diameter D° .

Then

$$m = m_{trans.} + \frac{[g_r(T^\circ P^\circ D^\circ) - g_w^*]}{h_g^* - h_{fc}} \quad (25)$$

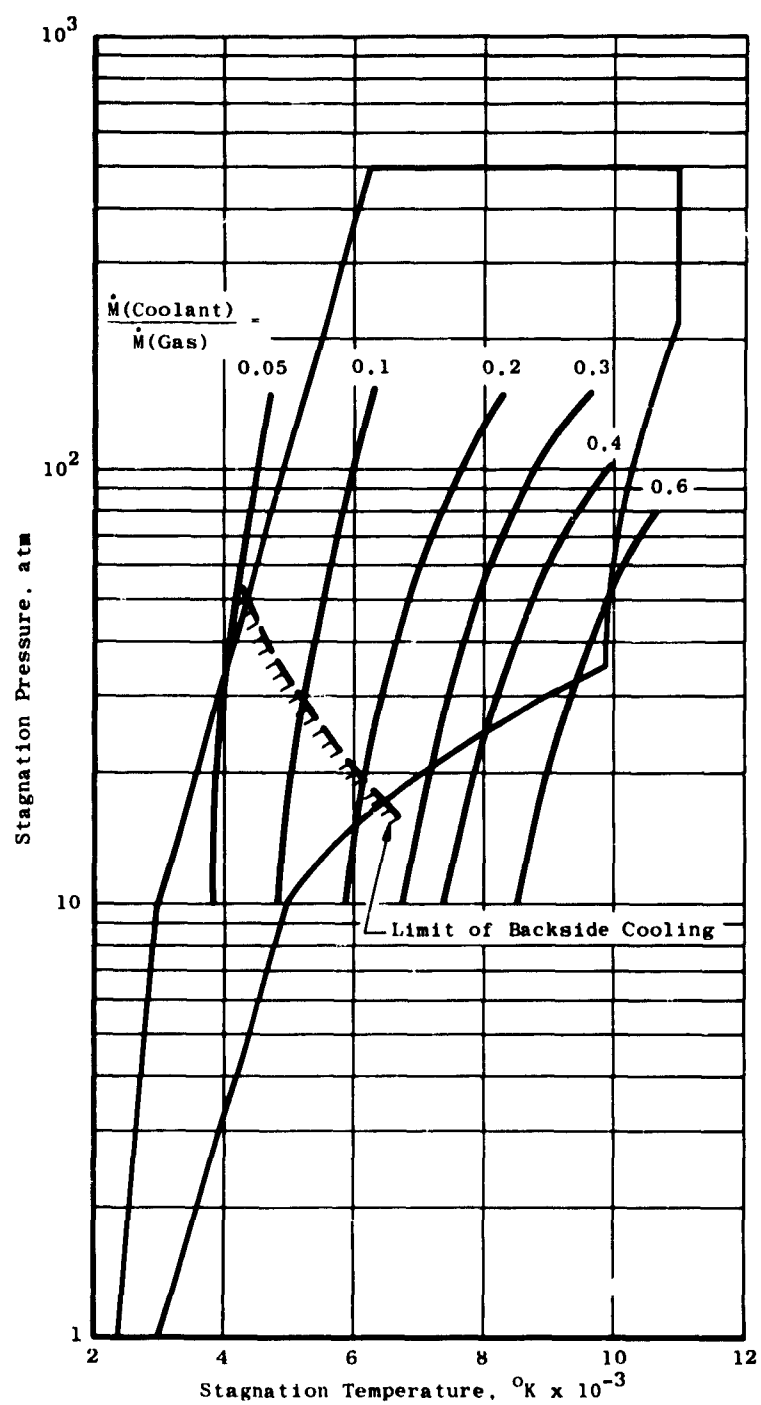


Fig. 16 Flow Ratios for Transpiration Cooling; Blocking Factor = 1.0;
 $D^* = 0.784''$

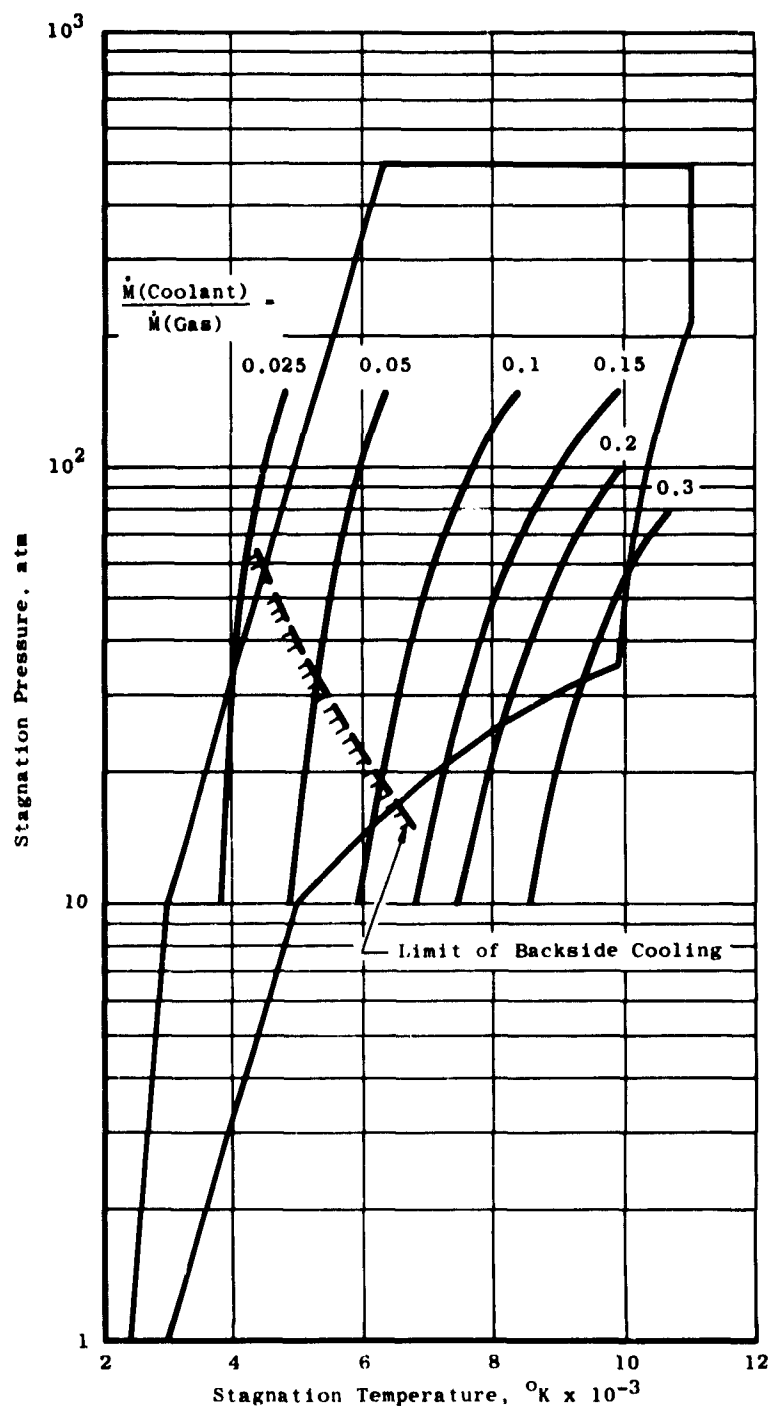


Fig. 17 Flow Ratios for Transpiration Cooling; Blocking Factor = 0.5;
 $D^* = 0.784''$

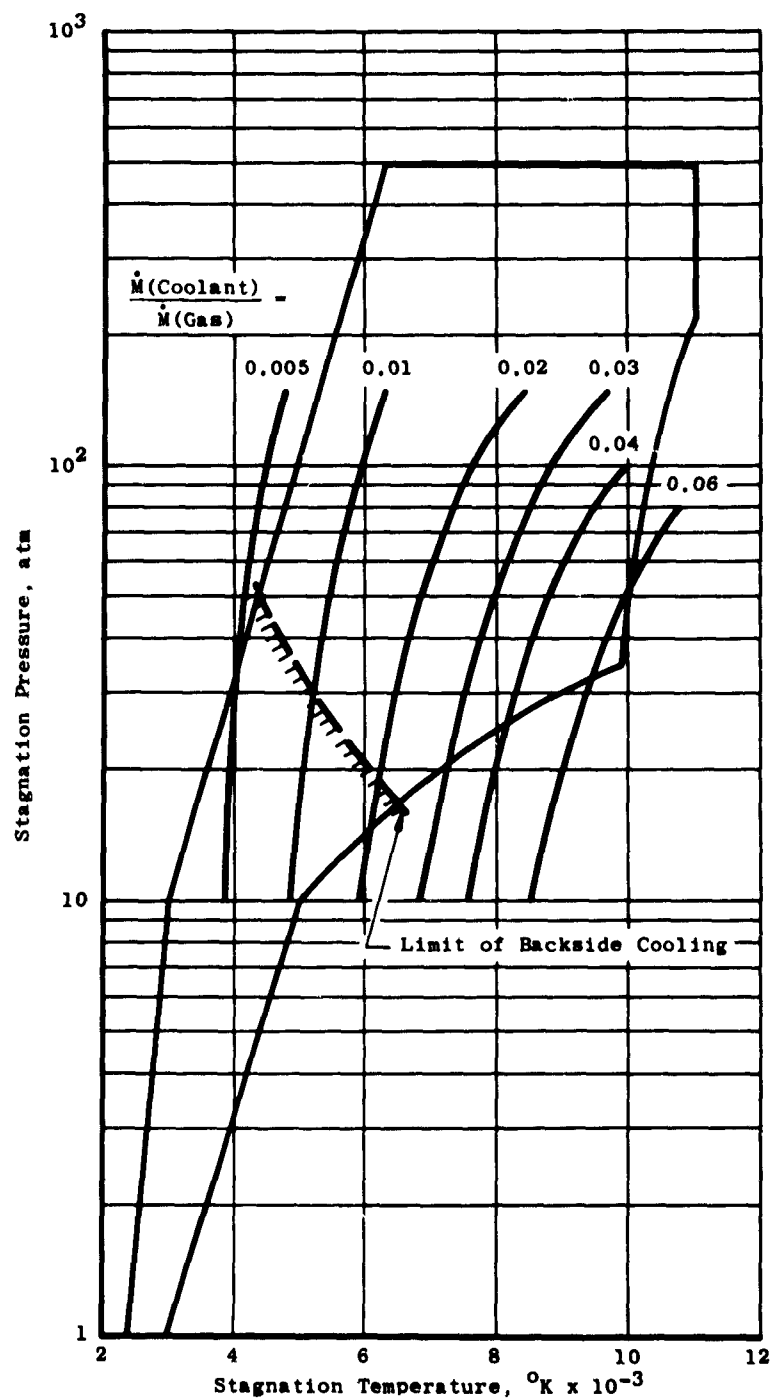


Fig. 18 Flow Ratios for Transpiration Cooling; Blocking Factor = 0.1;
 $D^* = 0.784''$

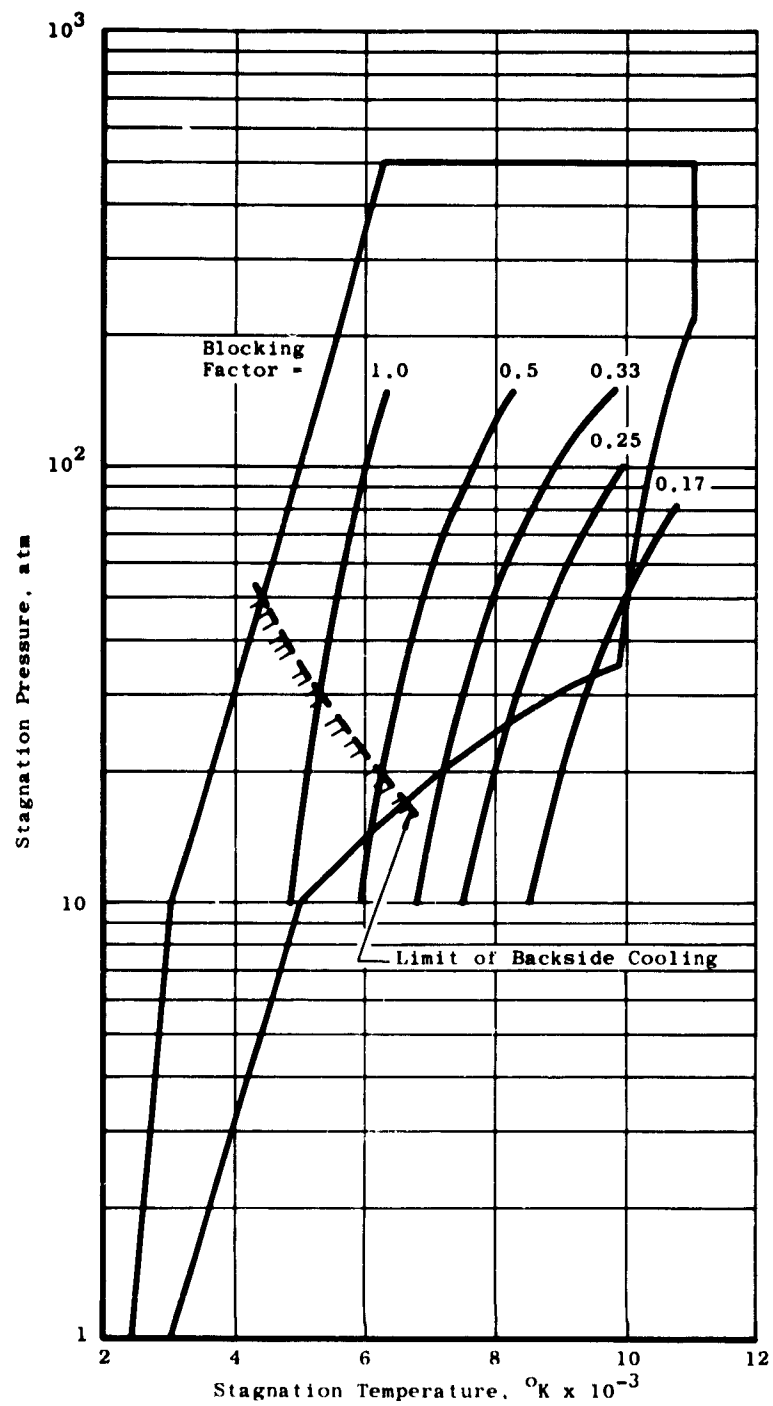


Fig. 19 Blocking Factors for Transpiration Cooling; $M(\text{coolant})/M(\text{gas}) = 0.1$; $D^* = 0.784''$

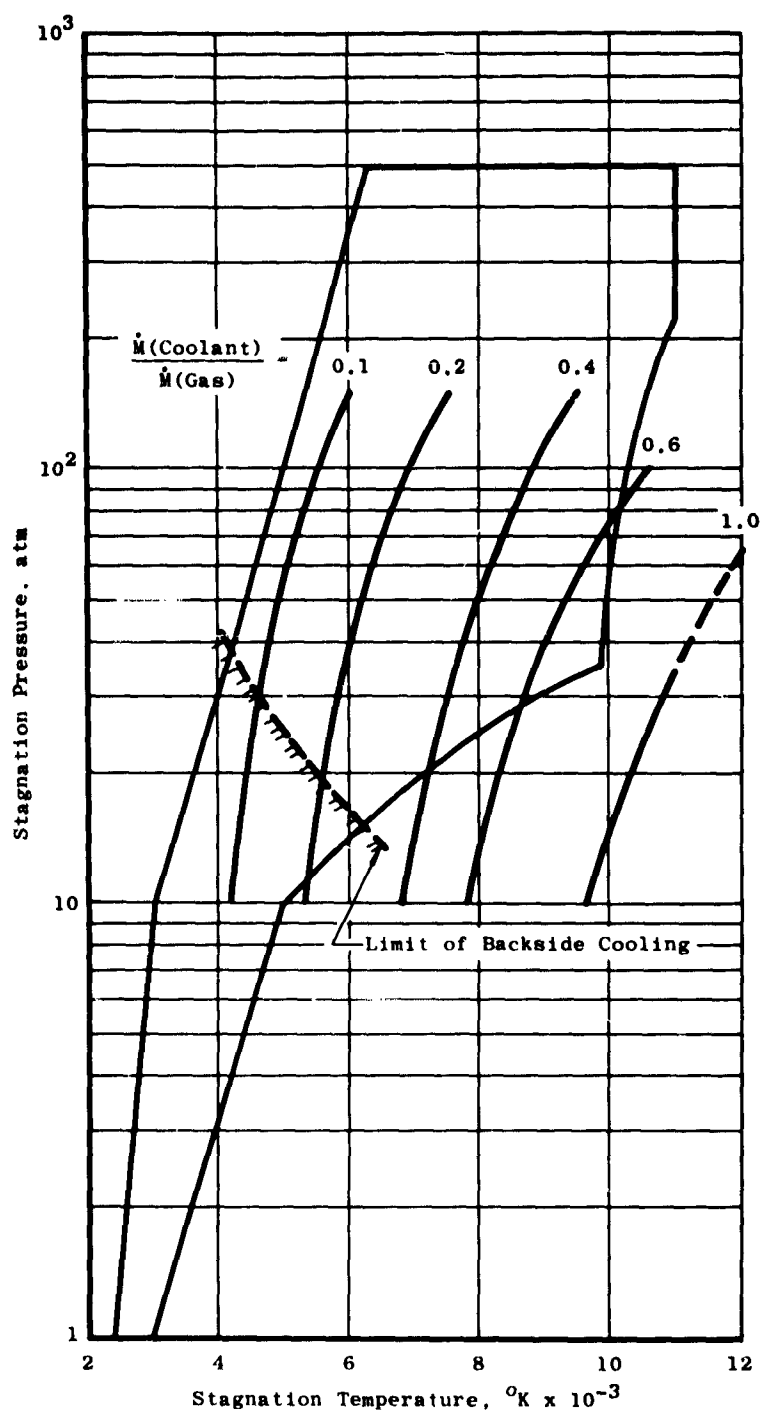


Fig. 20 Flow Ratios for Transpiration Cooling; Blocking Factor = 1.0;
 $D^* = 0.272''$

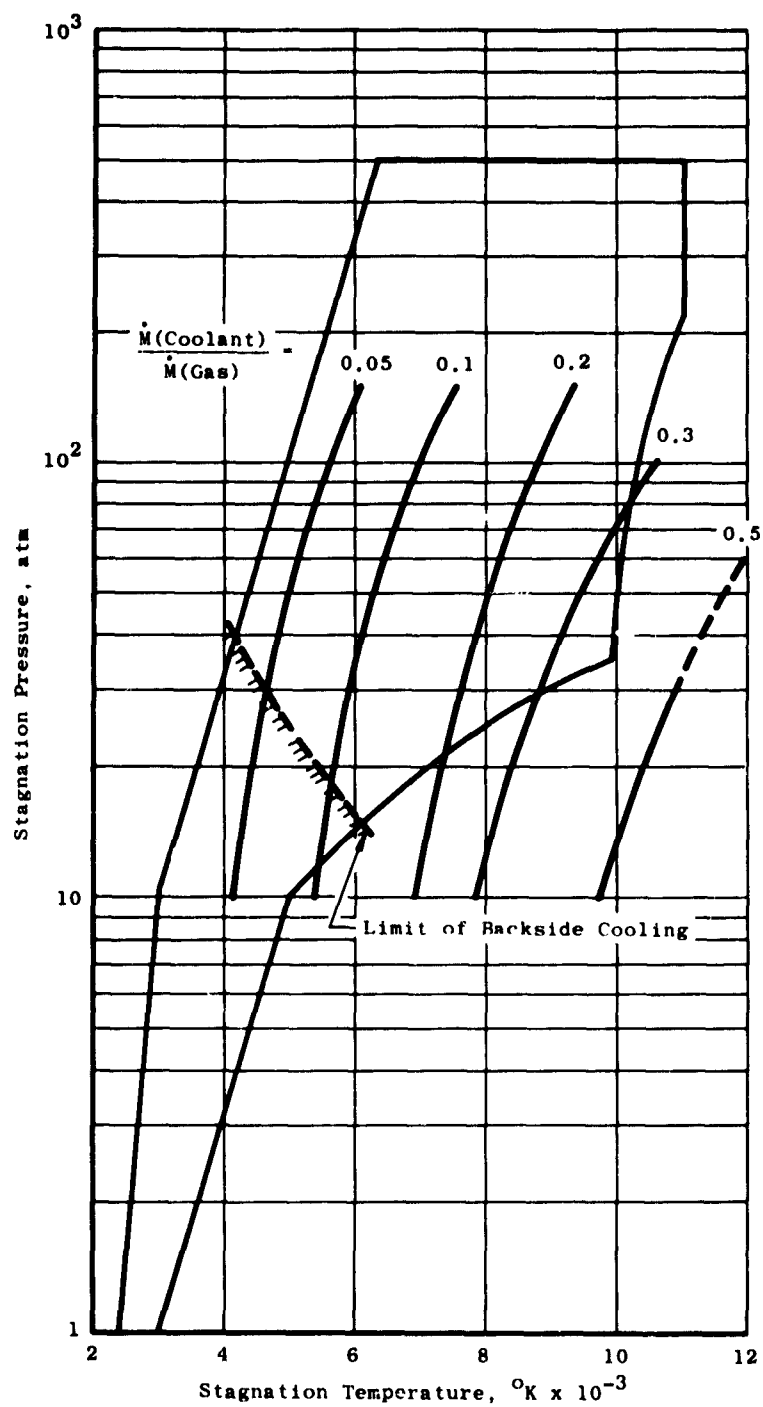


Fig. 21 Flow Ratios for Transpiration Cooling; Blocking Factor = 0.5;
 $D^* = 0.272''$

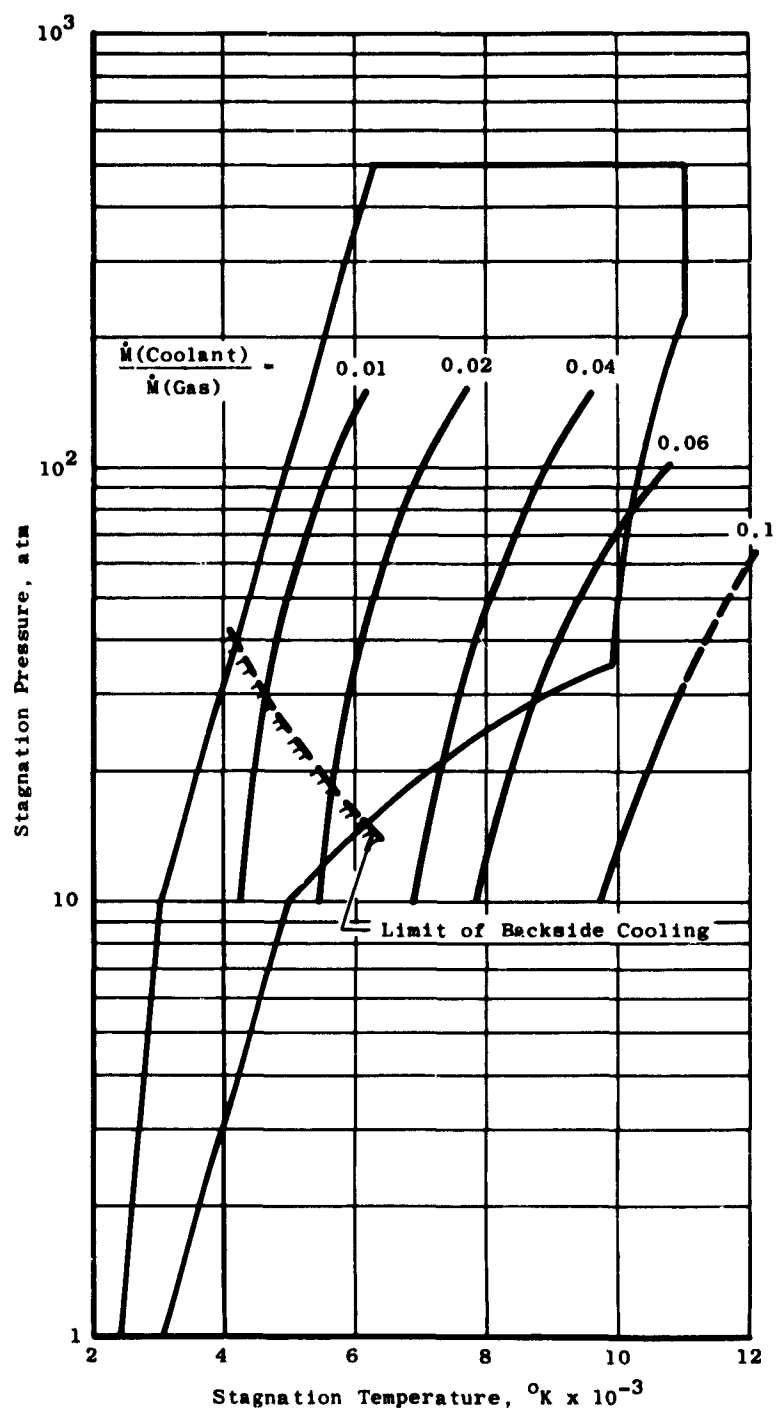


Fig. 22 Flow Ratios for Transpiration Cooling; Blocking Factor = 0.1;
 $D^* = 0.272''$

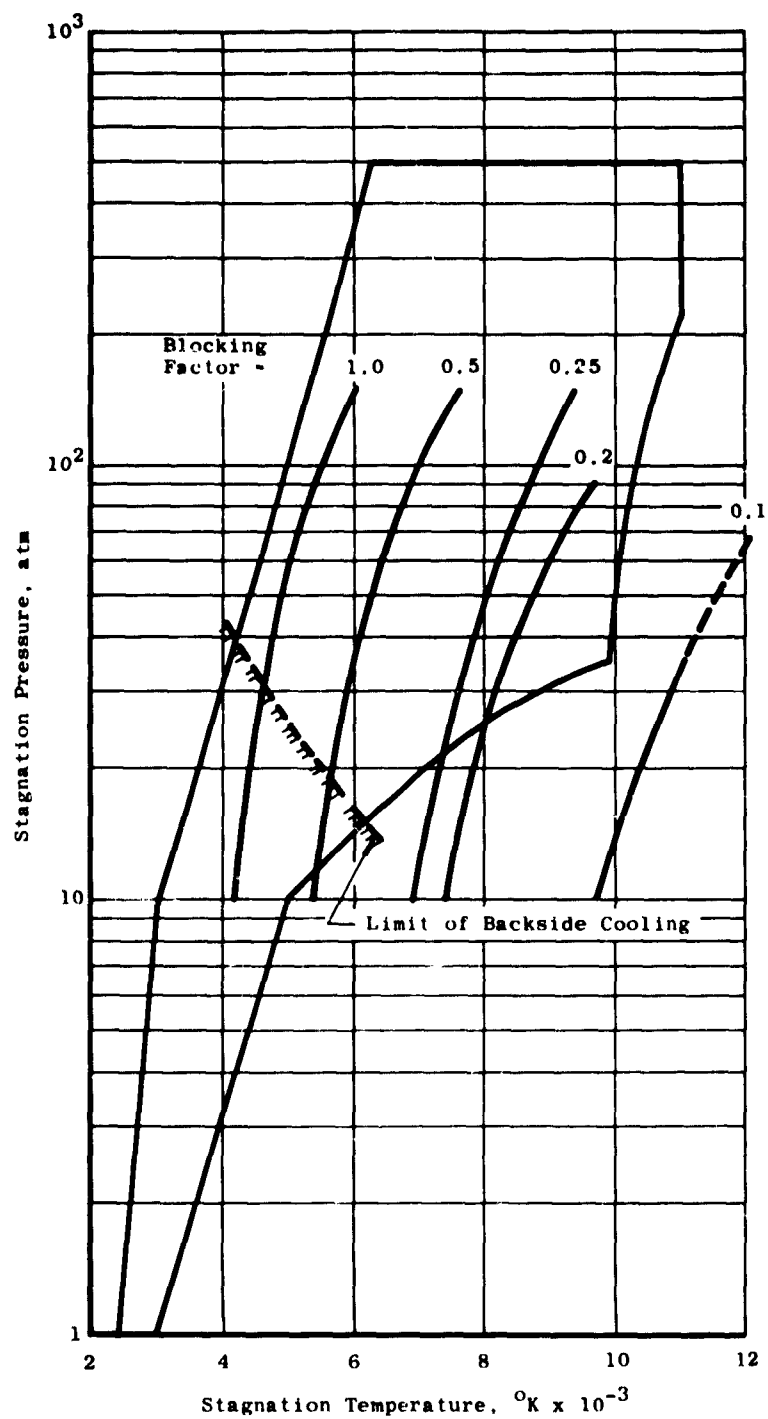


Fig. 23 Blocking Factors for Transpiration Cooling; $M(\text{coolant})/M(\text{gas}) = 0.1$; $D^* = 0.272''$

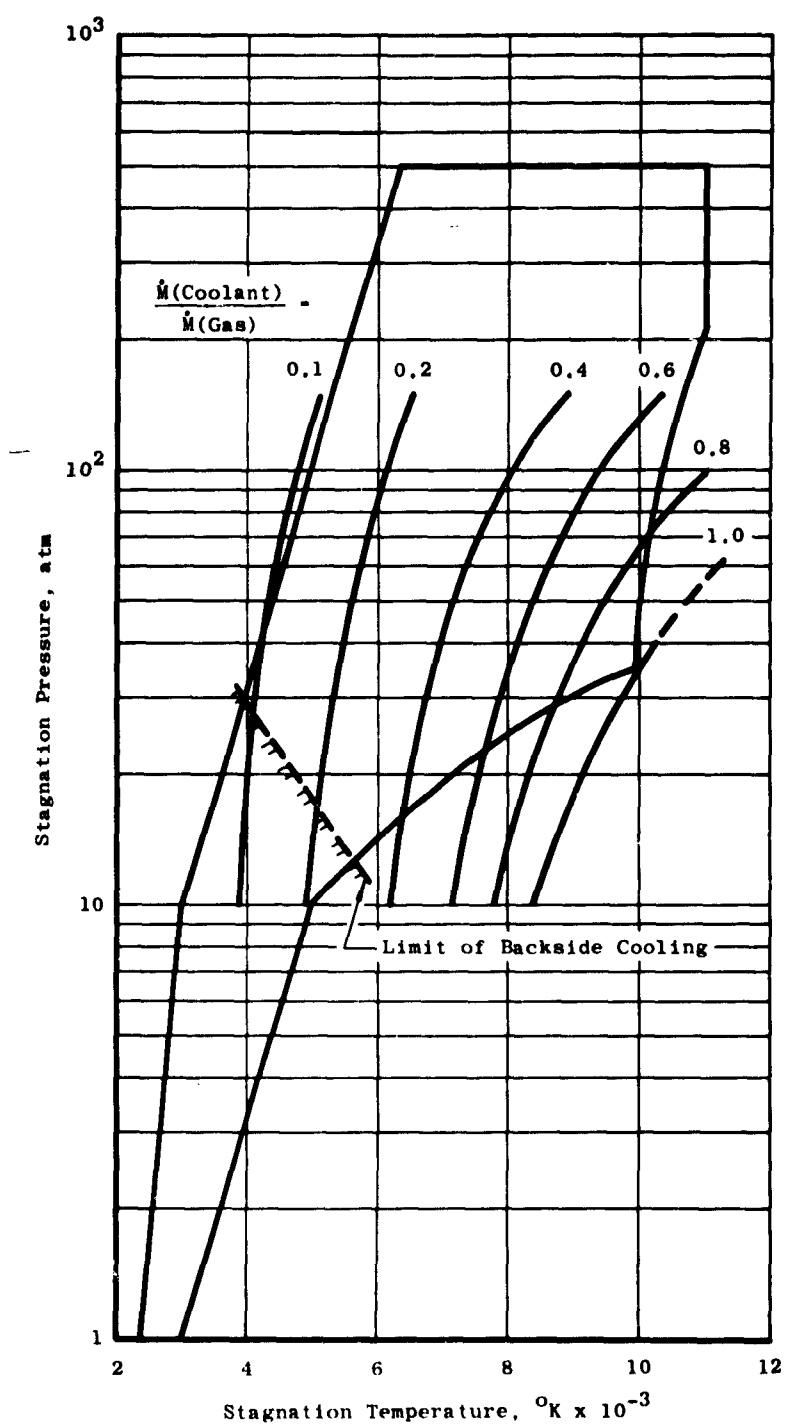


Fig. 24 Flow Ratios for Transpiration Cooling; Blocking Factor = 1.0;
 $D^* = 0.042''$

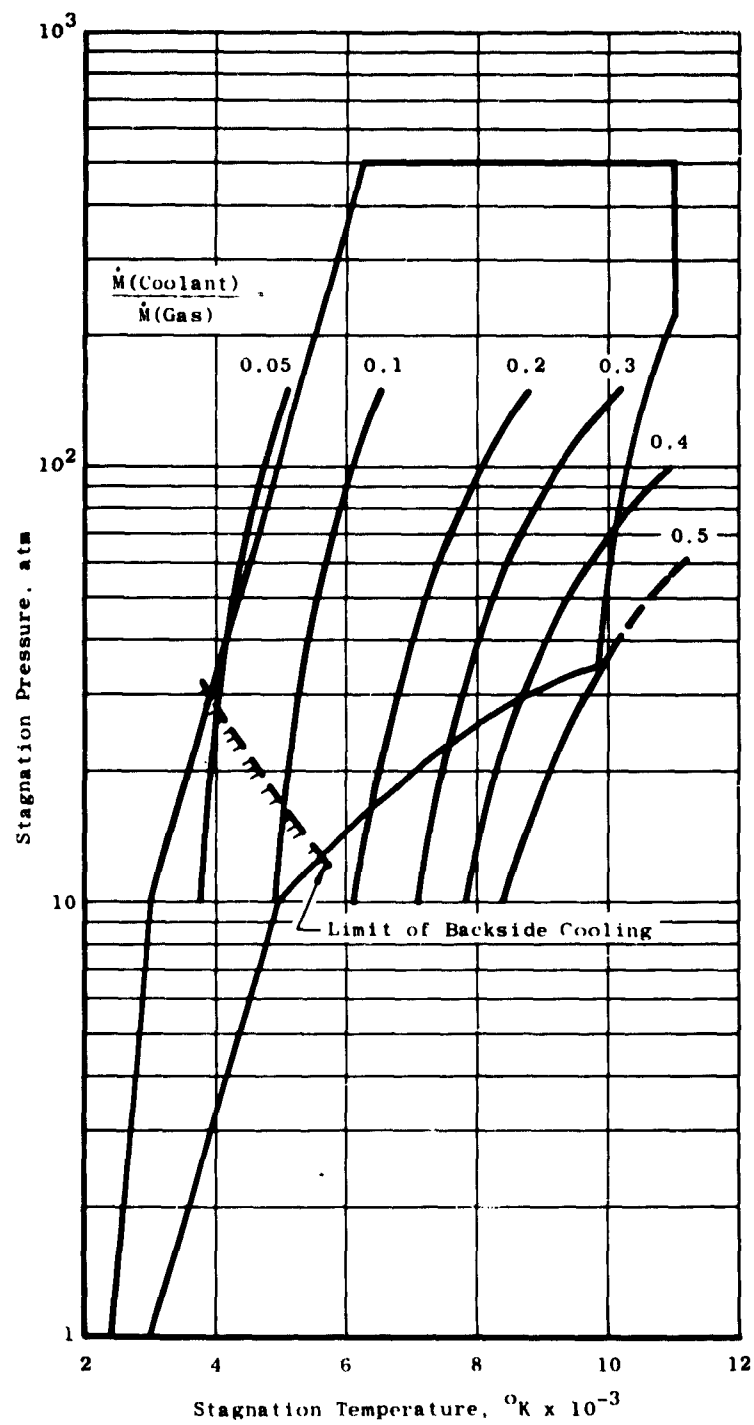


Fig. 25 Flow Ratios for Transpiration Cooling; Blocking Factor = 0.5;
 $D^* = 0.042''$

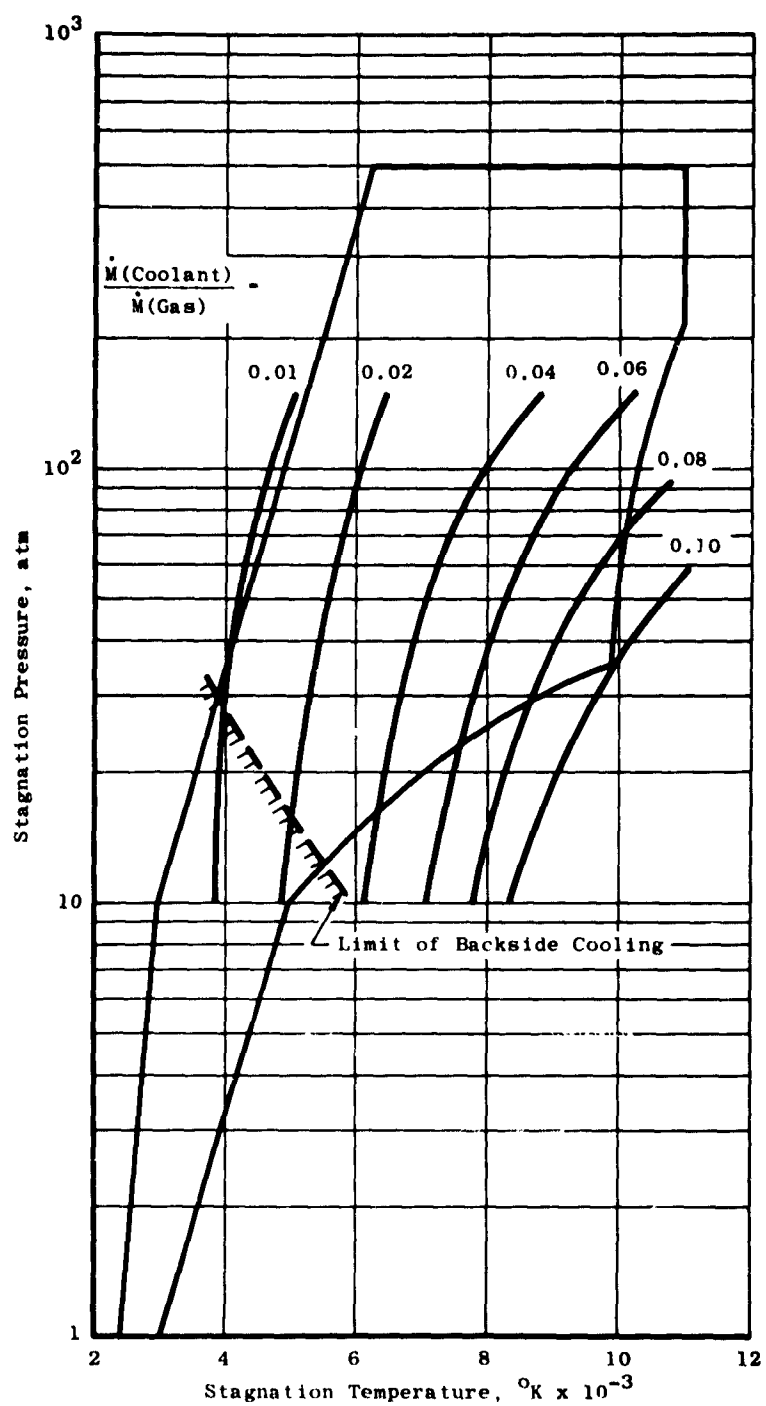


Fig. 26 Flow Ratios for Transpiration Cooling; Blocking Factor = 0.1;
 $D^* = 0.042''$

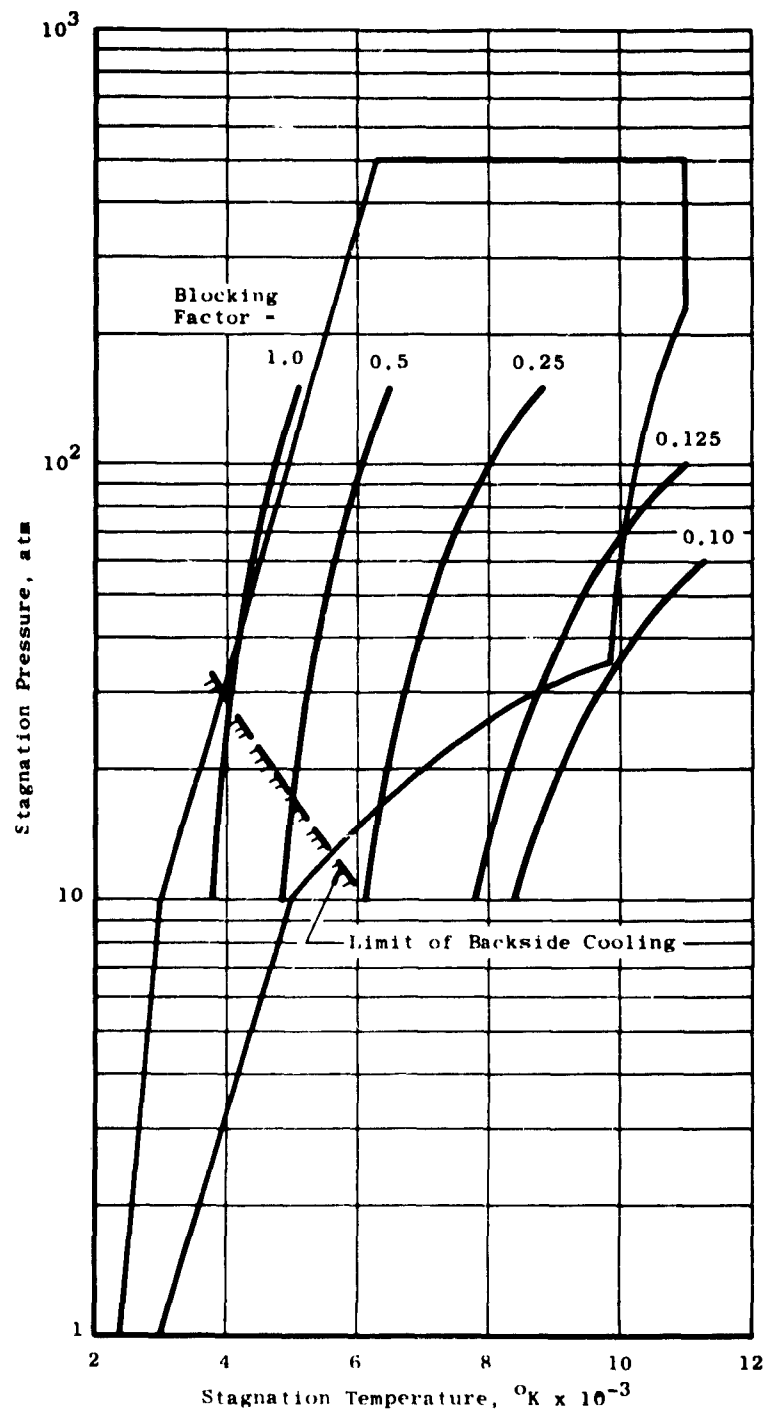


Fig. 27 Blocking Factors for Transpiration Cooling; $M(\text{coolant})/M(\text{gas}) = 0.1$;
 $D^* = 0.042''$

The magnitude of q_w^* is not necessarily determined by the available backside cooling, recall equation (23)

$$g_w = g_{wc} + \phi g_r$$

↓ (conservative approximation)

$$g_w^* = g_{wc}^* + \phi g_r(T^* p^* D^*) \quad (26)$$

The permissible values of q_{wc}^* are restricted to relatively low values because of the poor wall heat flux convective mechanisms which would exist in the coolant film. Stronger mechanisms within the film, i.e., turbulent exchanges, would most likely destroy the film. The removal of q_{wc}^* by backside cooling should improve the stability of the coolant film - the loss of which would certainly result in burnout. Also, under high radiation loads, q_w^* will comprise primarily ϕq_r which must be removed by backside cooling (film cooling only) because of the limited energy convection mechanisms which exist within the film. Without backside cooling, large radiative loads would raise the temperature of the nozzle walls until the film literally explodes away from the wall with subsequent burnout. It should be emphasized that transpiration cooling can handle all radiative and convective loads without backside cooling within the practical limits of pumping coolant through the porous walls and the compatibility of the ensuing coolant vapor with the plasma.

SUMMARY

The studies to date have demonstrated that either transpiration cooling or film cooling will extend the envelope of nozzle operation. However, it should be noted that the full extent of the new operating envelopes and the relative merits of the two concepts have not been fully established. Many questions are still unanswered - this information would be required for any nozzle design involving either concept. Problems requiring further study include:

- 1) determination of the blockage factors ψ_{trans} and ψ_{film}
- 2) backside cooling requirements using film cooling
- 3) mechanisms of handling the radiative load
- 4) interaction of the coolant vapor and plasma - special design problems
- 5) effect of injected coolant on nozzle dimensions
- 6) determination of the possible "burnout" conditions.

V. NOZZLE LINER STRESS ANALYSIS

There are three cases of interest in the stress analysis of a nozzle throat liner, namely, (1) an unrestrained liner (2) a partially restrained liner (3) a fully restrained liner.

By an unrestrained liner it is meant that the liner is mounted rigidly at one end to an entrance plenum or an exit expander but is not restrained by a sleeve or ribs. It is thus free to expand longitudinally and radially except for self restraint.

By a partially restrained liner it is meant that the liner is mounted rigidly at one or both ends and, in addition, it is restrained radially and possibly longitudinally also, by a surrounding sleeve. It is coupled to this sleeve by ribs between the liner and sleeve. The sleeve is thin enough that it expands some as the liner expands and thus the liner expansion is only partially restrained.

By a fully restrained liner it is meant that the radial and longitudinal expansion of the liner are completely constrained by the ribs, however, bending of the liner between ribs is possible. In the present analysis this case may then be studied by increasing the constraint in case (2) to the limit.

There are two fundamental areas of stress analysis, namely, elastic and plastic. Until a material is stressed past the yield point it is considered to follow Hooke's Law (stress proportional to strain), and the analysis for simple geometries is straight forward. When the yield point is passed the stresses are redistributed by yielding. The magnitude of the stress actually developed then depends on the stress-strain relationship of the material past the yield point. The problem, so far as the nozzle throat liner is concerned, is then one of determining if the yield point will be exceeded and if it will the number of cycles of operation before failure must be predicted.

To determine if the material will be stressed past the yield point for a given set of conditions the elastic analysis must be made. The stresses thus calculated are compared with some selected yield criterion to determine if yielding will occur.

For the elastic analysis the geometry was simplified somewhat. Except for the thrust load the liner and sleeve were considered to be concentric cylinders separated by a coolant annulus and ribs. The yield criterion selected was the critical octahedral shear stress (5).

In cases where the yield point of the material was exceeded the number of cycles to failure was predicted using the equation developed by Coffin (6):

$$N^{\frac{1}{2}} \epsilon_p = \text{Constant}$$

N = number of thermal cycles to failure
 ϵ_p = plastic yield, or plastic strain
 Const. = constant which varies from 0.25 - 0.75.

ELASTIC ANALYSIS

Case 1 - Unrestrained Liner

A thick walled cylinder is assumed in calculating hoop and thermal stresses in this analysis. The following general formulae for thick walled cylinders are available:

$$\sigma_T = \frac{a^2 p_i - b^2 p_o}{b^2 - a^2} + \frac{(p_i - p_o) a^2 b^2}{r^2 (b^2 - a^2)} \quad (27)$$

σ_T = tangential stress due to pressure (at inside or outside radius depending on choice of), psi
 a = inside radius, inches
 b = outside radius, inches
 p_i = inside pressure, psi
 p_o = outside pressure, psi
 $r = \begin{cases} a & \text{for } \sigma_T = \text{stress at inside radius} \\ b & \text{for } \sigma_T = \text{stress at outside radius} \end{cases}$

$$\sigma_{TT})_{r=a} = \frac{\alpha E \Delta T}{2(1-\mu) \ln \frac{b}{a}} \left(1 - \frac{2b^2}{b^2 - a^2} \ln \frac{b}{a} \right) \quad (28)$$

$$\sigma_{TT})_{r=b} = \frac{\alpha E \Delta T}{2(1-\mu) \ln \frac{b}{a}} \left(1 - \frac{2a^2}{b^2 - a^2} \ln \frac{b}{a} \right) \quad (29)$$

σ_{TT} = tangential thermal stress from self-restraint, psi
 α = thermal expansion coefficient, in/in °F
 μ = Poisson's ratio
 b = outside radius, inches
 a = inside radius, inches
 E = modulus of elasticity, psi
 ΔT = temperature difference across liner, °F.

Calculations of the airstream pressure variation along the nozzle axis show that the pressure remains almost constant until a very short distance from the minimum throat diameter. It then drops rapidly at this point and continues a gradual decrease in the expanding section. An approximate

thrust load on the nozzle may thus be calculated using the stagnation air pressure and the projected liner area in the direction of the axis.

Three end conditions for this case may be considered. In the first, the nozzle is fastened at the exit end and free to expand thermally at the entrance. In the second, the nozzle is fastened at the entrance and free to expand thermally at the exit. In the third condition, the nozzle is fastened at both ends and thus does not have free axial expansion. Since there must be smooth aerodynamic matching of the nozzle with the following expansion section in a wind tunnel, the second condition may be eliminated. Considering the third condition, it is noted that in the case of the smallest throat diameter, since the expansion forces must balance, there would be very high compressive stresses at the throat. This would be reduced some by bending, due to the geometry, but this would change the throat diameter and probably produce buckling at the small throat. For these reasons only condition one is analyzed.

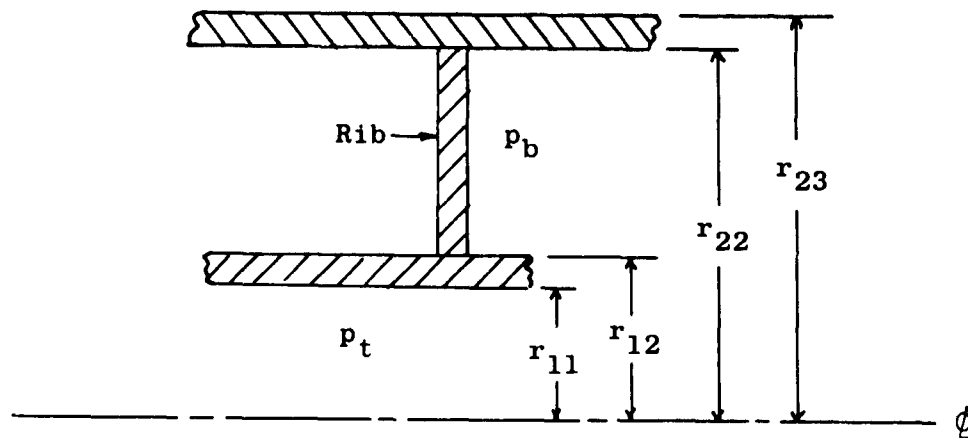


Fig. 28 Sketch of Liner, Rib, and Sleeve

(a) Compressive thrust stress at the throat (approximate):

$$\sigma_{PT} = - \frac{(P_t - P_b)(r_e^2 - r_{11}^2)}{(r_{12}^2 - r_{11}^2)} \quad (30)$$

P_t = airside pressure
 P_b = coolant pressure
 r_e = plenum inside radius
 r_{11} = throat inside radius
 r_{12} = throat outside radius

(b) The hoop stresses are given by:

$$\sigma_{H11} = \frac{r_{11}^2 P_t - r_{12}^2 P_b}{r_{12}^2 - r_{11}^2} + \frac{(P_t - P_b) r_{11}^2 r_{12}^2}{r_{11}^2 (r_{12}^2 - r_{11}^2)} \quad (31)$$

(Note that subscript 11 refers to position at the inside radius and 12 at the outside radius; t refers to the airside and b refers to the coolant side. See Figure 28).

$$\sigma_{H12} = \frac{r_{11}^2 P_t - r_{12}^2 P_b}{r_{12}^2 - r_{11}^2} + \frac{(P_t - P_b) r_{11}^2 r_{12}^2}{r_{12}^2 (r_{12}^2 - r_{11}^2)} \quad (32)$$

$$\text{letting } Z_1 = \frac{r_{11}^2 + r_{12}^2}{r_{12}^2 - r_{11}^2} \quad (33)$$

$$\text{and } Z_2 = \frac{r_{12}^2}{r_{12}^2 - r_{11}^2} \quad (34)$$

$$Z_3 = \frac{r_{11}^2}{r_{12}^2 - r_{11}^2} \quad (35)$$

$$\text{then } \sigma_{H11} = Z_1 P_t - Z_2 Z_3 P_b \quad (36)$$

$$\text{and } \sigma_{H12} = 2Z_3 p_e - Z_1 p_b \quad (37)$$

(c) Thermal stresses due to self-restraint are given by:

$$\sigma_{TH11} = \frac{\alpha E \Delta T}{2(1-\mu) \ln \frac{r_{12}}{r_{11}}} \left(1 - 2Z_2 \ln \frac{r_{12}}{r_{11}} \right) \quad (38)$$

$$\sigma_{TH12} = \frac{\alpha E \Delta T}{2(1-\mu) \ln \frac{r_{12}}{r_{11}}} \left(1 - 2Z_3 \ln \frac{r_{12}}{r_{11}} \right) \quad (39)$$

(These apply both longitudinally and tangentially).

(d) Radial pressure stresses on the airside and backside are:

$$\sigma_{R11} = -p_e \quad (40)$$

$$\sigma_{R12} = -p_b \quad (41)$$

The summation of the appropriate stresses from above gives the principle stresses at the inside and outside of the liner.

(e) The principle tangential stresses are:

Inside radius -

$$\sigma_{PC11} = Z_1 p_e - 2Z_2 p_b + \frac{\alpha E \Delta T}{2(1-\mu) \ln \frac{r_{12}}{r_{11}}} \left(1 - 2Z_2 \ln \frac{r_{12}}{r_{11}} \right) \quad (42)$$

Outside radius -

$$\sigma_{PC12} = 2Z_3 p_e - Z_1 p_b + \frac{\alpha E \Delta T}{2(1-\mu) \ln \frac{r_{12}}{r_{11}}} \left(1 - 2Z_3 \ln \frac{r_{12}}{r_{11}} \right) \quad (43)$$

(f) The principle longitudinal stresses are:

Inside radius -

$$\sigma_{PL11} = \frac{-(P_i - P_o)(r_o^2 - r_{11}^2)}{(r_{12}^2 - r_{11}^2)} + \frac{\alpha E \Delta T}{2(1-\mu) \ln \frac{r_{12}}{r_{11}}} (1 - 2z_2 \ln \frac{r_{12}}{r_{11}}) \quad (44)$$

Outside radius -

$$\sigma_{PL12} = \frac{-(P_i - P_o)(r_o^2 - r_{11}^2)}{(r_{12}^2 - r_{11}^2)} + \frac{\alpha E \Delta T}{2(1-\mu) \ln \frac{r_{12}}{r_{11}}} (1 - 2z_3 \ln \frac{r_{12}}{r_{11}}) \quad (45)$$

(g) The principle radial stresses are:

Inside radius -

$$\sigma_{PR11} = -P_i \quad (46)$$

Outside radius

$$\sigma_{PR12} = -P_o \quad (47)$$

The octahedral shear stresses are then calculated using the general formula:

$$\sigma_{oct} = \frac{1}{3} \left[(\sigma_1 - \sigma_2)^2 + (\sigma_2 - \sigma_3)^2 + (\sigma_1 - \sigma_3)^2 \right]^{1/2} \quad (49)$$

where $\sigma_1, \sigma_2, \sigma_3$ are the principle stresses at the point considered.

Case 2 - Partially Restrained Liner - Longitudinal Ribs

As in Case 1, it is assumed that the liner and the surrounding sleeve are thick walled cylinders in this case for restraint by longitudinal ribs.

For restraint by circumferential ribs it is assumed the liner is a thin walled cylinder, as the solution for this case was readily available and the approximation is good except at very small liner diameters.

The same notation is used in this case as in Case 1. When new terms are introduced they are defined. As in Case 1, the formulae for hoop and thermal stresses for thick walled cylinders (equations 27, 28, and 29) are used.

(a) For calculation of liner and sleeve tangential stresses assume a pseudo-pressure P_1 between the ribs and the liner and P_2 between the ribs and the sleeve

$$P_2 = P_1 \left(\frac{r_{12}}{r_{22}} \right) \quad (50)$$

P_2 and P_1 are thus equivalent uniformly distributed loads. (Subscript 22 refers to the inside of the sleeve).

$$2\delta_{12} \pi r_{12} = 2\delta_{22} \pi r_{22} \quad (51)$$

$$\therefore \frac{\delta_{12}}{\delta_{22}} = \frac{r_{22}}{r_{12}} \quad (52)$$

δ_{12} = unit strain of outside of liner, in/in
 δ_{22} = unit strain of inside of sleeve, in/in

$$\text{Since} \quad \delta = \frac{\sigma}{E} \quad (53)$$

$$\frac{\sigma_{H12}}{\sigma_{H22}} = \frac{r_{22} E_1}{r_{12} E_2} \quad (54)$$

(Subscript 1 refers to the liner, 2 to the sleeve).

$$\text{now } \sigma_{H11} = \frac{r_{11}^2 P_1 - (P_0 + P_1) r_{12}^2}{r_{12}^2 - r_{11}^2} + \frac{[P_1 - (P_0 + P_1)] r_{12}^2}{r_{12}^2 - r_{11}^2} \quad (55)$$

$$\sigma_{H11} = \left(\frac{r_{11}^2 + r_{12}^2}{r_{12}^2 - r_{11}^2} \right) P_t - 2 \left(\frac{r_{12}^2}{r_{12}^2 - r_{11}^2} \right) (P_b + P_i) \quad (56)$$

$$\sigma_{H11} = z_1 P_t - 2 z_2 (P_b + P_i) \quad (57)$$

In the same manner

$$\sigma_{H12} = 2 z_3 P_t - z_1 (P_b + P_i) \quad (58)$$

Since the outside pressure (gauge) on the sleeve is zero

$$\sigma_{H22} = \frac{(r_{23}^2 + r_{22}^2)}{(r_{23}^2 - r_{22}^2)} (P_b + P_i) \quad (59)$$

where r_{23} = outside sleeve radius

Letting $z_4 = \frac{r_{23}^2 + r_{22}^2}{r_{23}^2 - r_{22}^2}$ and substituting from equation (50)

$$\sigma_{H22} = z_4 (P_b + P_i \frac{r_{12}}{r_{22}}) \quad (60)$$

Substituting from equation (54)

$$\sigma_{H12} \frac{E_2 r_{12}}{E_1 r_{22}} = z_4 P_b + z_4 P_i \frac{r_{12}}{r_{22}} \quad (61)$$

Equating σ_{12} 's in equations (58) and (59)

$$2 z_3 P_t - z_1 (P_b + P_i) = \frac{z_4 E_1 r_{22}}{E_2 r_{12}} P_b + \frac{z_4 E_1}{E_2} P_i \quad (62)$$

Solving for P_i

$$P_i = \frac{2 z_3 P_t - P_b (z_1 + z_4 \frac{E_1 r_{22}}{E_2 r_{12}})}{z_1 + z_4 \frac{E_1}{E_2}} \quad (63)$$

substituting from equation (50)

$$P_2 = \frac{2 z_3 \frac{r_{12}}{r_{22}} P_4 - P_5 \frac{r_{12}}{r_{22}} \left(z_1 + z_4 \frac{E_1 r_{22}}{E_2 r_{12}} \right)}{z_1 + z_4 \frac{E_1}{E_2}} \quad (64)$$

Substitutions into equations (57), (58) and (60) give σ_{11} , σ_{12} , σ_{22} respectively.

(b) The hoop and longitudinal thermal stresses, due to self-restraint, are:

$$\sigma_{TH11} = \frac{\alpha E \Delta T}{2(1-\mu) \ln \frac{r_{12}}{r_{22}}} \left(1 - 2 z_2 \ln \frac{r_{12}}{r_{11}} \right) \quad (65)$$

$$\sigma_{TH12} = \frac{\alpha E \Delta T}{2(1-\mu) \ln \frac{r_{12}}{r_{22}}} \left(1 - 2 z_3 \ln \frac{r_{12}}{r_{11}} \right) \quad (66)$$

(c) The hoop stresses in (b) above are modified by the force between the liner and the ribs caused by the thermal expansion of the liner. Assuming pseudo-pressures P_4 between the ribs and liner and P_5 between the ribs and sleeve

$$\sigma_{NT11} = \sigma_{TH11} - 2 z_2 P_4 \quad (67)$$

$$\sigma_{NT12} = \sigma_{TH12} - z_1 P_4 \quad (68)$$

$$\sigma_{NT22} = z_4 P_5 \quad (69)$$

$\sigma_{NT} \equiv$ net thermal hoop stress

Since

$$P_5 = P_4 \frac{r_{12}}{r_{22}} \quad (70)$$

$$\sigma_{NT22} = z_4 P_4 \frac{r_{12}}{r_{22}} \quad (71)$$

but

$$\sigma_{NT22} = \sigma_{NT12} \frac{E_2 r_{12}}{E_1 r_{22}} \quad (72)$$

Substituting from equations (65), (66) and (68)

$$\sigma_{TH12} \left(\frac{E_2 r_{12}}{E_1 r_{22}} \right) - z_1 P_4 \left(\frac{E_2 r_{12}}{E_1 r_{22}} \right) = z_4 P_4 \left(\frac{r_{12}}{r_{22}} \right) \quad (73)$$

Solving for P_4

$$P_4 = \frac{\sigma_{TH12}}{\left(z_1 + z_4 \frac{E_1}{E_2} \right)} \quad (74)$$

Substituting from equation (74) into equations (67), (68) and (71)

$$\sigma_{NT11} = \sigma_{TH11} - 2z_2 \left(\frac{\sigma_{TH12}}{z_1 + z_4 \frac{E_1}{E_2}} \right) \quad (75)$$

$$\sigma_{NT12} = \sigma_{TH12} \left(1 - \frac{z_1}{z_1 + z_4 \frac{E_1}{E_2}} \right) \quad (76)$$

$$\sigma_{NT22} = \sigma_{TH12} \left(\frac{z_4 \frac{r_{12}}{r_{22}}}{z_1 + z_4 \frac{E_1}{E_2}} \right) \quad (77)$$

(d) Beam stresses are calculated from the general formulae:

(1) Over a rib

$$\sigma_B = \pm \frac{\Delta P}{2} \left(\frac{L}{t} \right)^2 \quad (78)$$

σ_B = bending tensile stress, psi
 ΔP = load per unit area, psi
 L = distance between supports, inches
 t = beam depth, inches

(2) Midway between ribs

$$\sigma_B = \pm \frac{\Delta P}{4} \left(\frac{L}{t} \right)^2 \quad (79)$$

in this case $\Delta P_L = P_1 + P_4$ (for liner) (80)

$$\Delta P_S = P_2 + P_5 \quad (\text{for sleeve}) \quad (81)$$

then inside the liner over a rib

$$\sigma_{B11} = \left(\frac{P_1 + P_4}{2} \right) \left(\frac{D_r}{r_{12} - r_{11}} \right)^2 \quad (82)$$

D_r = distance between ribs, inches

outside the liner over a rib

$$\sigma_{B121} = - \left(\frac{P_1 + P_4}{2} \right) \left(\frac{D_r}{r_{12} - r_{11}} \right)^2 \quad (83)$$

inside the liner midway between ribs

$$\sigma_{B112} = - \left(\frac{P_1 + P_4}{4} \right) \left(\frac{D_r}{r_{12} - r_{11}} \right)^2 \quad (84)$$

outside liner between ribs

$$\sigma_{B122} = \left(\frac{P_1 + P_4}{4} \right) \left(\frac{D_r}{r_{12} - r_{11}} \right)^2 \quad (85)$$

(e) The radial pressure stresses at the inside and outside of the liner are:

(1) Over a rib, inside and outside respectively

$$\sigma_{R11} = -P_t \quad (86)$$

$$\sigma_{R12} = -\left(P_t + P_s\right)\left(\frac{D_r}{t_r}\right) \quad (87)$$

t_r = rib circumferential thickness, inches

(2) Between ribs, inside and outside respectively

$$\sigma_{R12} = -P_t \quad (88)$$

$$\sigma_{R12} = -P_b \quad (89)$$

(f) If the liner is constrained longitudinally by the sleeve a uniform compressive stress will be introduced in the liner. In this case:

$$\delta_1 = \delta_2 \quad (90)$$

$$\text{now } \delta_1 = \alpha_1 \Delta T_m + \frac{\sigma_{TL1}}{E_1} \quad (91)$$

ΔT_m = rise in liner mean temperature

$$\delta_2 = \frac{\sigma_{TL2}}{E_2} \quad (92)$$

from a force balance

$$\pi(r_{23}^2 - r_{22}^2)\sigma_{TL2} = -\pi(r_{12}^2 - r_{11}^2)\sigma_{TL1} \quad (93)$$

from equations (90), (91) and (92)

$$\sigma_{TL1} = -\alpha_1 \Delta T_m E_1 + \sigma_{TL2} \frac{E_1}{E_2} \quad (94)$$

substituting for σ_{TL2} from equation (93)

$$\sigma_{TL1} = -\alpha_1 \Delta T_m E_1 - \sigma_{TL1} \frac{E_1}{E_2} \left(\frac{r_{12}^2 - r_{11}^2}{r_{23}^2 - r_{22}^2} \right) \quad (95)$$

$$\text{let} \quad z_s = \frac{r_{12}^2 - r_{11}^2}{r_{23}^2 - r_{22}^2} \quad (96)$$

solving for σ_{TL1} in equation (95)

$$\sigma_{TL1} = - \frac{\alpha_1 \Delta T_m E_1}{1 + z_s \frac{E_1}{E_2}} \quad (97)$$

substituting into equation (93)

$$\sigma_{TL2} = \frac{\alpha_1 \Delta T_m E_1 z_s}{1 + z_s \frac{E_1}{E_2}} \quad (98)$$

(g) The principle tangential stresses are:

(1) At the inside radius over a rib

$$\sigma_{PC111} = \sigma_{H11} + \sigma_{NT11} + \sigma_{B111} \quad (99)$$

(2) At the outside radius over a rib

$$\sigma_{PC121} = \sigma_{H12} + \sigma_{NT12} + \sigma_{B121} \quad (100)$$

(3) At the inside radius between ribs

$$\sigma_{PC112} = \sigma_{H11} + \sigma_{NT11} + \sigma_{B112} \quad (101)$$

(4) At the outside radius between ribs

$$\sigma_{PC122} = \sigma_{H12} + \sigma_{NT12} + \sigma_{B122} \quad (102)$$

(h) The principle longitudinal stresses are:

(1) At the inside radius

$$\sigma_{PL11} = \sigma_{TL1} + \sigma_{TH11} \quad (103)$$

(2) At the outside radius

$$\sigma_{PL12} = \sigma_{TL1} + \sigma_{TH12} \quad (104)$$

(i) The principle radial stresses are given in (e).

Case 2 - Partially Restrained Liner - Circumferential Ribs

The stresses for circumferential ribs were first analyzed using the pseudo-pressure method used for longitudinal ribs. A more exact analysis is that of Timoshenko (5) for an infinite cylinder with circumferential restraining bands. This latter analysis was used for the final calculations and is presented below. It assumes a thin walled cylinder.

(a) Bending stresses at ribs and midway between ribs must be calculated. When a distributed radial force is applied around a line on a cylinder the resistance to bending is analogous to that of a beam on an elastic foundation. The differential equation for the deflection of the strip is

$$D \frac{d^4 y}{dx^4} = - \frac{Et}{r^2} y \quad (105)$$

where $D = \frac{Et^3}{12(1-\mu^2)}$ the flexural rigidity of the wall, lb/in

(106)

t = wall thickness, inches
 r = cylinder mean radius, inches
 y = deflection from initial position, inches
 x = distance along a line in the surface parallel to the axis of the cylinder, inches

Defining

$$B \equiv \left(\frac{Et}{4Dr^2} \right)^{1/4} = \left(\frac{3-3\mu^2}{r^2 t^2} \right)^{1/4} \quad (107)$$

the general solution of equation (105) is

$$y = e^{Bx} (A \cos Bx + C \sin Bx) + e^{-Bx} (E \cos Bx + F \sin Bx) \quad (108)$$

A, C, E, and F are constants to be determined from known deflections, slopes, etc. at various values of x .

For the case of a single concentrated load P lb. acting at $x = 0$ on a beam of unit width and thickness t inches (part of the cylinder of radius r),

$$y = \frac{PBr^2}{2Et} e^{-Bx} (\cos Bx + \sin Bx) \quad (109)$$

$$M = -\frac{P}{4B} e^{-Bx} (\sin Bx - \cos Bx) \quad (110)$$

where M = bending moment (lb in)

Now

$$\sigma_B = \pm \frac{6M}{t^2} \quad (111)$$

thus

$$\sigma_B = \pm \frac{3}{2} \frac{P}{Bt^2} e^{-Bx} (\sin Bx - \cos Bx) \quad (112)$$

(When $x = 0$ the quantity in brackets is negative, so the positive sign gives the stress at the outside of the cylinder).

Since the general differential equation is linear the bending moment for multiple loads may be calculated by the principle of superposition, and thus, the stresses may be calculated by superposition. It is necessary to take only a few loads to get the approximate result for an infinite beam, as the terms become essentially negligible after $Bx \approx 7.0$.

The general solution for the bending stresses may now be written as an infinite series using equation (112)

$$\sigma_B \Big|_{x=0} = \pm \frac{3}{2 B t^2} \sum_{n=-\infty}^{\infty} \left[P_n e^{-B|x_n|} (\sin B|x_n| - \cos B|x_n|) \right] \quad (113)$$

The terms for negative n are the loads and their distances on one side of the point chosen as $x = 0$ for the stress calculation. The terms for positive n are the loads and distances on the other side. For $n = 0$, $x = 0$, P_0 is the load at $x = 0$. The absolute value signs apply to x since it can be shown from the general equation, equation (108), that the contribution from a load P_1 at a distance x_1 on one side of $x = 0$ is the same in sign and magnitude as that of the same load at the same distance on the other side of $x = 0$.

The deflection may also be written as an infinite series using the same notation

$$y = \frac{B r^2}{2 E t} \sum_{n=-\infty}^{\infty} \left[P_n e^{-B|x_n|} (\sin B|x_n| + \cos B|x_n|) \right] \quad (114)$$

Equation (114) is used to calculate the force P at each rib.

First assume all the ribs are the same, so $P_n = \text{Const.} = P$. Then

$$y = \frac{P B r^2}{2 E t} \sum_{n=-\infty}^{\infty} e^{-B|x_n|} (\sin B|x_n| + \cos B|x_n|) \quad (115)$$

The radial expansion of the liner due to pressure and increase in mean temperature (unrestrained) is

$$\Delta r = \frac{(P_i - P_o)r^2}{Et} + r\alpha \Delta T_m \quad (116)$$

A rib with cross sectional area A_r and modulus of elasticity E_r is increased in radius by a force P (lb/inch of circumference) an amount

$$\Delta r_r = \frac{Pr^2}{A_r E_r} \quad (117)$$

Then the deflection of the cylinder is

$$y = \frac{(P_i - P_o)r^2}{Et} + r\alpha \Delta T_m - \frac{Pr^2}{A_r E_r} \quad (118)$$

Using equations (115) and (118), and letting $E_r = E_1$,

$$\frac{PBr^2}{2E_1 t} \sum_{n=-\infty}^{\infty} e^{-B|x_n|} (\sin B|x_n| + \cos B|x_n|) = \frac{(P_i - P_o)r^2}{E_1 t} + r\alpha \Delta T_m - \frac{Pr^2}{A_r E_1} \quad (119)$$

solving for P

$$P = \frac{\frac{(P_i - P_o)r^2}{E_1 t} + r\alpha \Delta T_m}{\frac{Br^2}{2E_1 t} \sum_{n=-\infty}^{\infty} [e^{-B|x_n|} (\sin B|x_n| + \cos B|x_n|)] + \frac{r^2}{A_r E_1}} \quad (120)$$

Multiplying numerator and denominator in equation (120) by $\frac{E_1 t}{r^2}$

$$P = \frac{(P_i - P_o) + \frac{\alpha \Delta T_m E_1 t}{r}}{\frac{B}{2} \sum_{n=-\infty}^{\infty} [e^{-B|x_n|} (\sin B|x_n| + \cos B|x_n|)] + \frac{t}{A_r}} \quad (121)$$

For the case of $P = \text{Const.}$

$$\sigma_B = \pm \frac{3P}{2Bt^2} \sum_{n=-\infty}^{\infty} e^{-B|zn|} (\sin B|zn| - \cos B|zn|) \quad (122)$$

Since P is calculated at a rib, with constant distances between ribs (d_1) equation (121) may be written

$$P = \frac{(P_r - P_b) + \frac{\alpha \Delta T_m E_1 t}{r}}{B \left\{ \frac{1}{2} + \sum_{n=1}^{\infty} e^{-nBd_1} (\sin nBd_1 + \cos nBd_1) \right\} + \frac{t}{A_r}} \quad (123)$$

Equation (122) may be written, for the bending stresses at a rib

$$\sigma_{B111} = \frac{-3P}{2Bt^2} \left\{ -1 + 2 \sum_{n=1}^{\infty} e^{-nBd_1} (\sin nBd_1 - \cos nBd_1) \right\} \quad (124)$$

$$\sigma_{B121} = -\sigma_{B111} \quad (125)$$

For bending stresses midway between ribs

$$\sigma_{B112} = \frac{-3P}{2Bt^2} \left\{ 2 \sum_{n=0}^{\infty} e^{-\left(\frac{2n+1}{2}\right)Bd_1} \left[\sin\left(\frac{2n+1}{2}\right)Bd_1 - \cos\left(\frac{2n+1}{2}\right)Bd_1 \right] \right\} \quad (126)$$

$$\sigma_{B122} = -\sigma_{B112} \quad (127)$$

(b) Hoop stresses under and between the ribs are calculated using the deflection equation (115). The general hoop stress formula for a thin walled cylinder is:

$$\frac{\Delta}{r} = \frac{\sigma_{\text{hoop}}}{E} \quad (128)$$

so

$$\sigma_{\text{hoop}} = \Delta \left(\frac{E}{r} \right) \quad (129)$$

Now Δ is the deflection of the cylindrical surface. When the pressure difference $(P_t - P_b)$ and the rise in mean temperature ΔT_m occur the deflection is

$$\Delta_{PT} = \frac{(P_t - P_b) r^2}{E t} + r \alpha \Delta T_m \quad (130)$$

and the hoop stress is

$$\sigma_{PT} = \frac{(P_t - P_b) r}{t} \quad (131)$$

The ribs cause a deflection inward of

$$\Delta_R = \frac{(P_t - P_b) r^2}{E t} + r \alpha \Delta T_m - \frac{Pr^2}{A_r E_r} \quad (132)$$

and a stress of

$$\sigma_R = -\frac{(P_t - P_b) r}{t} - r \alpha \Delta T_m E_r + \frac{Pr}{A_r} \quad (133)$$

The net hoop stress under the ribs is thus

$$\sigma_{NH1} = \frac{Pr}{A_r} - r \alpha \Delta T_m E_r \quad (134)$$

The deflection caused by the ribs between ribs is

$$\Delta_{R2} = \frac{Pr^2}{E_r t} \sum_{n=0}^{\infty} e^{-\left(\frac{2n+1}{2}\right) \beta d_r} \left[\sin\left(\frac{2n+1}{2}\right) \beta d_r + \cos\left(\frac{2n+1}{2}\right) \beta d_r \right] \quad (135)$$

The net hoop stress between ribs is thus

$$\sigma_{HH2} = \frac{(P_t - P_b)r}{t} - \frac{PBr}{t} \sum_{n=0}^{\infty} e^{-(\frac{2n+1}{2})Bd_L} \left[\sin(\frac{2n+1}{2}Bd_L) + \cos(\frac{2n+1}{2}Bd_L) \right] \quad (136)$$

(c) The thermal stresses due to self-restraint are, for a thin wall, both circumferentially and longitudinally

$$\sigma_{TH} = \pm \frac{\alpha \Delta T E_t}{2(1-\mu)} \quad (137)$$

(d) The radial pressure stresses are:

(1) Inside radius under a rib

$$\sigma_{R11} = -P_t \quad (138)$$

(2) Outside radius under a rib

$$\sigma_{R12} = -\frac{P}{t_r} \quad (139)$$

t_r = rib thickness, inches

(3) Inside radius between ribs

$$\sigma_{R112} = -P_t \quad (140)$$

(4) Outside radius between ribs

$$\sigma_{R122} = -P_b \quad (141)$$

(e) The calculation of longitudinal stresses from the thrust load with circumferential ribs is not so straight forward. In the case of no restraint the entire thrust is taken by the liner. In the case of longitudinal ribs essentially all the thrust is taken by the sleeve through the ribs. In the case of circumferential ribs the thrust component of the

pressure which will be taken by the ribs depends on the number, thickness, radial width, end constraint, and angle of the ribs. If the ribs are placed at all points perpendicular to the liner they will take the thrust load largely in compression, but if they are placed perpendicular to the flow axis they will take the thrust load mainly in bending.

It was at first proposed that the ribs be placed perpendicular to the liner but difficulties in fabrication and assembly led to the conclusion the ribs should be placed perpendicular to the flow axis if circumferential ribs were used. This causes a problem in determining the distribution of the thrust between the tensile (or compressive) stresses in the liner and the bending stresses in the ribs.

For a model to use to approximate these stresses, assume a contour as shown below in cross-section

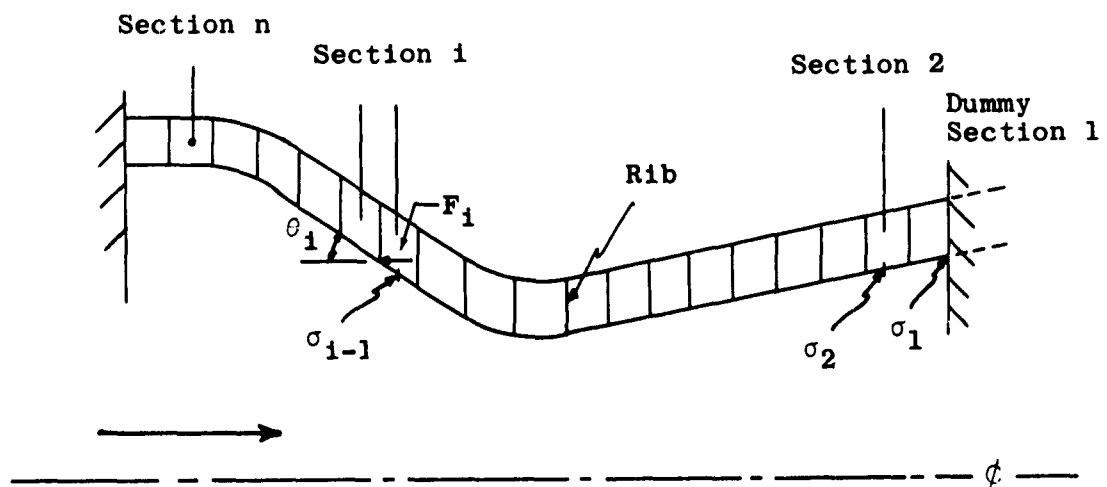


Fig. 29 Sketch of Nozzle with Ribs Perpendicular to Flow of Gas

A force balance may be made on the i^{th} section. Forces to the right are taken as positive.

$$0 = P_i A_i \sin \theta_i - F_i - \left[\sigma_i w_i t_i \cos\left(\frac{\theta_i + \theta_{i+1}}{2}\right) - \sigma_{i+1} w_i t_i \cos\left(\frac{\theta_i + \theta_{i+1}}{2}\right) \right] \quad (142)$$

P_i = pressure difference, air minus coolant, psi
 A_i = area, inches
 F_i = rib restraining force, pound
 w_i = liner circumference at position of σ_i , inches
 t_i = liner thickness at position of σ_i , inches

(Note that the pressure force on the expansion end is negative). Since the rib is a circular plate fixed in the liner and sleeve, in the exact analysis of the relationship between force and displacement, one obtains the equation

$$F = \frac{\delta E t_r^3}{\kappa_i a^3} \quad (143)$$

where

δ = rib displacement
 E = rib modulus of elasticity
 t_r = rib thickness
 a = outside radius of rib
 b = inside radius of rib
 κ_i = some function of $\left(\frac{a}{b}\right)$ given in Table I.

This same result may be closely approximated by an analytical expression based on a simple beam analysis. Treating the rib as a beam of length $(a - b)$ and width $2\pi \bar{r}$

$$\delta = \frac{F(a-b)^3}{2\pi \bar{r} t_r^3 E} \quad (144)$$

$$F = \frac{2\pi \bar{r} \delta E t_r^3}{(a-b)^3} \quad (145)$$

Setting equations (143) and (145) equal gives

$$\kappa_i = \frac{(a-b)^3}{2\pi \bar{r} a^3} \quad (146)$$

The expressions for K_1 for several definitions of \bar{r} are given below:

\bar{r}	K_1
a	$\left[\left(\frac{a}{b} \right)^3 - 3 \left(\frac{a}{b} \right)^2 + 3 \left(\frac{a}{b} \right) - 1 \right] / 2\pi \left(\frac{a}{b} \right)^3$
b	$\left[\left(\frac{a}{b} \right)^3 - 3 \left(\frac{a}{b} \right)^2 + 3 \left(\frac{a}{b} \right) - 1 \right] / 2\pi \left(\frac{a}{b} \right)^2$
$\frac{a+b}{2}$	$\left[\left(\frac{a}{b} \right)^2 - 4 \left(\frac{a}{b} \right) + 7 - \frac{8}{1 + \left(\frac{a}{b} \right)} \right] / \pi \left(\frac{a}{b} \right)^2$
$\frac{a-b}{\ln \frac{a}{b}}$	$\left\{ \ln \frac{a}{b} \left[\left(\frac{a}{b} \right)^2 - 2 \left(\frac{a}{b} \right) + 1 \right] \right\} / 2\pi \left(\frac{a}{b} \right)^2$

Some values of K_1 , as given by Timoshenko (5) and as calculated from the above expressions are tabulated below:

TABLE I
THE FUNCTION K_1

\bar{r}	$\frac{a}{b}$	1.10	1.25	1.50	2.0	3.0	4.0	5.0
a	K_1	.000120	.00127	.0059	.0198	.047	.067	.082
b	K_1	.000132	.00159	.0088	.0396	.141	.268	.408
$\frac{a+b}{2}$	K_1	.000132	.00142	.0071	.0265	.071	.107	.136
$\frac{a-b}{\ln a/b}$	K_1	.000125	.00141	.0072	.0275	.078	.122	.164
Table	K_1	_____	.00129	.0064	.0237	.062	.092	.114

These values show that the best choice for \bar{r} is the mean radius. They also show that this choice should give forces which are within $\sim 10\%$ of those obtained from equation (143) for $\frac{a}{b} < 1.25$. Equation (145) was used with $\bar{r} = \frac{a+b}{2}$ for this analysis.

Equation (142) may now be written

$$P_i A_i \sin \theta_i = \frac{\pi(a_i+b_i)d_i E t_i^3}{(a_i-b_i)^3} + \sigma_i w_i t_i \cos\left(\frac{\theta_i + \theta_{i+1}}{2}\right) - \sigma_{i-1} w_{i-1} t_i \cos\left(\frac{\theta_i + \theta_{i-1}}{2}\right) \quad (147)$$

Let $C_i = P_i A_i \sin \theta_i$ (148)

$$G_i = \frac{\pi(a_i+b_i) E t_i^3}{(a_i-b_i)^3} \quad (149)$$

$$D_i = w_i t_i \cos\left(\frac{\theta_i + \theta_{i+1}}{2}\right) \quad (150)$$

The general equation for the force balance is now

$$C_i = G_i d_i + D_i \sigma_i - D_{i-1} \sigma_{i-1} \quad (151)$$

In order to solve these equations d_i must be expressed in terms of σ or vice versa. In general Hooke's Law is

$$E = \frac{\sigma}{\Delta/l} \quad (152)$$

E = modulus of elasticity, psi

σ = stress, psi

Δ = strain, inches

l = length, inches

If d_i is the amount the i^{th} segment has elongated due to tensile stresses

$$d_i \approx \frac{(\sigma_i + \sigma_{i-1}) l_i}{2E} \quad (153)$$

The axial movement is then

$$x_i \approx \frac{(\sigma_i + \sigma_{i-1}) l_i}{2E \cos \theta_i} \quad (154)$$

Stresses in the liner and rib displacements may be related using equation (154). The average stress in a section is taken as the mean of the stresses at the ends. Ribs removed from a fixed end must yield the total elongation in the axial direction of all sections between that rib and the fixed end, plus one-half the elongation of their own section, thus

$$\delta_i = \frac{1}{2} \left(\frac{\sigma_i + \sigma_{i-1}}{2} \right) \frac{L_i}{E \cos \theta_i} + \sum_{j=1}^{j=n-1} \left(\frac{\sigma_j + \sigma_{j+1}}{2} \right) \frac{L_{j+1}}{E \cos \theta_{j+1}} \quad (155)$$

This equation holds for all except the section numbered n where

$$\delta_n = \frac{1}{2} \left(\frac{\sigma_n + \sigma_{n-1}}{2} \right) \frac{L_n}{E \cos \theta_n} \quad (156)$$

When these equations are substituted into equation (151) a series of $(n - 1)$ equations in n unknowns is obtained. The "extra" unknown is the stress at the exit end,

The "extra" stress, σ_1 , must be picked to satisfy the condition that the integrated displacement over the length of the liner is zero, that is, the ends are fixed. This is done as follows:

(1) The end stress σ_1 is arbitrarily specified, together with the other stresses, and equation (151) solved by relaxation of residuals. This gives a value of σ_2 , and δ_2 is calculated from equation (155).

(2) The fixed exit end condition requires that

$$\delta_2 + \frac{1}{2} \left(\frac{\sigma_2 + \sigma_1}{2} \right) \frac{L_1}{E \cos \theta_1} = 0 \quad (157)$$

Letting the calculated value of the left side of this equation be

$$\gamma = \delta_2 + \left(\frac{\sigma_2 + \sigma_1}{4} \right) \frac{L_1}{E \cos \theta_1} \quad (158)$$

(3) If $\gamma > 0$ the liner extends too far in the direction of flow, and to shorten it σ_1 must be more compressive so σ_1 must be reduced. If $\gamma < 0$, σ_1 must be increased. γ may be made as close to 0 as desired by changing σ_1 in the proper direction and repeating the calculation in (1).

Calculations were made for a representative liner configuration with a Mo-Ti liner and ~ 200 atm. entrance air pressure. The liner had 20 ribs .025 inches thick and spaced .25 inches apart along the axis. Results are given in Table II. The computer program used for the calculations was written in Fortran II language and is included in Appendix A. The calculations were made on an IBM 1620 Digital Computer.

(f) If the liner in this case is fixed at the ends, compressive longitudinal stresses will be developed. For restraint by the sleeve only these will be the same as in Case I, Part (f), thus

$$\sigma_{TL1} = - \frac{\alpha, \Delta T_m E_1}{\left(1 + Z_s \frac{E_1}{E_2}\right)} \quad (159)$$

and

$$\sigma_{TL2} = \frac{\alpha, \Delta T_m E_1 Z_s}{\left(1 + Z_s \frac{E_1}{E_2}\right)} \quad (160)$$

(g) The principle tangential stresses for this case are:

(1) At the inside radius over a rib

$$\sigma_{PC111} = \sigma_{NH1} - \sigma_{TH} \quad (161)$$

(2) At the outside radius over a rib

$$\sigma_{PC121} = \sigma_{NH1} - \sigma_{TH} \quad (162)$$

(3) At the inside radius between ribs

$$\sigma_{PC112} = \sigma_{NH2} - \sigma_{TH} \quad (163)$$

(4) At the outside radius between ribs

$$\sigma_{PC122} = \sigma_{NH2} + \sigma_{TH} \quad (164)$$

TABLE II
RESULTS FOR A REPRESENTATIVE LINER CONFIGURATION

Section Number	Assumed Air Pressure (psi)	Diameter (inches)	Liner Thickness (inches)	Tensile Stress (psi)
1	2800	1.32	.034	200
2	2800	1.24	.033	510
3	2800	1.16	.032	695
4	2800	1.08	.031	895
5	2800	1.00	.030	1,220
6	1400	.92	.029	990
7	1300	.84	.028	625
8	1200	.76	.028	45
9	1100	.68	.027	- 300
10	1000	.60	.026	- 440
11	900	.52	.025	- 400
12	800	.44	.024	- 2,540
13	700	.36	.023	- 4,700
14	600	.28	.022	- 8,220
15	500	.24	.025	- 7,940
16	400	.60	.028	- 4,100
17	300	1.04	.031	- 2,100
18	200	1.41	.033	10,475
19	100	1.50	.034	8,185
20	5	1.50	.035	7,930

(h) The principle longitudinal stresses for this case are:

(1) At the inside radius over a rib

$$\sigma_{PL11} = \sigma_{THRUST} + \sigma_{TL1} - \sigma_{TH} + \sigma_{B11} \quad (165)$$

(2) At the outside radius over a rib

$$\sigma_{PL21} = \sigma_{THRUST} + \sigma_{TL1} + \sigma_{TH} + \sigma_{B121} \quad (166)$$

(3) At the inside radius between ribs

$$\sigma_{PL12} = \sigma_{THRUST} + \sigma_{TL1} - \sigma_{TH} + \sigma_{B112} \quad (167)$$

(4) At the outside radius between ribs

$$\sigma_{PL22} = \sigma_{THRUST} + \sigma_{TL1} + \sigma_{TH} + \sigma_{B122} \quad (168)$$

Note: The ribs cause a small additional bending stress which is neglected here.

(i) The radial principle stresses are given in (d).

Case 3 - Fully Restrained Liner

This is the case of real interest in the present analysis as sample calculations of Case 2 show that unless the sleeve is made thinner than the liner little is gained stresswise.

This case is calculated from the equations developed in Case 2 (Longitudinal Ribs) by letting the outside radius of the sleeve be much larger than the inside radius, thus, using a very thick sleeve. In Case 2 - (Circumferential Ribs) this case is calculated by assuming a very large rib cross-sectional area.

Since a large number of variables were involved these equations were programmed in Fortran II language for the IBM 1620 Digital Computer. This program is attached and described in Appendix A.

CONCLUSIONS

Parametric stress studies and coolant flow considerations show that longitudinal ribs offer the best possibilities for backside cooling. If circumferential ribs are placed perpendicular to the flow axis high bending stresses are introduced in the ribs and liner due to the thrust load. The problem of getting proper coolant flow at each section is also complicated and causes design and fabrication difficulties.

The maximum design pressure is 500 atmospheres in the entrance tube. This would produce a pressure of approximately 250 atmospheres at the throat. Calculations were made using these pressures and assuming a heat load of 60 B/in²sec for a Mo-Ti-Zr liner. A backside cooling coefficient of 150,000 B/hr ft² °F was assumed. The bulk coolant temperature was assumed to be 85°F. A heavy sleeve was used and the liner thickness varied. The results of these calculations are presented graphically on pages 75 through 78. Some properties of Mo-Ti-Zr are shown graphically on page 79.

Several observations may be made from these graphs: the critical octahedral shear stress for yielding, τ_{oct} , is exceeded for all liner thicknesses and at all four locations for the 1.5 inch diameter entrance sections; at two positions τ_{oct} is exceeded for the 0.78 inch diameter throat; the octahedral shear stresses for the 0.27 inch diameter throat may be made $\leq \tau_{critical}$ by making the liner thickness ≤ 10 mils; the octahedral shear stresses for the 0.042 inch throat are $\leq \tau_{critical}$ for a liner thickness ≤ 14 mils. It should be noted that although the curves are not plotted below 10 mils liner thickness, all the octahedral shears approach infinity as the liner thickness approaches 0. An optimum thickness for the liner may be picked from the curves to minimize the plastic strain, and for this thickness the mean longitudinal compressive stress, which is the maximum mean stress, may be found. These values are:

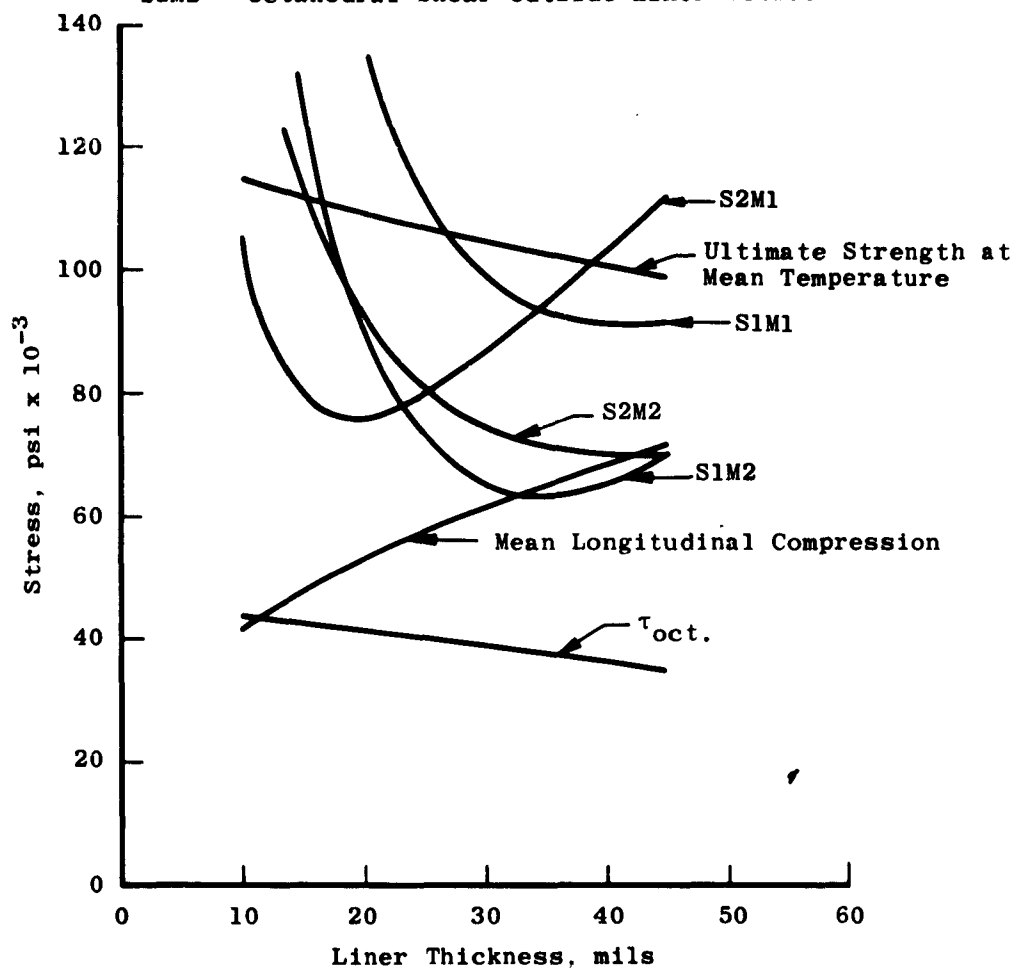
Liner Diameter (Inches)	Liner Thickness (Inches)	Rib Spacing (Inches)	Mean Longitudinal Stress (psi)
1.50	.034	.226	-65,000
.784	.018	.120	-52,000
.272	.012	.059	-47,000
.042	.006	.014	-40,000

The mean longitudinal stress is compressive, and does not exceed the ultimate strength of the liner material for any of the conditions.

A brief calculation may be made to predict the operating cycles before failure for these nozzles. The maximum principle stress occurs midway between ribs at the inside of the liner and at the 1.5 inch diameter section.

Longitudinal Ribs
 $Q = 60 \text{ Btu/in.}^2 \text{ sec}$
 Material - Mo-Ti-Zr
 Diameter - 1.5 in.
 Pressure - 500 atm
 Backside Coefficient - $150,000 \text{ Btu/hr ft}^{20} \text{ F}$

S1M1 - Octahedral Shear Inside Liner over a Rib
 S1M2 - Octahedral Shear Outside Liner over a Rib
 S2M1 - Octahedral Shear Inside Liner between Ribs
 S2M2 - Octahedral Shear Outside Liner between Ribs



121 172 212 247

Rib Spacing for Indicated Liner Thickness, mils

Fig. 30 Stress versus Liner Thickness; Diameter = 1.5"

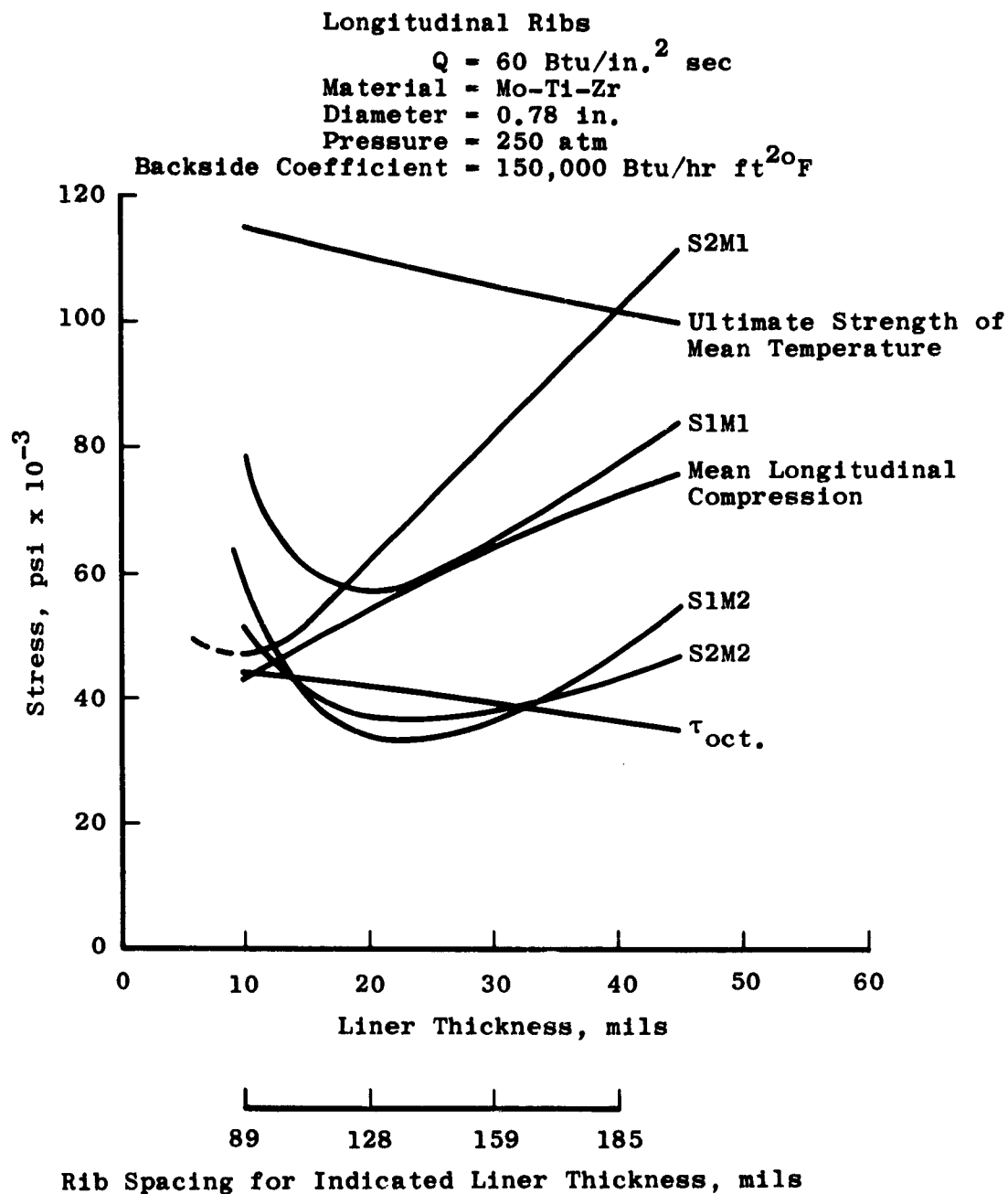


Fig. 31 Stress Versus Liner Thickness; Diameter = 0.78"

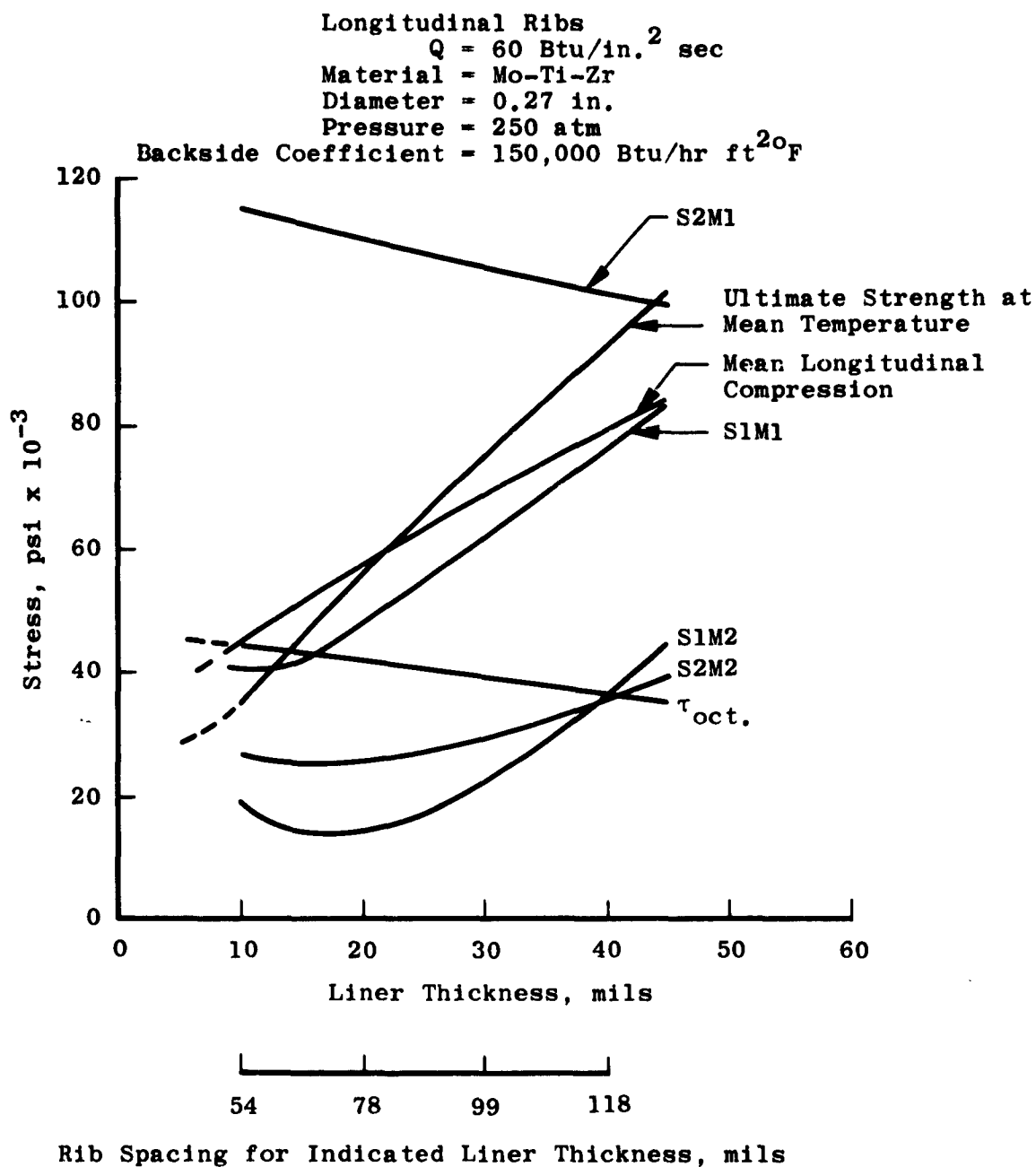


Fig. 32 Stress versus Liner Thickness; Diameter = 0.27"

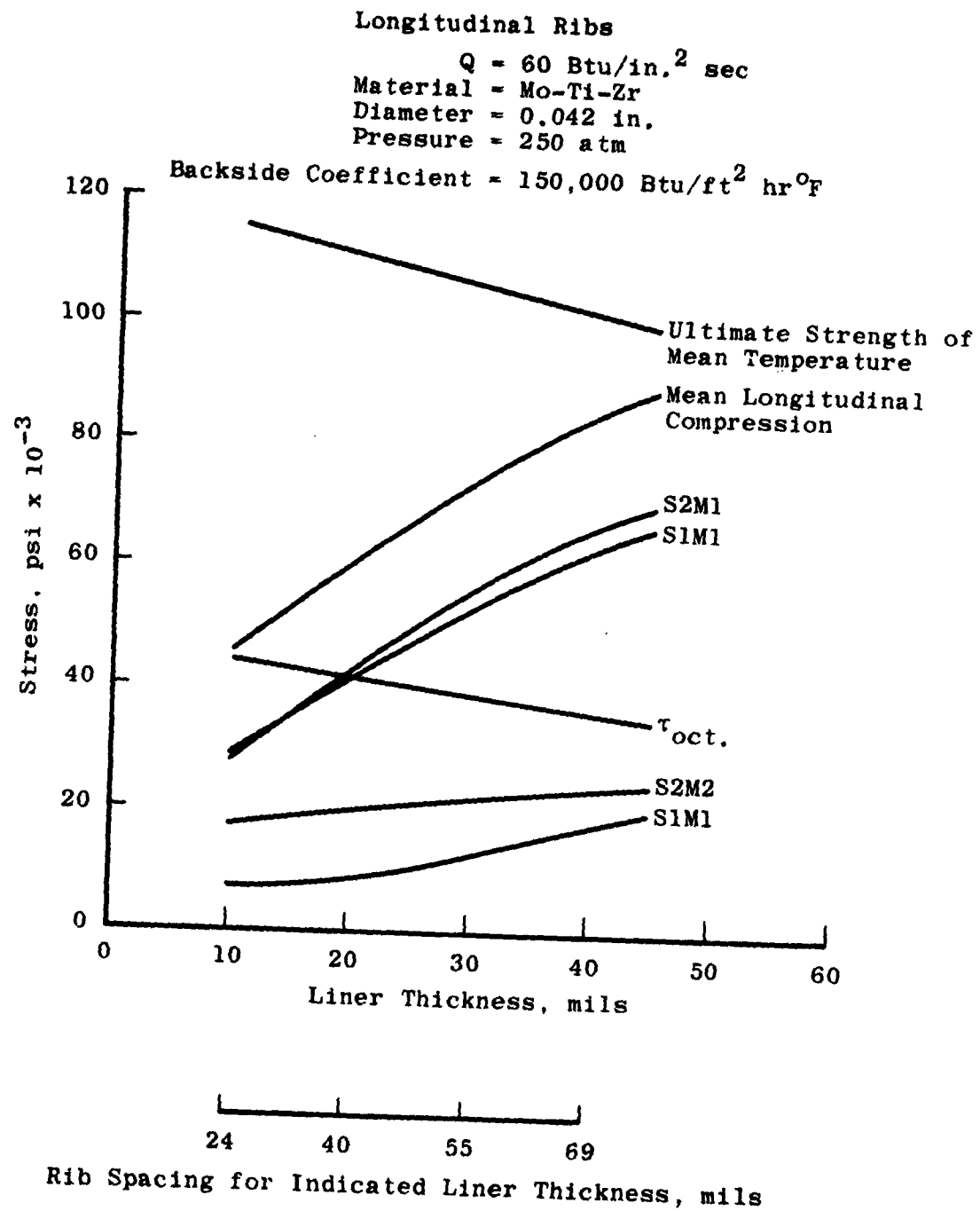


Fig. 33 Stress versus Liner Thickness; Diameter = 0.042 in.

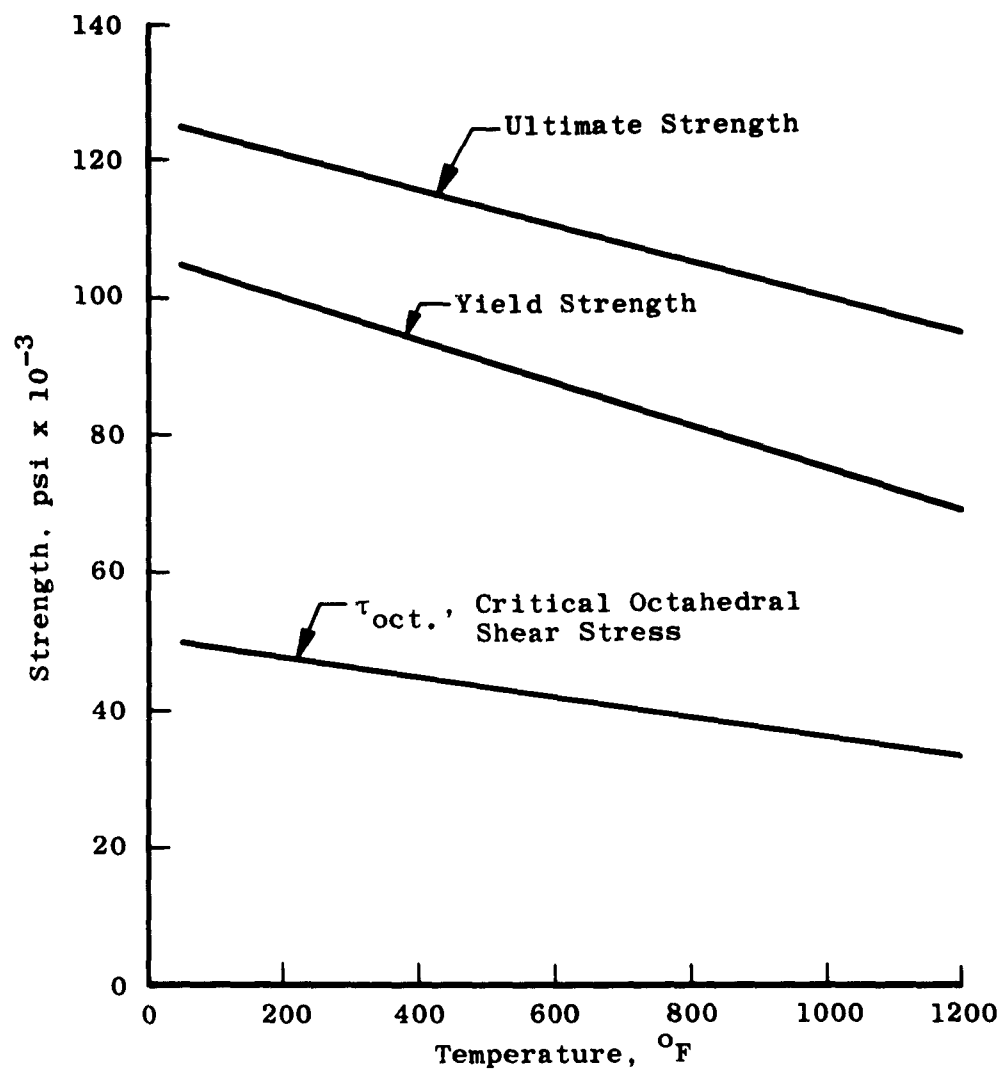


Fig. 34 Strength versus Temperature for Mo-Ti-Zr

The computed value of this stress is -232,000 psi, which exceeds the yield strength of the material by $\sim 172,000$ psi when the inside temperature is 1470°F. The modulus of elasticity at this temperature is 35,000,000 psi. The plastic strain is thus

$$\Delta \epsilon_p \approx \frac{172,000}{35,000,000} = 0.00492 \text{ in/in}$$

Using an average value of 0.36 for the constant in Coffin's (6) equation

$$N = \left[\frac{0.36}{0.00492} \right]^2$$

and $N \approx 5000$ cycles to failure.

Though not presented graphically in this report, calculations for Mo-Ti-Zr liners at lower pressures and heat loads indicate that these same liner thickness and rib spacing values are acceptable. Calculations may be rapidly made for any assumed conditions using the Nozzle Stress Program.

In the actual nozzle design it is proposed that the ribs will terminate just before reaching the throat as the pressure drops sharply at this point. This simplifies the nozzle construction and reduces the coolant pressure loss in the longer expansion section. It also alleviates the problem of close rib spacing at the throat of the .042 inch nozzle. The ribs may be terminated when the liner diameter is $\sim .3$ inch and a rib spacing of $\sim .1$ inch.

A sketch of a typical nozzle design is shown on page 81. In this sketch the ribs are shown attached to the sleeve rather than the liner. This offers some advantage in so far as construction and longitudinal compressive stresses are concerned. However, there may be some distortion at the throat and some heat transfer problems on the backside. It is, therefore, recommended that the ribs be machined integral with the liner if costs are not prohibitive.

VI. MATERIALS STUDY

The selection of the best material to use for a nozzle liner for high pressure-high temperature air must be based on the following considerations:

(a) Ability to stand the imposed stresses. A stress parameter will include as factors:

- (1) Thermal conductivity
- (2) Strength at working temperatures
- (3) Modulus of elasticity
- (4) Thermal expansion coefficient.

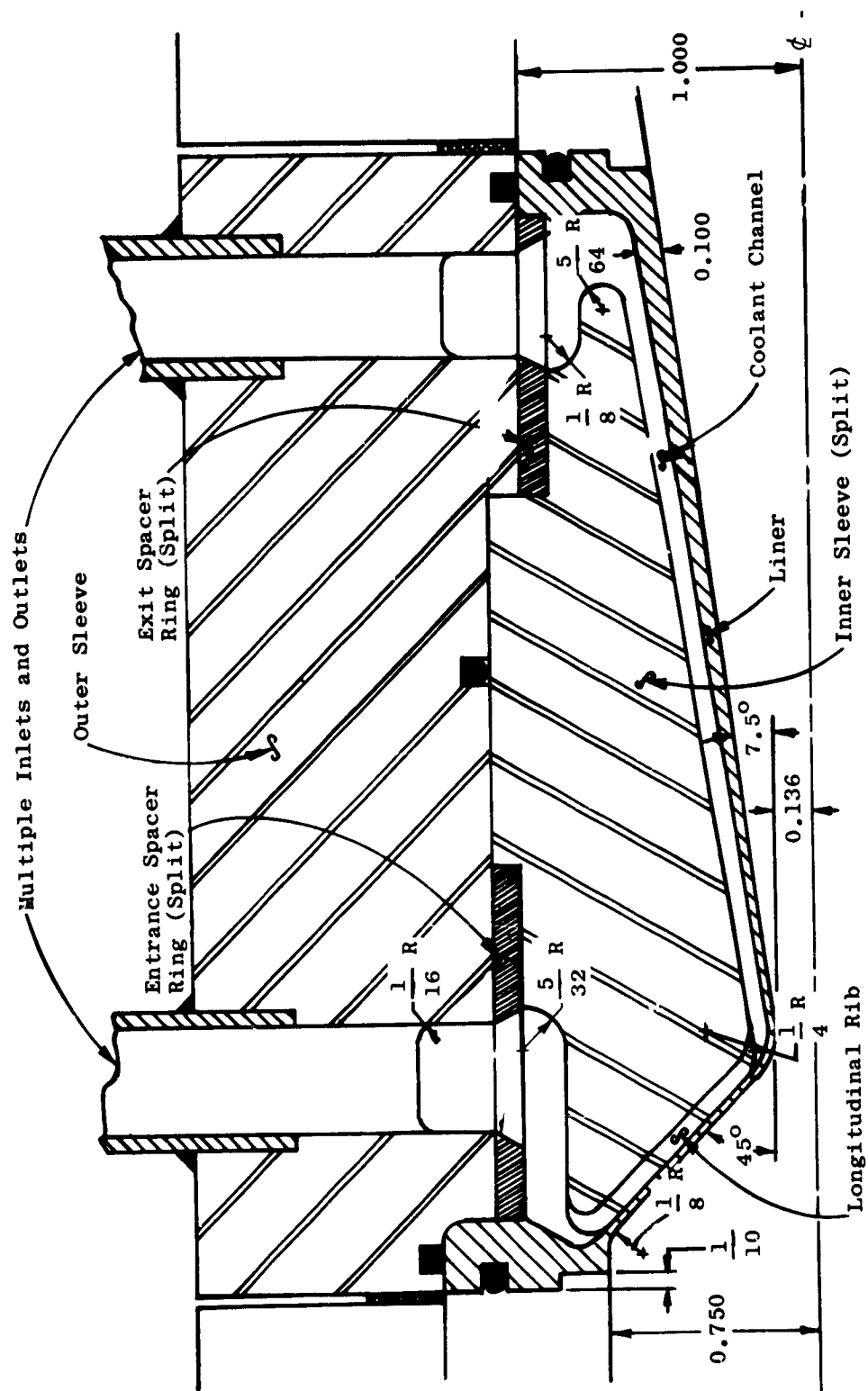


Fig. 35 Sketch of Typical Nuzzle Design

All dimensions are in inches.

(b) Resistance to oxidation at elevated temperatures. This factor includes:

- (1) Oxidation resistance of the material chosen.
- (2) Possibility of protection by coatings.

(c) Fabricability, which includes:

- (1) Machinability.
- (2) Joining methods.

STRESS PARAMETER

It is noted that the thermal stress in a structural member across which there is a temperature difference is directly proportional to the temperature difference, the thermal expansion coefficient, and the modulus of elasticity. For a given heat load the temperature difference is inversely proportional to the thermal conductivity. A thermal stress parameter should also include the ultimate strength. Thus:

$$P_s = \frac{S_u k}{E \alpha} \quad (169)$$

P_s = stress parameter, B/hr ft

k = thermal conductivity, $\frac{B}{hr ft ^\circ F}$

E = modulus of elasticity, lb/in²

α = thermal expansion coefficient, in/in $^\circ F$

S_u = ultimate strength, lb/in²

Figure 36, page 83, shows this parameter plotted vs temperature ($^\circ F$) for the following materials: Cu-Be alloy, Cu-Zr alloy, Mo-0.5 Ti-0.07 Zr, AM 350 steel, modified H-11 steel. It is evident from the curves shown that above approximately 900 $^\circ F$ the Mo-Ti-Zr alloy is a much better material to use so far as the thermal stresses are concerned and, at the high heat loads expected in the nozzle, these stresses are dominant.

OXIDATION RESISTANCE

The oxidation rate of pure copper is given by:

$$w^2 = kt$$

where w = weight of oxide formed in grams/cm²

t = time in seconds

k = function of temperature in $^\circ F$

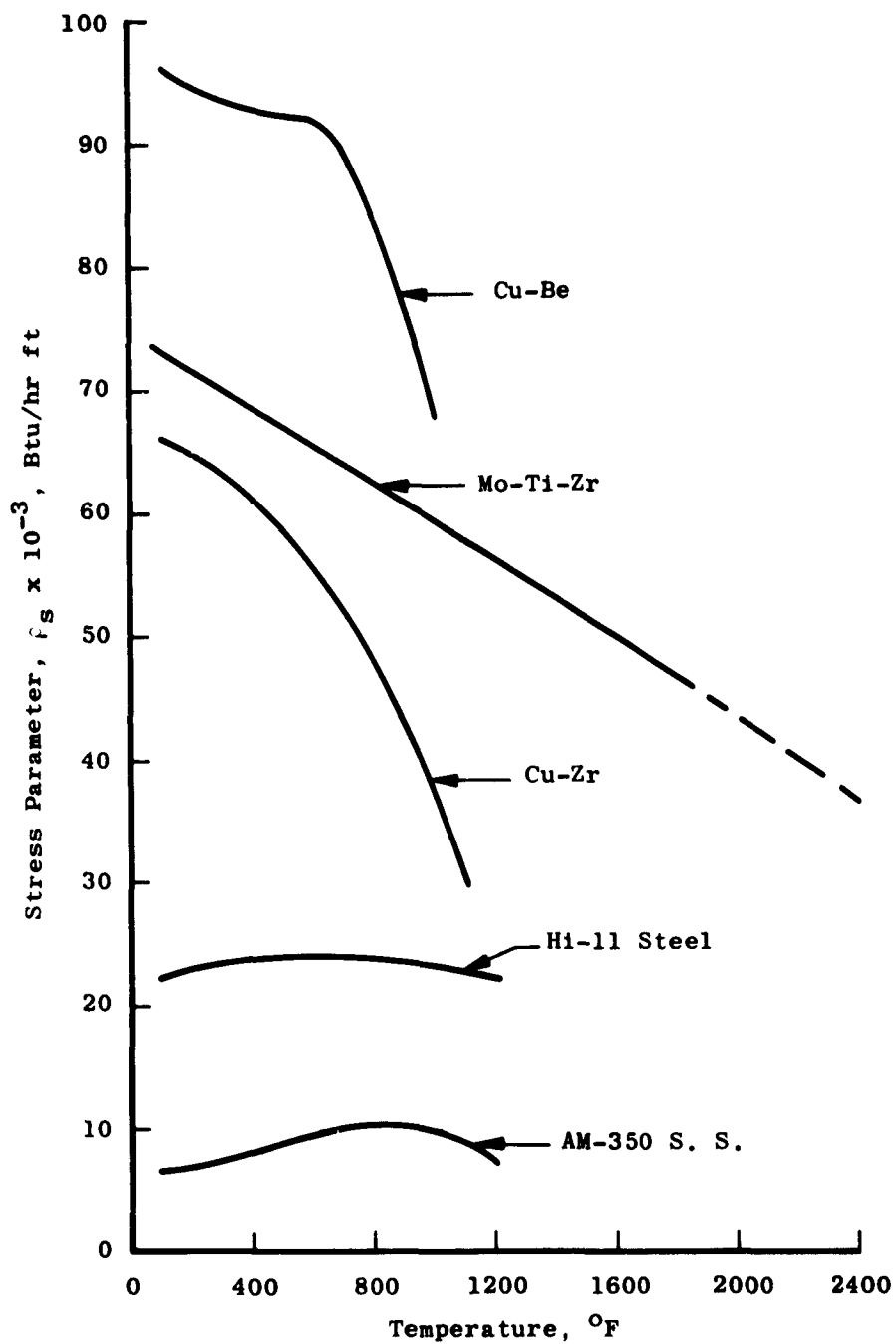


Fig. 36 Temperature Effect on the Stress Parameter of Various Nozzle Liner Materials

Some values of k are (7):

<u>Temp. °F</u>	<u>$k \times 10^{10}$</u>	
	<u>Pure O₂</u>	<u>Air</u>
750	.044	-
950	.440	-
1100	3.24	-
1300	16.0	8.03

Assuming that the rate in air at the lower temperatures is half that in pure O₂ the penetration in cm/hr is:

$$p_o = \frac{(kt)^{1/2}}{d}$$

p_o = cm/hr of oxidation
 k = function of temperature
 t = time in seconds
 d = density in grams/cm³

$$p_o)_{1100F} = \frac{[(1.62 \times 10^{-10} \times 3.6 \times 10^3)]^{1/2}}{8.96}$$

$$p_o)_{1100F} \approx 10^{-4} \text{ cm/hr.}$$

Even if the oxide is continuously removed the rate of loss is very small at 1100°F, and the inside temperature of the copper alloys would not exceed this temperature except at extremely high heat loads ($> 200 \text{ B/in}^2 \text{ sec}$). Oxidation of the copper alloys does not appear to be a large problem if they are used.

The Mo-Ti and Mo-Ti-Zr alloys are not as resistant to oxidation as the Cu alloys. The oxide of Mo is also volatile, so there is no self protection. There are metallic coatings available, however, such as electroplated or hot dipped Ni, which will protect Mo in the 1300-1500°F range.

For protection at much higher temperatures, say 2000-2500°F, a silicide coating known as Chromalloy W-3 is available. It is thus possible to provide oxidation protection for Mo and Mo alloys for several hours at the temperatures of interest.

FABRICABILITY

Fabricability is an important consideration, as the optimum thickness of the liner at some positions is 10-15 mils. The thrust load requirements must be met by using ribs on either the liner or the sleeve. If the ribs are a part of the liner they must be machined on this surface and thus, the machinability of the material is very important.

The copper alloys, including Cu-Be and Cu-Zr, have a machinability index of 20 (based on free-cutting brass = 100). Cu-Be and Cu-Zr may both be joined by soldering and brazing (8).

Molybdenum and its alloys Mo-Ti and Mo-Ti-Zr machine much like cast iron (8). Tungsten carbide tools should be used (8). The machinability index is approximately the same as that of the copper alloys.

CONCLUSION

The following observations are made:

(a) If the backside cooling technique (forced convection or boiling), the heat load, and the liner thickness are such that the temperatures at the inside of a Cu-Be liner remain below 800°F, Cu-Be is the preferred liner material. Under these conditions it has the largest stress parameter and does not require oxidation coating.

(b) If the backside cooling technique (forced convection or boiling), the heat load, and the liner thickness are such that temperatures at the inside of a Cu-Zr liner are between 800°F and 1000°F, and if it is desired to avoid the added expense, complication, and uncertainty of coating the liner, Cu-Zr is attractive.

(d) If the heat loads and backside cooling technique (forced convection or boiling) are such that the conditions in (1) and (2) are not met, Mo-Ti or Mo-Ti-Zr are plainly superior.

As the heat load is increased for any given backside cooling technique, the inside liner temperature rises. Studies of the heat load in the upper region of the envelope show that with radiation included this load may easily be several hundred B/in²sec. This would produce inside surface temperatures of > 800°F using Cu-Be. Since Mo-Ti and Mo-Ti-Zr have higher stress parameters than Cu-Zr and this advantage increases as the heat load is increased, it is recommended that Mo-Ti-Zr be used in order to push as far as possible in the envelope. At lower heat loads

and inside temperatures, metallic coatings should be used. At higher heat loads and temperatures ($\sim 2000^{\circ}\text{F}$), Chromalloy W-3 coating should be used.

VII. SHARP EDGED NOZZLE

Since the heat transfer rate across a laminar boundary layer is small compared to the heat transfer rate across a turbulent boundary layer, it is desirable to design a nozzle in which a laminar boundary layer exists as far downstream as possible. For this reason, the sharp edged nozzle shown in Figure 37, is proposed for an analysis. The primary advantage of this type of nozzle is the short distance of the upstream air-metal contact relative to a conventional nozzle approach section.

From the above arguments, it is concluded that it will be desirable to have the radius of curvature of the nozzle as small as possible; therefore, it becomes necessary to attain the shape of the sonic line for any proposed nozzle of this type since this information is required for the design of the downstream section of the nozzle. Other questions which need to be answered about the proposed nozzle are: (1) how much water is carried downstream by the air, (2) does the water jet transport air out of the main water stream, and, if so, how much, and (3) what influence will the eddies have on the design of the nozzle? The analysis which has been accomplished to date is briefly outlined in the following sections.

The first region of analysis was confined to the water air interface, see Figure 37. Since the water emerges from the jet at a high velocity (~ 125 ft per sec), it was assumed that the water velocity was large relative to the adjacent air velocity. This assumption implies that the emergent water can be treated as a wall jet flowing into a semi-infinite medium. The Reynolds number of the jet based on the diameter of the inlet annulus is about 6×10^4 ; therefore, the problem is that of a turbulent wall jet (with the implicit assumption of equivalent static pressures in the air and water streams). Some analytical work and experimental results were found for wall jets for the case of a fluid emergent into a large medium which is filled with the same fluid, but no information was found for the case of dissimilar fluids. Since the static pressure in the two streams is assumed to be equivalent, it was concluded that the only driving force to cause mixing would be the momentum flux, and hence, the only physical properties of significance would be the density and viscosity. On this basis, it was decided to treat the jet as water emergent into water and calculate a Reynolds number of the fluid crossing into the jet. This Reynolds number is based on the component of velocity normal to the jet axis. Assume that the air "sucked" into the water jet would be of such magnitude that it would have an equivalent Reynolds number to that calculated above.

M. B. Glauert (9) developed an analytical solution for the wall jet assuming a similarity solution. His results show that the characteristic jet width is essentially proportional to the distance along the axis parallel to the jet wall raised to the first power. An experimental in-

vestigation of a wall jet was carried out by P. Bakke (10) and independently by W. H. Schwarz and W. P. Cosart (11).

From the above references it was concluded that the jet would spread at about 3.5° ; therefore, the dimension "a" (see Figure 37) is known. Since "a" is chosen to include the water "spread", there will be no water carried into the air stream due to mixing; however, the model chosen requires entrainment of the surrounding fluid into the jet. It should be observed that the model under analysis neglects diffusion of the water into the air stream; however, it is felt that the water transported into the air stream by this mechanism will be small because of the short distance of water travel in the nozzle.

Referring to Figure 37, it is seen that the length of the water jet is less than three equivalent diameters; therefore, the velocity profiles will not be susceptible to a similarity type solution since the similarity solution is valid only at far downstream conditions. Since the entrance stream is not subject to similarity analysis, the conclusions drawn might be questioned; however, direct observation of an air jet under analysis at The University of Tennessee shows that the air wall jet pulls in air (smoke) from the surrounding medium in the entrance region as well as far downstream. On this basis, it is felt that the conclusions drawn from a similarity analysis are quantitatively correct. No attempt will be made to use the similarity velocity profile to attain the quantity of air pulled into the water jet.

If eddies are developed in the region near the throat it is possible that they will change the effective throat geometry; therefore, it would be difficult, if not impossible, to calculate the shape of the sonic line (hence design of the downstream section of the nozzle). Since air is being pulled into the water jet the eddies will be depressed, and conceivably can be controlled to the point where there are essentially no eddies formed in the section near the throat. On this basis, it was concluded that the formation of eddies would be of no consequence in the design of the nozzle.

Before considering the preceding problems in a more rigorous fashion, it was decided to examine the shape of the sonic line at the throat for different throat diameters and wall geometries, and then determine what flow regime exists in the boundary layer.

The determination of the sonic line is not complete, but the equations to be solved have been developed. The development of the equations to be used for determining the shape of the sonic line is as follows.

The solution to the potential flow problem in a region near the throat outlined here follows the procedure described by Oswatitsch and Rothstein (13).

Use the nomenclature as presented in Figure 38. The equation of continuity is written as

$$\frac{\partial}{\partial y}(\rho v y) = -y \frac{\partial}{\partial x}(\rho u) \quad (170)$$

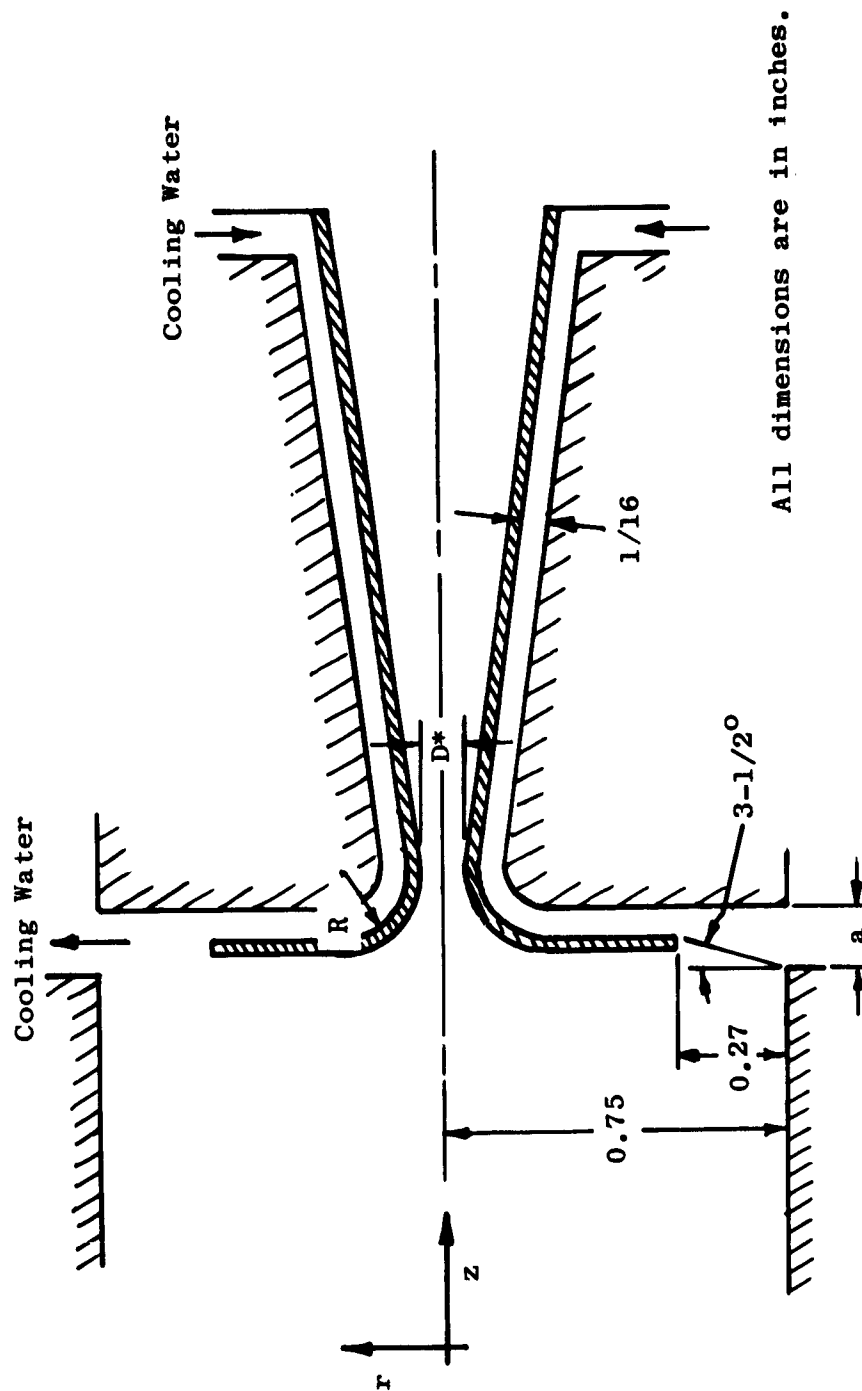


Fig. 37 Sketch of Sharp Edged Nozzle (Not to Scale)

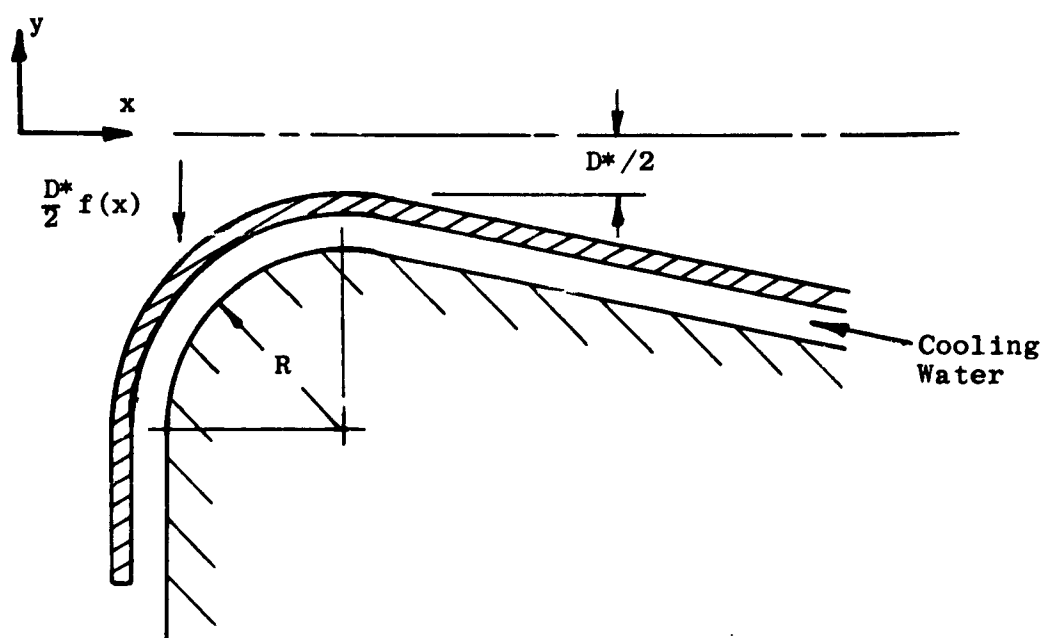


Fig. 38 Nomenclature Used Near Throat of Sharp Edged Nozzle

where u and v are the velocity components in x and y directions, and

$$\omega^2 = u^2 + v^2 \quad (171)$$

Solve equation (170) for v by making an approximation for ρu . Take the value of ρu to be the stream filament value designated by $\rho_s u_s$. The equation of energy can be written as

$$\frac{1}{2} \omega^2 + \frac{\gamma}{\gamma-1} \frac{P}{\rho} = \frac{\gamma}{\gamma-1} \frac{P^0}{\rho^0} \quad (172)$$

where γ is the ratio of specific heats and the superscript 0 refers to stagnation conditions. In equation (172) let $T \rightarrow 0$, and define $\omega = c$ at this condition, then

$$c^2 = \frac{2\gamma}{\gamma-1} \frac{P^0}{\rho^0} \quad (173)$$

Let

$$\omega' = \frac{\omega}{c} \quad (174)$$

and

$$\rho' = \frac{\rho}{\rho^0} \quad (175)$$

Since the main flow is assumed to be non-viscous, the flow is isentropic, i.e.,

$$\frac{P}{\rho^0} = \left(\frac{\rho}{\rho^0} \right)^\gamma \quad (176)$$

Substitute equations (173) through (176) into equation (172), then equation (172) becomes

$$\omega'^2 = 1 - (\rho')^{\gamma-1} \quad (177)$$

Since equation (177) is in a simple form the quantities c and ρ^0 will be used to make all velocities and density non-dimensional henceforth; consequently, the primes will be dropped.

The equation of continuity for the stream filament is

$$M = f^2 \pi \rho_s u_s \quad (178)$$

where f is as indicated in Figure 38.

Differentiation of equation (178) yields

$$\frac{1}{\rho_s u_s} \frac{d}{dx} (\rho_s u_s) = -2 \frac{f'}{f} \quad (179)$$

Equation (170) becomes (using equation (179))

$$\frac{d}{dy} (\rho v y) \approx 2 y \rho_s u_s \frac{f'}{f} \quad (180)$$

Since there is symmetry about the centerline, $v = 0$ at $y = 0$.

Integration of equation (180) (with $\frac{\rho}{\rho_s} \approx 1$) yields

$$v \approx \frac{f'}{f} y u_s \quad (181)$$

Assume u to be given by,

$$u(x, y) = u_0 + \frac{1}{2!} a_2 y^2 + \dots \quad (182)$$

Potential flow (irrotational flow) requires that

$$\frac{\partial u}{\partial y} = \frac{\partial v}{\partial x} \quad (183)$$

Using equation (181), the first two terms of equation (182), and carrying out the operations indicated in equation (183), the result is

$$u = u_0 + \frac{1}{2} (u_s f f'' + f f' u_s' - u_s f'^2) \frac{y^2}{f^2} \quad (184)$$

The parameter u_0 in equation (184) is attained from the equation of continuity

$$M = 2\pi \int_0^f u \rho y dy \quad (185)$$

From equation (171) and equation (177)

$$\rho = (1 - w^2)^{\frac{1}{r-1}} = (1 - u^2 - v^2)^{\frac{1}{r-1}} \quad (186)$$

Define

$$\Theta(u, v^2) \equiv u(1 - u^2 - v^2)^{\frac{1}{r-1}} \quad (187)$$

then equation (185) reads as

$$M = 2\pi \int_0^f \Theta(u, v^2) y dy \quad (188)$$

Solution of equation (188) yields

$$u_s - u_0 \approx \frac{1}{4} (u_s f f'' + \frac{3}{2} u_s' f f') \quad (189)$$

Solving equation (171) for u_0 and substituting the result into equation (184) yields

$$\begin{aligned} u = u_s + \frac{1}{4} (u_s f f'' + \frac{3}{2} u_s' f f') \\ + \frac{1}{2} (u_s f f'' + f f' u_s' - u_s f'^2) \frac{y^2}{f^2} \end{aligned} \quad (190)$$

For the nozzle presented in Figure 38, f is found to be

$$f = \frac{2R}{D^*} + 1 - 2 \left[\frac{2xR}{D^{*2}} - \left(\frac{x}{D^{*2}} \right)^2 \right]^{\frac{1}{2}} \quad (191)$$

Equations (190) and (191) have not been solved; however, the solution of these equations should yield the flow field in the region near the throat, and in particular, the shape of the sonic line with the radius of curvature of the nozzle as a parameter. D^* and u_s will be specified by the design criteria.

VIII. BACKSIDE COOLING STUDY

The heat loads on the liner of any proposed nozzle are calculated to be very high. The heat load postulated for the stress analysis is $60 \text{ B/in}^2\text{sec}$ or $30 \times 10^6 \text{ B/hr ft}^2$. If only backside cooling without film or transpiration assistance is used the loads in the upper portion of the envelope may exceed this value several times. This not only causes problems in liner materials, temperatures, and stresses, but also in problems with the removal of the heat at the backside of the liner. Unless a high heat transfer coefficient on the coolant side can be attained, an excessive rise in the liner temperature will occur.

It is proposed that water be used as the backside coolant since it is readily available in sufficient quantities at high pressures. The thermodynamic and heat transfer properties are known and several equations are available which give a good prediction of the heat transfer coefficient at various flow conditions. Water boils at fairly low temperatures (at low pressures) offering the possibility of a high heat transfer coefficient with a low flow rate and pressure drop.

Two heat transfer modes are of interest using water as the coolant, namely, forced convection and boiling. Forced convection exists at all positions along the coolant channel when the static pressure is high enough to cause the saturation temperature to equal or exceed the liner coolant surface temperature. Boiling heat transfer exists when the liner surface temperature is allowed to exceed the saturation temperature of the coolant by an amount sufficient to cause vaporization of the coolant at spots on the surface. This is called nucleate boiling, and in conjunction with the forced fluid flow, will be referred to as surface boiling.

FORCED CONVECTION

In order to design the coolant annulus for forced convection cooling, it is necessary to calculate the static pressure, bulk temperature, surface temperature, and heat transfer coefficient at each position along the coolant channel. The inlet pressure, flow rate, and coolant channel geometry must then be adjusted to assure that the heat will be transferred without causing the surface temperature to exceed the saturation temperature of the coolant at any location. Since the properties of the coolant such as viscosity, Prandtl's number, and density are functions of the bulk temperature and these vary with the flow rate and the heat load distribution along the channel, a stepwise fluid flow and heat transfer calculation along the channel is required.

The static pressure distribution is calculated from the general equation

$$P_e = P_i - \Delta P_f - \Delta P_d \quad (192)$$

where P_e = static pressure at exit of a section, psi
 P_i = static pressure at entrance to a section, psi
 ΔP_f = loss of pressure due to frictional drag, psi
 ΔP_d = loss of pressure due to acceleration, psi.

The frictional pressure loss is calculated from the Blasius formula for fully developed turbulent flow with fluid properties evaluated at the bulk temperature,

$$\Delta P_f = \frac{0.00219 \Delta x}{D_h} \left(\frac{\rho V^2}{2g_c} \right) R_e^{-\frac{1}{4}} \quad (193)$$

where Δx = length of channel section, inches
 D_h = hydraulic diameter of channel, inches
 ρ = density of coolant, lbm/ft³
 V = coolant mean velocity, ft/sec
 g_c = 32.2 lbm ft/lbf sec²
 R_e = Reynolds number
 μ = coolant viscosity, lbm/ft sec.

The dynamic pressure loss, ΔP_d , is calculated from

$$\Delta P_d = \frac{R_e V_e^2 - P_i V_i^2}{2g_c} \quad (194)$$

The pressure loss due to the sharp bend at the coolant channel entrance is calculated from the Blasius formula, equation (193), using an equivalent section length in place of Δx . The equivalent section length used in the present calculations is $\sim 45 D_h$, thus,

$$\Delta P_{f \text{ ent.}} \approx 0.10 \left(\frac{\rho V^2}{2g_c} \right)_{\text{ent.}} R_{e \text{ ent.}}^{-\frac{1}{4}} \quad (195)$$

The surface heat transfer coefficient is calculated using the Colburn equation modified by evaluating Reynolds number and Prandtl's number at the film temperatures

$$h_c = 0.023 C_p G R_{e_f}^{-0.2} P_{r_f}^{-\frac{2}{3}} \quad (196)$$

where h_c = surface heat transfer coefficient, B/hr ft²°F
 C_p = specific heat of coolant, B/lbm °F
 G = mass flow rate, lbm/hr ft²
 Re_f = Reynolds number (film)
 Pr_f = Prandtl's number (film).

The bulk temperature along the coolant channel is calculated from the heat balance equation on each section,

$$T_{b_2} = T_{b_1} + \frac{Q A_s}{G A_c C_p} \quad (197)$$

where T_{b_2} = bulk temperature at section exit, °F
 T_{b_1} = bulk temperature at section entrance, °F
 Q = liner heat load, B/hr ft²
 A_s = liner section surface area, ft²
 G = coolant mass flow rate, lbm/hr ft²
 A_c = coolant channel cross-sectional area, ft²
 C_p = coolant specific heat, B/lbm °F.

The calculational procedure is to choose a nozzle geometry, coolant flow rate, and entrance pressure for a given heat load distribution. The bulk temperature and static pressure distributions are first calculated using equations (192), (193), (194), (195), and (197). The heat transfer coefficients are calculated using equation (196) by successive approximation from the surface temperature calculation where

$$T_s = T_b + \frac{Q}{h_c} \quad (193)$$

with T_s = surface temperature, °F
 T_b = bulk temperature, °F
 Q = liner heat load, B/hr ft²
 h_c = heat transfer coefficient based on film temperature, B/hr ft² °F.

If the surface temperature exceeds the saturation temperature by more than 10 °F at any section, adjustments are made in entrance pressure, channel geometry, and flow rate and the calculation repeated until the desired conditions are achieved.

A general computer program was written for the calculations. It includes the boiling heat transfer calculations described below. The computer program, entitled Backside Cooling Program, is discussed in Appendix B.

BOILING HEAT TRANSFER

The problem with the backside cooling is in obtaining high heat transfer coefficients in order to hold down the liner coolant side surface temperature. With forced convection cooling extremely high velocities are required to achieve heat transfer coefficients from 75,000 to 100,000 B/hr ft² °F. This causes high entrance pressures, large frictional pressure loss in the coolant channel, large pumping power, etc. With surface boiling, high heat transfer coefficients may be obtained at much lower velocities and consequently with less pressure loss, pumping power etc. As a safety feature it should be noted that a small change in flow rate is not so critical as in forced convection (provided one is not too close to "burnout", which will be discussed below).

The general form of the boiling heat transfer curve for pool boiling can be found in any standard text on heat transfer. In the nucleate boiling region it is noted that the heat load rises very rapidly with a small change in ΔT_{sat} , thus, giving a large heat transfer coefficient. A point is reached called the "burnout" point, or the point of burnout heat load Q_{Bo} . For a condition of constant Q when this heat load is exceeded, there is a very large increase in ΔT_{sat} . The hot metal surface melts or vaporizes at this temperature, and thus, the term burnout point arises.

Two calculations are required in the design of a system for surface boiling heat transfer. Calculations must first be made to determine the surface temperature required to transfer the given heat load at a given coolant flow rate in a given channel. The burnout heat flux Q_{Bo} , must then be checked to see that for these conditions it exceeds the given heat load.

Since the heat load is essentially fixed by the gas temperature on the air side of the liner the first calculation reduces to a determination of the liner surface temperature for a given bulk coolant temperature, channel geometry and flow rate. The method of Rohsenow as described by Kreith (16) is used for this calculation. The heat flux is separated into two parts, the convective heat flux, and the boiling heat flux.

$$\text{Then} \quad Q_{Total} = Q_{convective} + Q_{boiling} \quad (199)$$

$$\text{Now} \quad Q_{convective} = h_c(T_s - T_b) \quad (200)$$

$$\text{thus} \quad Q_{boiling} = Q_{Total} - h_c(T_s - T_b) \quad (201)$$

In these equations, h_c is calculated from equation (196). Using the data of McAdams, et al (17) the boiling heat flux may be calculated using the equation

$$Q_{\text{Boiling}} = 0.2 (\Delta T_{\text{sat}})^{3.86} \quad \text{B/hr ft}^2 \quad (202)$$

Then

$$Q_{\text{Total}} = 0.2 (\Delta T_{\text{sat}})^{3.86} + h_c (T_s - T_b) \quad (203)$$

Using the results of the convective heat transfer calculations, T_b , h_c , and T_{sat} are known. Equation (203) is then solved by trial and error for T_s , the surface temperature.

Equations for predicting Q_{Bo} for various flow conditions do not show very good agreement. A summary by Kreith (16) of recent correlations gives the following equations:

$$Q_{\text{Bo}} = (4 \times 10^5 + 4800 \Delta T_{\text{sub}}) U^{1/3} \quad (204)$$

$$Q_{\text{Bo}} = 7000 \Delta T_{\text{sub}} U^{1/2} \quad (205)$$

$$Q_{\text{Bo}} = C G \times 10^{-6} M (\Delta T_{\text{sub}})^{0.22} \quad (206)$$

where $\Delta T_{\text{sub}} = T_{\text{sat}} - T_b$

U = velocity, ft/sec

G = mass flow rate, lbm/ft² hr

c and m are tabulated functions of the static pressure.

Another correlating equation by McGill and Sibbitt (18) for a tube with $L/D = 21$ is

$$Q_{\text{Bo}} = 0.475 U^{1/2} (\Delta T_{\text{sub}})^{0.28} \quad \text{B/in}^2 \text{ sec.} \quad (207)$$

To show the lack of agreement in the above equations for Q_{Bo} assume for equations (204) and (205)

$$\begin{aligned} \Delta T_{\text{sub}} &= 100^\circ \text{F} \\ U &= 20 \text{ ft/sec.} \end{aligned}$$

These values are in the range supposedly correlated by equations (204) and (205).

From equation (204):

$$Q_{Bo} = 2.38 \times 10^6 \text{ B/hr ft}^2$$

From equation (205):

$$Q_{Bo} = 3.14 \times 10^6 \text{ B/hr ft}^2$$

From equation (206), using the same values for u and ΔT_{sub} and a pressure of 500 psia

$$Q_{Bo} = 0.806 \times 10^6 \text{ B/hr ft}^2$$

From equation (207)

$$Q_{Bo} = 4.0 \times 10^6 \text{ B/hr ft}^2$$

The total variation is thus from 800,000 to 4,000,000 B/hr ft², a factor of 5.

As another approach, the effects of sub-cooling, velocity, and static pressure may be considered to be independent and another equation proposed.

Lowering the pool temperature below the saturation temperature increases Q_{Bo} for pool boiling. For degassed distilled water, lowering the pool temperature to $\Delta T_{sub} = 50^\circ\text{F}$ doubles Q_{Bo} and lowering it to $\Delta T_{sub} = 100^\circ\text{F}$ quadruples Q_{Bo} . An equation which correlates the data of M. E. Ellion (as given by Kreith, not taken from original report) is,

$$Q_{Bo} = 4 \times 10^5 + 5000 \Delta T_{sub} + 80 \Delta T_{sub}^2 \quad (208)$$

or

$$Q_{Bo} = 4 \times 10^5 \left(1 + 0.0125 \Delta T_{sub} + 0.0002 \Delta T_{sub}^2 \right) \quad (209)$$

Equation (209) is plotted in Figure 39. Ellion also gives data for water with some detergent added to lower the surface tension, the same type effect as would be obtained from gas in the water. An equation which correlates this data well is,

$$Q_{Bo} = 4 \times 10^5 \left(1 + 0.0217 \Delta T_{sub} \right) \quad (210)$$

Equation (210) is plotted in Figure 39.

Experiments by M. T. Ciechelli and C. F. Bonilla (19) using various liquids showed that, for pool boiling, increasing the static pressure increased Q_{Bo} up to a pressure of one-third the critical pressure. An equation which correlates their data well is,

$$Q_{Bo} = 4 \times 10^5 \left[1 + 30 \left(\frac{P_s}{P_c} \right) - 31 \left(\frac{P_s}{P_c} \right)^{1.33} \right] \quad (211)$$

where P_s/P_c = ratio of static to critical pressure. Equation (211) is plotted in Figure 40.

Combining equations (210) and (211) and using $u^{1/3}$ as a conservative choice for the velocity dependence gives

$$Q_{Bo} = 4 \times 10^5 (1 + 0.0217 \Delta T_{sub}) \left[1 + 30 \left(\frac{P_s}{P_c} \right) - 31 \left(\frac{P_s}{P_c} \right)^{1.33} \right] u^{1/3} \quad (212)$$

This equation is plotted for three values of p_s and four values of u in Figures 41, 42, and 43. For the values $u = 20$, $P_s = 500$, and $\Delta T_{sub} = 100$ as used in previous calculations, this equation gives

$$Q_{Bo} = 4 \times 10^5 (1 + 2.17) (1 + 4.68 - 2.64) (2.71)$$

$$\text{or } Q_{Bo} = 10.4 \times 10^6 \text{ B/hr ft}^2$$

Though this value is considerably higher than the highest value previously calculated from these conditions there is some indication it might be achieved. Equation (205) was proposed by Gunther (20), and for these flow conditions gave $Q_{Bo} = 3.14 \times 10^6 \text{ B/hr ft}^2$. In his article Gunther noted that unpublished data by McKenney for a tube with .012" walls gave burnout limits 'well above' those predicted by equation (205). This was attributed to the increased heat capacity of a heavier tube which handled transients better. Since the nozzle liner will have a minimum thickness of approximately .012" it is possible that equation (212) gives a better prediction of Q_{Bo} than those cited.

Since equation (212) is unproved and there is a large scatter in Q_{Bo} predictions, using suggested equations, several values of Q_{Bo} are calculated in the computer study so a comparison may be made.

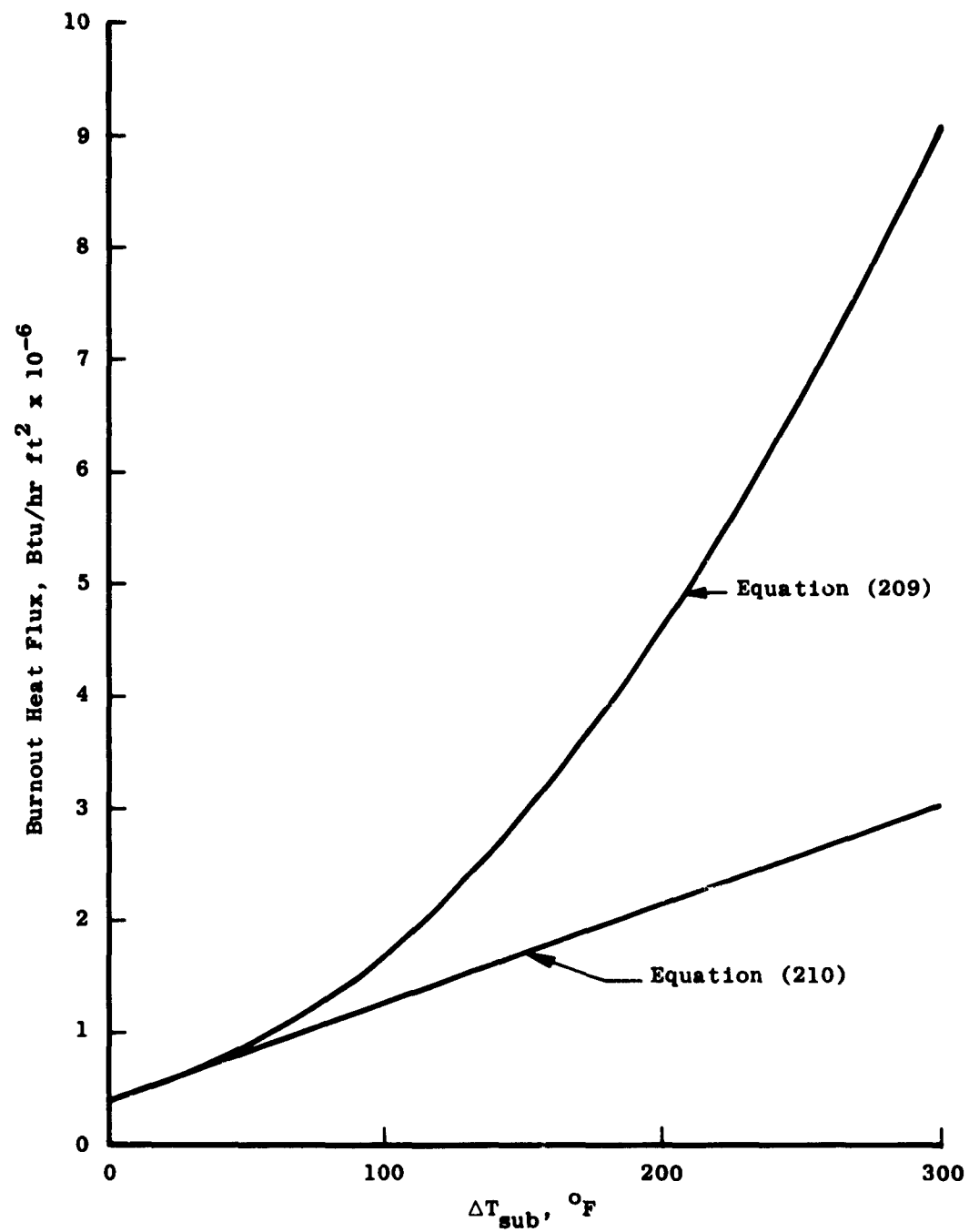


Fig. 39 Comparison of Burnout Heat Flux Equations

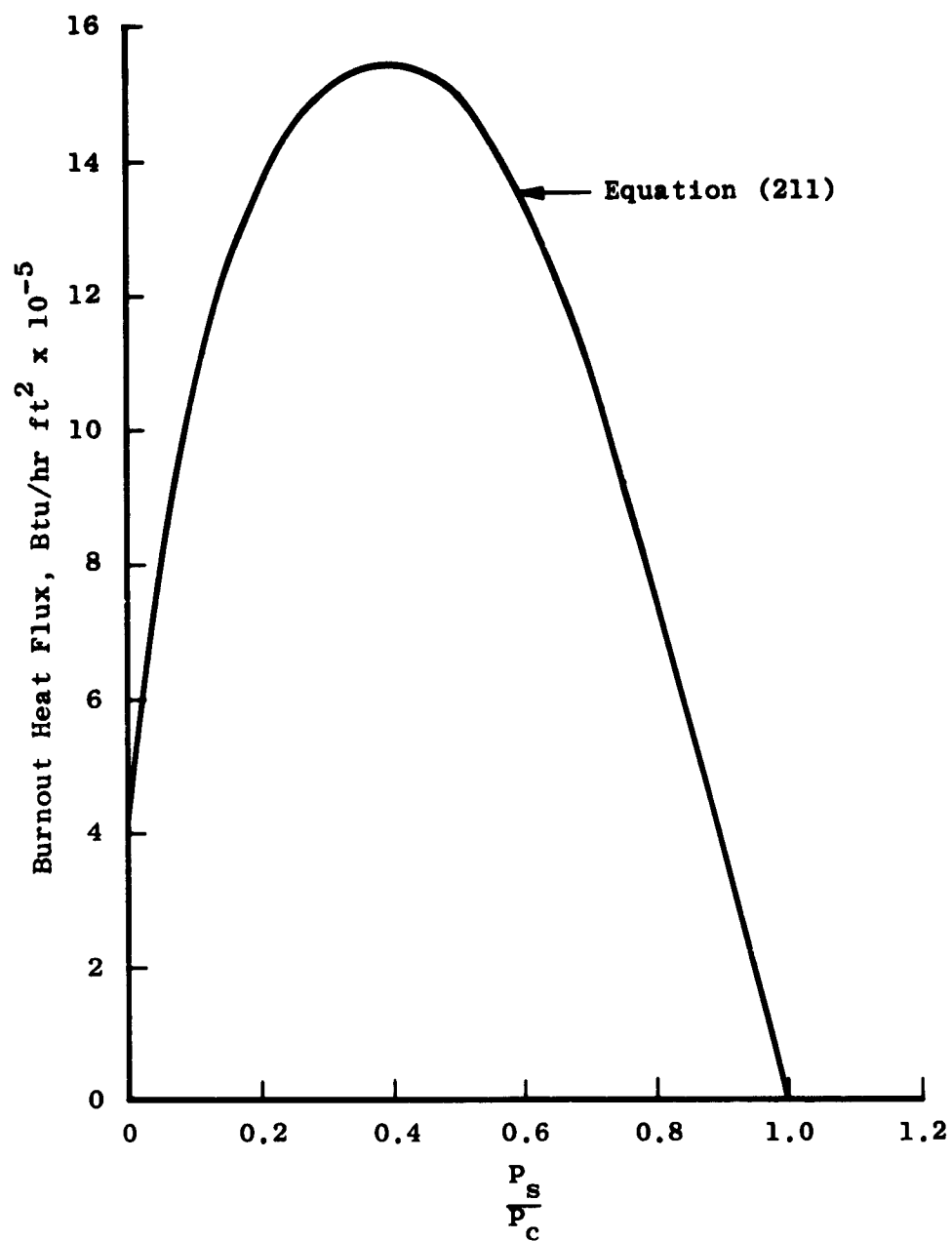


Fig. 40 Burnout Heat Flux versus Pressure Ratio

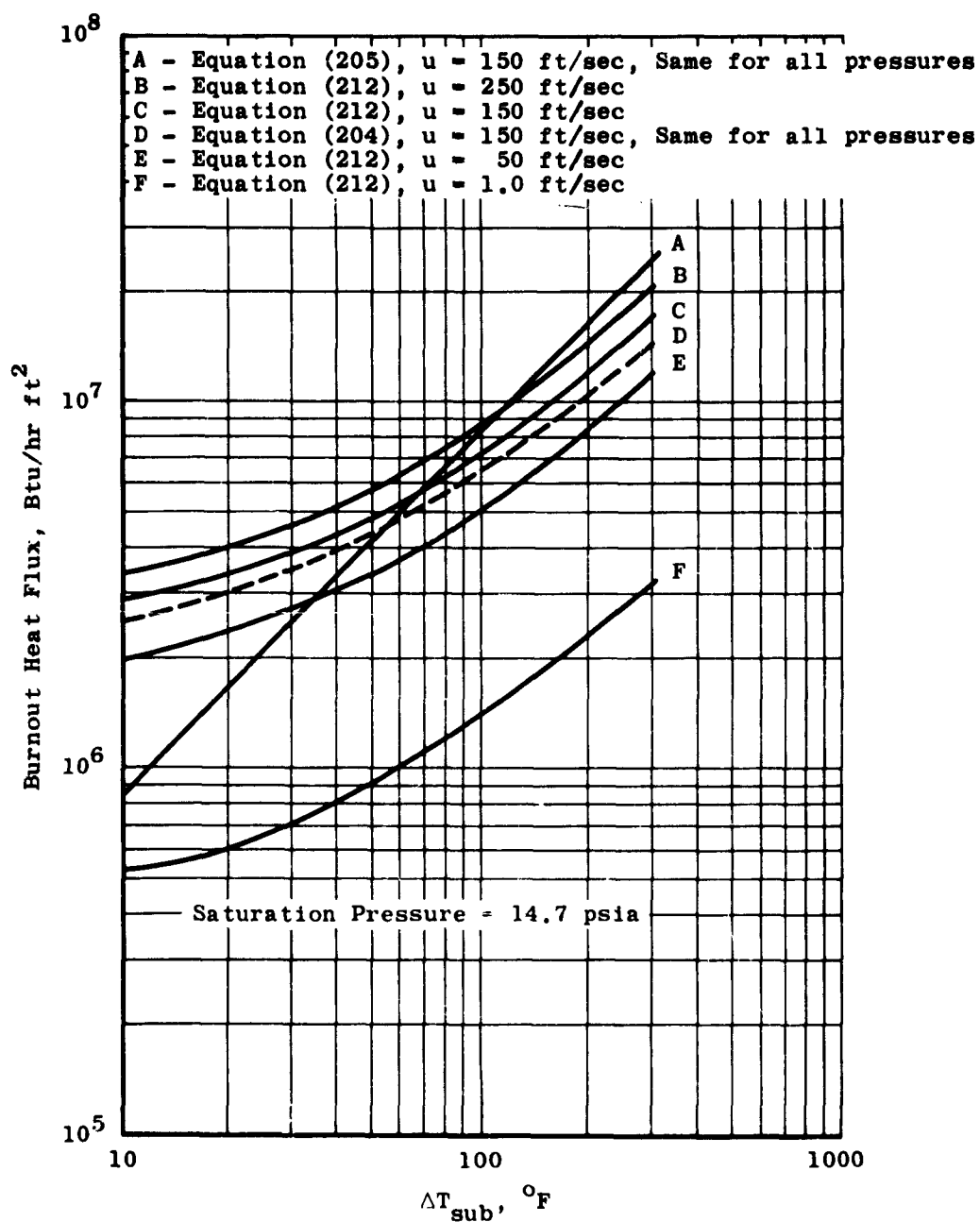


Fig. 41 Comparison of Burnout Heat Flux Equations

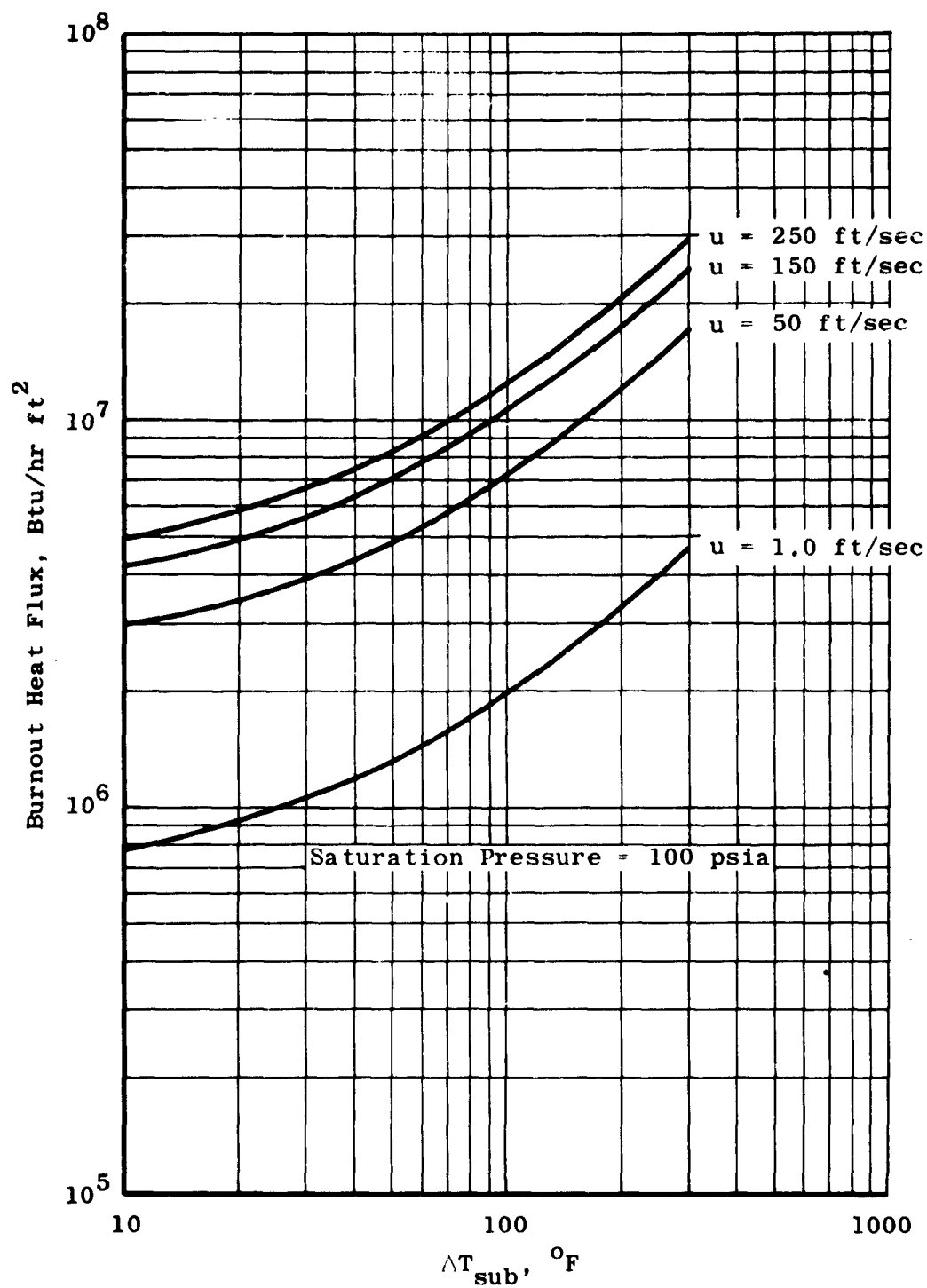


Fig. 42 Plot of Equation (212); Pressure = 100 psia

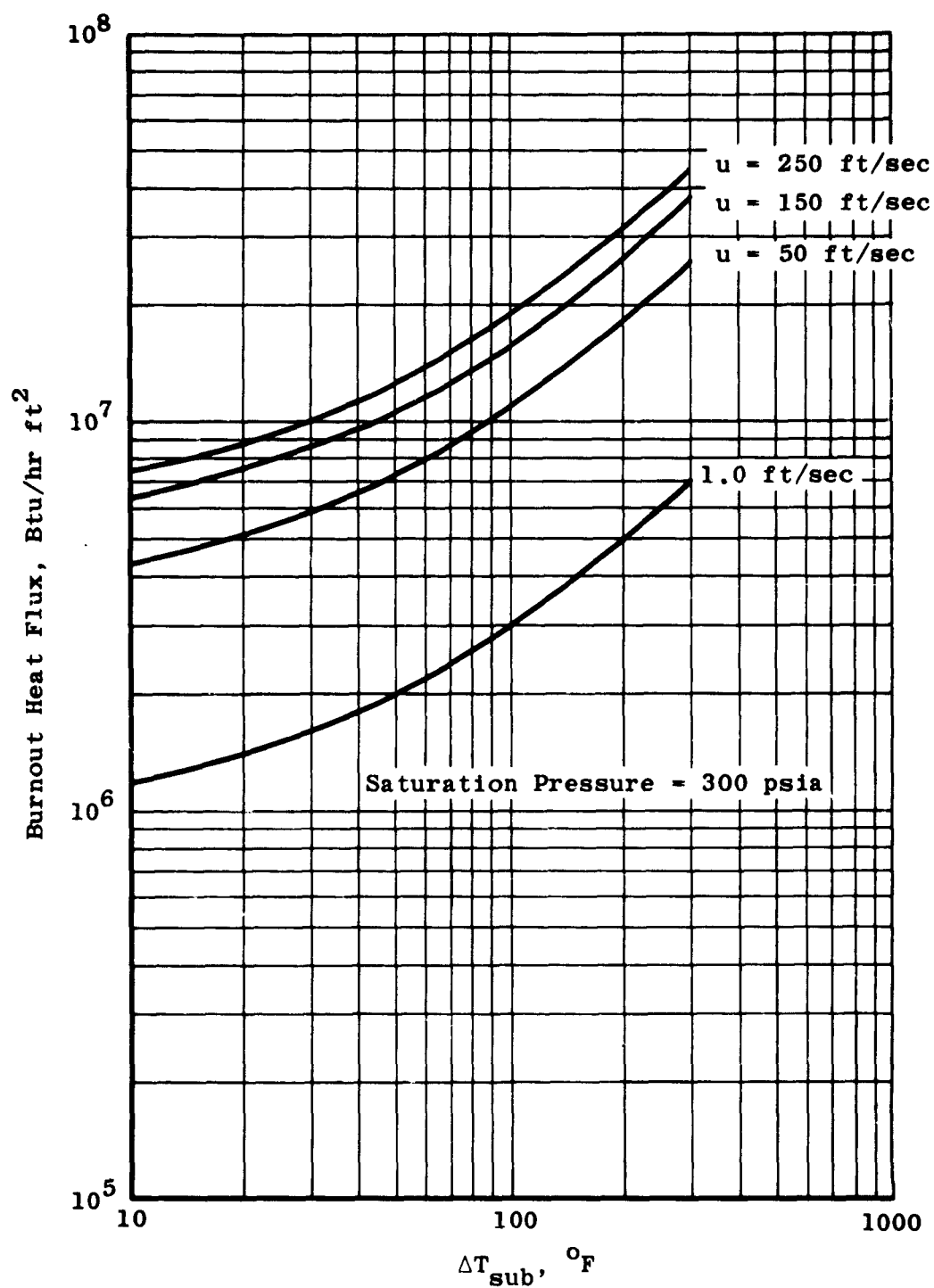


Fig. 43 Plot of Equation (212); Pressure = 300 psia

CONCLUSIONS

Studies of the backside cooling were made using the computer program. The results of three cases of particular interest are shown on pages 147 through 155. The nozzle used for the studies had an entrance diameter of 1.5 inches, a 46 degree converging section, a .25 inch diameter throat and a 7.5 degree diverging section. The heat load distribution assumed is given under Q in the input data.

Since subcooling and velocity of the coolant both affect the boiling burnout heat load, a flow rate of 20 lbs/sec gave good results for the cases with boiling. A flow rate of 25 lbs/sec was used for the third case where boiling was not allowed.

The first case presented shows the conditions necessary to achieve approximately the required boiling burnout heat load with equation (212) used for Q_{Bo} . These are summarized as follows:

Coolant Flow Rate = 20 lbm/sec₂
 Coolant Annulus Area = 0.35 in²
 Coolant Velocity = 133 ft/sec
 Maximum Surface Temperature = 489 °F
 Surface Coefficient = 76,000 B/hr ft² °F.

The second case presented shows the conditions necessary to achieve the required boiling burnout heat load with equation (205) used for Q_{Bo} . These are summarized as follows:

Coolant Flow Rate = 20 lbm/sec
 Coolant Annulus Area = 0.200 in²
 Coolant Velocity = 232 ft/sec
 Maximum Surface Temperature = 498 °F
 Surface Coefficient = 75,000 B/hr ft² °F.

The third case presented shows the conditions necessary to achieve forced convection heat transfer at all sections. These are summarized as follows:

Coolant Flow Rate = 25 lbm/sec
 Coolant Annulus Area = 0.160 in²
 Coolant Velocity = 363 ft/sec
 Maximum Surface Temperature = 478 °F
 Surface Coefficient = 78,000 B/hr ft² °F.

Several conclusions may be drawn from these calculations based on the heat load and coolant used:

- (1) The maximum heat transfer coefficient obtainable while satisfying the burnout requirements is $\sim 80,000$ B/hr ft² °F.
- (2) No appreciable reduction in surface temperature may be obtained by boiling as compared with high velocity forced convection.

- (3) The required inlet pressure to prevent boiling is ~ 1620 psia at a flow rate of 25 lbm/sec and a cooling annulus of 0.16 in^2 .
- (4) The required inlet pressure with boiling is ~ 325 psia, and little is gained by using equation (212) rather than equation (205) for the burnout calculation.
- (5) There is room for doubt that this heat load may be transferred by boiling without burnout, due to the fact that equation (204) predicts burnout in all cases calculated where boiling is allowed.

It is, therefore, recommended that provisions be made to supply the coolant water at sufficient pressure to prevent surface boiling and the coolant annulus be designed for high velocity, high pressure, forced convection heat transfer.

BIBLIOGRAPHY

- (1) Cohen and Reshotko, NACA 1289, 1956.
- (2) Bartz, D. R., A Simple Equation for Rapid Estimation of Rocket Nozzle Convective Heat Transfer Coefficients, Jet Propulsion, January 1957.
- (3) Eckert and Drake, Heat and Mass Transfer, McGraw-Hill Publishing Company.
- (4) Kivel, B. and Bailey, K., Tables of Radiation from High Temperature Air, Avco Research Report 21.
- (5) Timoshenko, S., Strength of Materials - Part II, D. Van Nostrand Company, 1956.
- (6) Coffin, L. F., Thermal Stress and Thermal Stress Fatigue, Proceedings for Short Course Materials Engineering Design for High Temperatures, Pennsylvania State University, June 1958.
- (7) Metals Handbook, 8th Edition, Volume 1, American Society for Metals, 1961.
- (8) Materials Selector Issue, Materials in Design Engineering, Reinhold Publishing Corporation, October 1962.
- (9) Glauert, M. B., The Wall Jet, Journal of Fluid Mechanics, Volume 1, 1956.
- (10) Bakke, P., An Experimental Investigation of a Wall Jet, Journal of Fluid Mechanics, Volume 2, 1957.
- (11) Schwarz, W. H. and Cosart, W. P., The Two-Dimensional Wall Jet, Journal of Fluid Mechanics, Volume 10, February-June, 1961.
- (12) Hagler, G. E., M. S. Thesis - To be published, Chemical Engineering Department, University of Tennessee.
- (13) Oswatitsch, K. and Rothstein, W., Flow Pattern in a Converging-Diverging Nozzle, National Advisory Committee for Aeronautics, Technical Memorandum Number 1215.
- (14) Yuan, S. W., Cooling by Protective Fluid Films, Turbulent Flows and Heat Transfer, Princeton University Press, 1959.
- (15) Van Driest, E. R., Investigation of Laminar Boundary Layer in Compressible Fluids Using the Crocco Method, NACA TN 2597, 1952.

- (16) Kreith, F., Principles of Heat Transfer, International Textbook Company, 1960.
- (17) McAdams, W. M., et al., Heat Transfer at High Rates to Water With Surface Boiling, Industrial Engineering Chemistry, Volume 41, 1945.
- (18) McGill, H. L. and Sebbitt, W. L., Argonne National Laboratory, Reports ANL-4603, 1951 and ANL-4915, 1952.
- (19) Clechelli, M. T. and Bonilla, C. F., Heat Transfer to Liquids Boiling Under Pressure, AIChE Transactions, Volume 41, 1945.
- (20) Gunther, F. C., Photographic Study of Surface Boiling Heat Transfer to Water With Forced Convection, Transactions of The American Society of Mechanical Engineers, February 1951.

APPENDIX A

**FORTRAN PROGRAMS
FOR
NOZZLE AND RIB STRESSES**

NOZZLE STRESS PROGRAM

This computer program is written in the Fortran II language. It accepts data which describe the liner, rib, and sleeve as to dimensions, configuration, materials, heat load, etc. It then calculates the principle stresses, octahedral shear stresses, etc. as described in the Output section below. The equations used for the calculations are given in the Stress Analysis discussion under Case 1 and Case 2.

INPUT DATA

First Card

The first data card is a title card with up to forty-nine alphabetic or numeric characters to identify the case being studied.

Second Card

The second data card gives, according to FORMAT (E12.1, E12.1, E12.1, E12.1, E12.1, E12.1) the following data in order:

- PT - The airside pressure at the throat, psi.
- Q - The liner heat load, Btu/hr ft².
- D11 - The liner inside diameter, inches.
- DS - Liner inside diameter at nozzle inlet, inches.
- DC - Coolant annulus width, radially, inches.
- TCOOL - Coolant bulk temperature, °F.

Third Card

The third data card gives, according to FORMAT (E12.1, E12.1, E12.1, E12.1, E12.1, E12.1) the following data in order:

- C1 - Liner thermal conductivity at temperature T11, B/hr ft °F.
- C2 - Liner thermal conductivity at temperature T12, B/hr ft °F.
- C3 - Liner thermal conductivity at temperature T13, B/hr ft °F.
- A1 - Liner thermal expansion coefficient at temperature T11, in/in °F.
- A2 - Liner thermal expansion coefficient at temperature T12, in/in °F.
- A3 - Liner thermal expansion coefficient at temperature T13, in/in °F.

Fourth Card

The fourth data card gives, according to FORMAT (E12.1, E12.1, E12.1, E12.1, E12.1, E12.1) the following data in order:

- E1 - Liner modulus of elasticity at temperature T11, psi.
- E2 - Liner modulus of elasticity at temperature T12, psi.
- E3 - Liner modulus of elasticity at temperature T13, psi.
- U - Poisson's ratio for the liner.
- ES - Sleeve modulus of elasticity, psi.
- ER - Rib modulus of elasticity, psi.

Fifth Card

The fifth data card gives, according to FORMAT (E12.1, E12.1, E12.1, E12.1, E12.1, E12.1) the following data in order:

HT - The limiting liner high temperature, °F.
 HW - The coolant-liner heat transfer coefficient, B/hr ft² °F.
 T11- First material property reference temperature, °F.
 T12- Second material property reference temperature, °F.
 T13- Third material property reference temperature, °F.
 TYPE-A number from 1-6 inclusive which specifies the configuration for which calculations are wanted. These are as follows:
 1.0 = circumferential ribs only
 2.0 = longitudinal ribs only
 3.0 = unrestrained liner and circumferential ribs
 4.0 = unrestrained liner and longitudinal ribs
 5.0 = unrestrained only
 6.0 = unrestrained, longitudinal ribs and circumferential ribs.

Sixth Card

The sixth data card gives, according to FORMAT (E12.1, E12.1, E12.1, E12.1, E12.1) the following data in order:

TR - Rib thickness, inches.
 DL - Distance between circumferential ribs, inches.
 AR - Cross-sectional area of circumferential ribs, inches.
 THK- Stepwise increase in thickness of liner for calculations, inches.
 T10- Starting thickness of liner for calculations, inches.

Seventh Card

The seventh card gives, according to FORMAT (E12.1, E12.1) the following data in order:

DR - Distance between longitudinal ribs, inches.
 ST - Liner thrust stress for circumferential ribs, psi.

PROGRAM OPERATION

The program operates automatically using the above input data for each case.

Starting with a liner thickness given by T10 this thickness is increased in seven steps by the amount THK. The sleeve thickness is constant at 1.0 inches, as the configurations with ribs will be fully restrained.

For each liner thickness the calculations for stresses are made for zero coolant pressure and then for coolant pressure equal to air pressure. Other pressure values may be used by altering statement number 49. If the equal pressure case is not desired the program is run with SENSE SWITCH 2 ON.

The program is so written that if the limiting high liner temperature HT is exceeded at the inside surface the maximum possible liner thickness which does not cause an over temperature is calculated and used for the last thickness.

To speed up the running of the program for cases which do not involve circumferential ribs it is run with SENSE SWITCH 3 ON. This by-passes the summing operations necessary for circumferential ribs.

OUTPUT

Unrestrained Nozzle:

PB - Coolant pressure, psi.
 T1 - Liner thickness, inches.
 TI - Liner inside surface temperature, °F.
 TB - Liner outside surface temperature, °F.
 SPC1-Principle circumferential stress, inside surface, psi.
 SPC2-Principle circumferential stress, outside surface, psi.
 SPL1-Principle longitudinal stress, inside surface, psi.
 SPL2-Principle longitudinal stress, outside surface, psi.
 SIM -Octahedral shear stress, inside surface, psi.
 S2M -Octahedral shear stress, outside surface, psi.

Longitudinal Rib Nozzle:

PB - Coolant pressure, psi.
 T2 - Sleeve thickness.
 T1 - Liner thickness, inches.
 TI - Liner inside surface temperature, °F.
 TB - Liner outside surface temperature, °F.
 DR - Distance between ribs, inches.
 SIP1-Principle circumferential stress, inside surface over rib, psi.
 SIP2-Principle circumferential stress, outside surface over rib, psi.
 S2PC1-Principle circumferential stress, inside surface between ribs, psi.
 S2PC2-Principle circumferential stress, outside surface between ribs, psi.
 SPL1- Principle longitudinal stress, inside surface, psi.
 SPL2- Principle longitudinal stress, outside surface, psi.
 SR12- Pressure between liner and rib, psi.
 SSC22-Sleeve bending stress (negligible), psi.
 SLS - Sleeve longitudinal stress (negligible), psi.
 SIM1- Octahedral shear, inside surface over rib, psi.
 SIM2- Octahedral shear, outside surface over rib, psi.
 S2M1- Octahedral shear, inside surface between ribs, psi.
 S2M2- Octahedral shear, outside surface between ribs, psi.

Circumferential Rib Nozzle:

PB - Coolant pressure, psi.
 T2 - Sleeve thickness, inches.
 T1 - Liner thickness, inches.

TI - Liner inside surface temperature, °F.
TB - Liner outside surface temperature, °F.
DL - Distance between ribs, inches.
S1LC1-Principle circumferential stress, inside surface over rib, psi.
S1LC2-Principle circumferential stress, outside surface over rib, psi.
S2LC1-Principle circumferential stress, inside surface between ribs, psi.
S2LC2-Principle circumferential stress, outside surface between ribs, psi.
S1LL1-Principle longitudinal stress, inside surface over rib, psi.
S1LL2-Principle longitudinal stress, outside surface over rib, psi.
S2LL1-Principle longitudinal stress, inside surface between ribs, psi.
S2LL2-Principle longitudinal stress, outside surface between ribs, psi.
S1M1 -Octahedral shear, inside surface over rib, psi.
S1M2 -Octahedral shear, outside surface over rib, psi.
S2M1 -Octahedral shear, inside surface between ribs, psi.
S2M2 -Octahedral shear, outside surface between ribs, psi.
B - Parameter used in stress calculation (See derivation).
P - Force per inch of length on ribs, lb/in.
PII - Bending stress on liner at rib, psi.
SR2I- Pressure between liner and rib, radial, psi.

The program and a sample output for longitudinal rib calculation follow on page 114.

```

C C H.C. ROLAND * * NOZZLE STRESS PROGRAM 1
C FIRST INPUT IS TITLE WITH UP TO 49 ALPHAMERIC CHARACTERS 2
C TYPE 6.0 = UNRESTRAINED, LONGITUDINAL, AND CIRCUMFERENTIAL RIBS 3
C 5.0 = UNRESTRAINED ONLY 4
C 4.0 = UNRESTRAINED AND LONGITUDINAL RIBS, SENSE SWITCH 3 ON 5
C 3.0 = UNRESTRAINED AND CIRCUMFERENTIAL RIBS 6
C 2.0 = LONGITUDINAL RIBS ONLY, SENSE SWITCH 3 ON 7
C 1.0 = CIRCUMFERENTIAL RIBS ONLY 8
C SENSE SWITCH 2 ON BYPASSES AUTOMATIC PRESSURE EQUALIZATION 8A
90 FORMAT (49H ) 9
91 FORMAT (E12.1, E12.1, E12.1, E12.1, E12.1, E12.1) 10
92 FORMAT (E12.1, E12.1, E12.1, E12.1, E12.1, E12.1) 11
93 FORMAT (10H INPUT DATA) 12
100 FORMAT (6X, 2HPB, 12X, 2HT1, 9X, 2HT1, 9X, 2HTB) 13
101 FORMAT (3X, 4HSPC1, 7X, 4HSPC2, 9X, 4HSP1, 8X, 4HSP2, 9X, 3HSM1, 9X, 3HSM2) 14
102 FORMAT (19H UNRESTRAINED NOZZLE) 15
103 FORMAT (F12.3, F12.3, F12.3, F12.3, F12.3, F12.3) 16
104 FORMAT (F12.3, F12.3, F12.3, F12.3) 17
110 FORMAT (23H LONGITUDINAL RIB NOZZLE) 18
111 FORMAT (6X, 2HPB, 12X, 2HT2, 10X, 2HT1, 8X, 2HT1, 10X, 2HTB, 13X, 2HDL) 19
112 FORMAT (3X, 5HSPC1, 7X, 5HSPC2, 7X, 5HSPC1, 7X, 5HSPC2) 20
113 FORMAT (3X, 4HSP1, 8X, 4HSP2, 8X, 4HSP1, 7X, 5HSPC2, 9X, 3HSP1) 21
114 FORMAT (3X, 4HSP1, 8X, 4HSP2, 8X, 4HSP1, 8X, 4HSP2) 22
115 FORMAT (F12.3, F12.3, F12.3, F12.3, F12.3, F12.3) 23
120 FORMAT (26H CIRCUMFERENTIAL RIB NOZZLE) 24
121 FORMAT (6X, 2HPB, 12X, 2HT2, 10X, 2HT1, 8X, 2HT1, 10X, 2HTB, 13X, 2HDL) 25
126 FORMAT (6X, 1HB, 11X, 1HP, 9X, 3HP1, 8X, 4HSP2) 26
128 FORMAT (5X, 5HSP1, 7X, 5HSP2, 7X, 5HSP1, 7X, 5HSP2) 27
129 FORMAT (5X, 5HSP1, 7X, 5HSP2, 7X, 5HSP1, 7X, 5HSP2) 28
130 FORMAT (E12.1, E12.1) 29
DO 51 I=1, 100 30
READ 90 31
PUNCH 90 32
READ 91, PT, Q, D11, DS, DC, TCOOL 33
READ 91, C1, C2, C3, A1, A2, A3 34
READ 91, E1, E2, E3, U, ES, ER 35
READ 91, HT, HW, T11, T12, T13, TYPE 36
READ 92, TR, DL, AR, THK, T10 37
READ 130, DR, ST 38
PUNCH 93 39
PUNCH 91, PT, Q, D11, DS, DC, TCOOL 40
PUNCH 91, C1, C2, C3, A1, A2, A3 41
PUNCH 91, E1, E2, E3, U, ES, ER 42
PUNCH 91, HT, HW, T11, T12, T13, TYPE 43
PUNCH 92, TR, DL, AR, THK, T10 44
PUNCH 130, DR, ST 45
COUNT=0.0 46
T1=T10 47
DO 52 J=1, 8 48
IF (J-1) 8, 8, 2 49
2 T1=T1+THK 50
8 D12=D11+2.*T1 51
DRCAL=SQRTF(D12*T1) 52
IF (DRCAL) 3, 7, 7 53
3 DR=DRCAL 54
7 RL=LOGF(D12/D11) 55

```

	DLRAT=DL/TR	56
	TLRAT=TR/DL	57
	TRL=DC/6.	58
	IF (TRL-DH/4.) 4,4,5	59
4	GO TO 6	60
5	TRL=DR/4.	61
6	DT1=Q*D11*RL/(24.*C2)	62
	TB=TCOOL+Q/HW	63
	T1=TB+DT1	64
	TM=DT1/LOGF(T1/TB)	65
	IF (TM-T12) 10,30,20	66
10	DO 15 K=1,3	67
	TC=(TM-T11)/(T12-T11)	68
	CM=C1+TC*(C2-C1)	69
	DT1=Q*D11*RL/(24.*CM)	70
	T1=TB+DT1	71
	TM=DT1/LOGF(T1/TB)	72
	IF (TM-T12) 15,30,20	73
15	CONTINUE	74
	GO TO 30	75
20	DO 25 L=1,3	76
	TC=(TM-T12)/(T13-T12)	77
	CM=C2+TC*(C3-C2)	78
	DT1=Q*D11*RL/(24.*CM)	79
	T1=TB+DT1	80
	TM=DT1/LOGF(T1/TB)	81
	IF (TM-T12) 10,30,25	82
25	CONTINUE	83
	GO TO 35	84
30	TC=(TM-T11)/(T12-T11)	85
	AL=A1+TC*(A2-A1)	86
	EL=E1+TC*(E2-E1)	87
	IF (T1-HT) 40,40,32	88
32	COUNT=COUNT+1.	89
33	T1=T1-.001	90
	D12=D11+2.*T1	91
	RL=LOGF(D12/D11)	92
	DT1=Q*D11*RL/(24.*CM)	93
	T1=TB+DT1	94
	IF (T1-HT) 34,34,33	95
34	IF (COUNT-1.5) 40,40,38	96
38	GO TO 51	97
35	TC=(TM-T12)/(T13-T12)	98
	AL=A2+TC*(A3-A2)	99
	EL=E2+TC*(E3-E2)	100
	IF (T1-HT) 40,40,32	101
40	T2=1.0	102
	DTM=TM-TCOOL	103
	D22=D12+2.*DC	104
	D23=D22+2.*T2	105
	RMN=(D11+T1)/2.	106
	IF (SENSE SWITCH 3) 81,41	107
41	B=SQRTF(SQRTF(2.73/((RMN**2)*(T1**2))))	108
	D=0.	109
	F=1.	110
	SUM1=-.5	111

```

SUM2=0. 112
DO 80 LM=1,8 113
ARG1=B*D*DL 114
ARG2=B*F*DL/2. 115
SUM1=SUM1+(2.718**(-ARG1))*(COSF(ARG1)+SINF(ARG1)) 116
SUM2=SUM2+(2.718**(-ARG2))*(COSF(ARG2)+SINF(ARG2)) 117
D=D+1. 118
F=F+2. 119
80 CONTINUE 120
A=B*DL 121
CHB=.5*((2.718**A)+(2.718**(-A))) 122
CB=COSF(B*DL) 123
SHB=.5*((2.718**A)-(2.718**(-A))) 124
SB=SINF(B*DL) 125
81 PB=0. 126
D12SQ=(D12**2) 127
D11SQ=(D11**2) 128
D22SQ=(D22**2) 129
D23SQ=(D23**2) 130
D5SQ=(D5**2) 131
Z1=(D12SQ+D11SQ)/(D12SQ-D11SQ) 132
Z2=D12SQ/(D12SQ-D11SQ) 133
Z3=D11SQ/(D12SQ-D11SQ) 134
Z4=(D22SQ+D12SQ)/(D22SQ-D12SQ) 135
Z5=D22SQ/(D22SQ-D12SQ) 136
Z6=D12SQ/(D22SQ-D12SQ) 137
Z7=(D23SQ+D22SQ)/(D23SQ-D22SQ) 138
Z8=(D12SQ-D11SQ)/(D23SQ-D22SQ) 139
Z9=(D5SQ-D11SQ)/(D12SQ-D11SQ) 140
Z10=(D5SQ-D12SQ)/(D12SQ-D11SQ) 141
F1=AL*DT1*EL/(2.*(1.-U)*RL) 142
F2=1.-2.*Z3*RL 143
F4=1.-2.*Z2*RL 144
DO 50 N=1,2 145
IF (N-1) 67,67,68 146
68 IF (SENSE SWITCH 2) 69,67 147
69 GO TO 50 148
67 IF (TYPE-2.5) 70,60,60 149
70 IF (TYPE-1.5) 48,42,42 150
60 PS=PT/.528 151
28 SPC1=Z1*PT-2.*Z2*PB+F1*F4 152
SPC2=2.*Z3*PT-Z1*PB+F1*F2 153
SPL12=(PS/(DS-D11))*(.528*DS-D11)*Z9) 154
SPL13=(PS/(DS-D11))*3148*((DS**3)-(D11**3))/(D12SQ-D11SQ) 155
SPL1=F1*F4-(SPL12+SPL13)+PB*Z10 156
SPL2=F1*F2-(SPL12+SPL13)+PB*Z10 157
S1M=SQRTE(((SPC1-SPL1)**2)+((SPC1+PT)**2)+((SPL1+PT)**2))/3. 158
S2M=SQRTE(((SPC2-SPL2)**2)+((SPC2+PB)**2)+((SPL2+PB)**2))/3. 159
PUNCH 102 160
PUNCH 100 161
PUNCH 104,PB,T1,T1,TB 162
PUNCH 101 163
PUNCH 103,SPC1,SPC2,SPL1,SPL2,S1M,S2M 164
29 IF (TYPE-5.5) 61,42,42 165
61 IF (TYPE-4.5) 62,49,49 166
62 IF (TYPE-3.5) 48,42,42 167

```

```

42  P1N=2.*Z3*PT-Z1*PB-Z7*EL*D22*PB/(ES*D12)      168
    P1D=Z1+Z7*EL/ES      169
    P1=P1N/P1D      170
    P2=P1*D12/D22      171
    S11=Z1*PT-2.*Z2*(PB+P1)      172
    S12=2.*Z3*PT-Z1*(PB+P1)      173
    S22=Z7*(PB+P2)      174
    P1P=F1*F2/(Z1+Z7*EL/ES)      175
    S11P=F1*F4-2.*Z2*P1P      176
    S12P=F1*F2-Z1*P1P      177
    S22P=Z7*P1P*D12/D22      178
    SB11=.5*P1*((DR/T1)**2)      179
    SB12=-SB11      180
    SB11P=.5*P1P*((DR/T1)**2)      181
    SB12P=-SB11P      182
    SR12=-(P1+P1P)*(DR/TR)      183
    SLT1=F1*F4      184
    SLT2=F1*F2      185
    SILT=-AL*DTM*EL/(1.+Z8*EL/ES)      186
    S22PP=Z7*(PB+(D12/D22)*(P1+P1P))      187
    SB22=-.5*(D22/D12)*(P1+P1P)*((DR/T2)**2)      188
    SB22P=-.5*SB22      189
    S2LT=AL*DTM*EL/(EL/ES+1.+Z8)      190
    S1PC1=S11+S11P+SB11+SB11P      191
    S1PC2=S12+S12P+SB12+SB12P      192
    S2PC1=S11+S11P+.5*SB12+.5*SB12P      193
    S2PC2=S12+S12P+.5*SB11+.5*SB11P      194
    SPL1=SLT1+SILT      195
    SPL2=SLT2+SILT      196
    SSC22=S22P+SB22P      197
    SLS=S2LT      198
    S1M1=SQRTF(((S1PC1-SPL1)**2)+((S1PC1+PT)**2)+((SPL1+PT)**2))/3.      199
    S1M2=SQRTF(((S1PC2-SPL2)**2)+((S1PC2-SR12)**2)+((SPL2-SR12)**2))      200
    S1M2=S1M2/3.      201
    S2M1=SQRTF(((S2PC1-SPL1)**2)+((S2PC1+PT)**2)+((SPL1+PT)**2))/3.      202
    S2M2=SQRTF(((S2PC2-SPL2)**2)+((SPL2+PB)**2)+((S2PC2+PB)**2))/3.      203
    PUNCH 110      204
    PUNCH 111      205
    PUNCH 103,PB,T2,T1,T1,TR,DR      206
    PUNCH 112      207
    PUNCH 104,S1PC1,S1PC2,S2PC1,S2PC2      208
    PUNCH 113      209
    PUNCH 115,SPL1,SPL2,SR12,SSC22,SLS      210
    PUNCH 114      211
    PUNCH 104,S1M1,S1M2,S2M1,S2M2      212
    IF (TYPE-5.5) 64,48,48      213
64  GO TO 40      214
48  PNI=PT-PB+AL*DTM*EL*T1/4*RN      215
    P=PNI/(3*SUM1+T1/AR)      216
    PMO=P*(SUM-SB)/(4.*B*(CH3-CB))      217
    P11=6.*PMO/(T1**2)      218
    S1LL1=F1*F4+P11*ST      219
    S1LL2=F1*F2-P11*ST      220
    S2LL1=F1*F4-.5*P11*ST      221
    S2LL2=F1*F2+.5*P11*ST      222
    SR21=-P/TR      223

```

	S1LC1=P*RMN/AR-AL*DTM*EL+F1*F4	224
	S1LC2=P*RMN/AR-AL*DTM*EL+F1*F2	225
	SLC21=(PT-PB)*RMN/T1+F1*F2-P*B*RMN*SUM2/T1	226
	SLC23=(PT-PB)*RMN/T1+F1*F4-P*B*RMN*SUM2/T1	227
	S2LC1=SLC23	228
	S2LC2=SLC21	229
	S1M1=SQRTF(((S1LL1-S1LC1)**2)+((S1LL1+PT)**2)+((S1LC1+PT)**2))/3.	230
	S1M4=SQRTF(((S1LL2-S1LC2)**2)+((S1LL2-SR21)**2)+((S1LC2-SR21)**2))	231
	S1M2=S1M4/3.	232
	S2M1=SQRTF(((S2LL1-S2LC1)**2)+((S2LL1+PT)**2)+((S2LC1+PT)**2))/3.	233
	S2M2=SQRTF(((S2LL2-S2LC2)**2)+((S2LL2+PB)**2)+((S2LC2+PB)**2))/3.	234
	PUNCH 120	235
	PUNCH 121	236
	PUNCH 103,PB,T2,T1,TI,TB,DL	237
	PUNCH 129	238
	PUNCH 104,S1LC1,S1LC2,S2LC1,S2LC2	239
	PUNCH 128	240
	PUNCH 104,S1LL1,S1LL2,S2LL1,S2LL2	241
	PUNCH 114	242
	PUNCH 104,S1M1,S1M2,S2M1,S2M2	243
87	PUNCH 126	244
	PUNCH 104,B,P,P11,SR21	245
49	PB=PT	246
50	CONTINUE	247
52	CONTINUE	248
51	CONTINUE	249
	END	250

H.C.ROLAND * NOZZLE-STRESS MO-TI 100ATM .78DIA
INPUT DATA

15000.0E-01 20000.0E+03 78400.0E-05 15000.0E-04 12500.0E-05 85000.0E-03
78000.0E-03 65000.0E-03 52000.0E-03 30000.0E-10 30000.0E-10 30000.0E-10
7000.0E+03 35000.0E+03 22000.0E+03 31000.0E-05 30000.0E+03 47000.0E+03
25000.0E-01 15000.0E+01 80000.0E-03 15000.0E-01 35000.0E-01 20000.0E-04
30000.0E-06 30000.0E-05 10000.0E-06 50000.0E-07 10000.0E-06

LONGITUDINAL RIB NOZZLE

PB	T2	T1	T1	TB	DR
0.000	.150	.010	435.298	218.333	.089
S1PC1	S1PC2	S2PC1	S2PC2		
37273.467	-58848.215	-66838.347	45263.599		
SPL1	SPL2	SR12	SSC22	SLS	
-50481.115	-8013.607	-5160.472	1630.772	1278.018	
S1M1	S1M2	S2M1	S2M2		
35906.323	24663.672	27760.480	23455.556		

LONGITUDINAL RIB NOZZLE

PB	T2	T1	T1	TB	DR
0.000	.150	.015	543.416	218.333	.110
S1PC1	S1PC2	S2PC1	S2PC2		
6922.805	-44673.096	-79588.817	41838.526		
SPL1	SPL2	SR12	SSC22	SLS	
-65091.374	-1964.038	-7829.187	3367.455	2180.655	
S1M1	S1M2	S2M1	S2M2		
32146.945	18903.071	33914.763	20201.713		

LONGITUDINAL RIB NOZZLE

PB	T2	T1	T1	TB	DR
0.000	.150	.020	651.199	218.333	.128
S1PC1	S1PC2	S2PC1	S2PC2		
-13598.211	-38471.732	-95691.718	43621.775		
SPL1	SPL2	SR12	SSC22	SLS	
-79037.995	4389.749	-11368.618	5602.869	3208.340	
S1M1	S1M2	S2M1	S2M2		
34060.160	17701.253	41044.070	19610.878		

LONGITUDINAL RIB NOZZLE

PB	T2	T1	T1	TB	DR
0.000	.150	.025	758.614	218.333	.144
S1PC1	S1PC2	S2PC1	S2PC2		
-30158.264	-34726.437	-112463.090	47578.395		
SPL1	SPL2	SR12	SSC22	SLS	
-92445.664	10936.377	-15833.241	8275.086	4336.720	
S1M1	S1M2	S2M1	S2M2		
37965.063	18733.969	48286.856	20346.836		

LONGITUDINAL RIB NOZZLE

PB	T2	T1	T1	TB	DR
0.000	.150	.030	865.640	218.333	.159
S1PC1	S1PC2	S2PC1	S2PC2		
-44708.344	-31756.228	-129121.060	52656.492		
SPL1	SPL2	SR12	SSC22	SLS	
-105400.650	17601.154	-21219.544	11335.277	5547.330	
S1M1	S1M2	S2M1	S2M2		
42616.963	21224.229	55422.706	21887.034		

LONGITUDINAL RIB NOZZLE

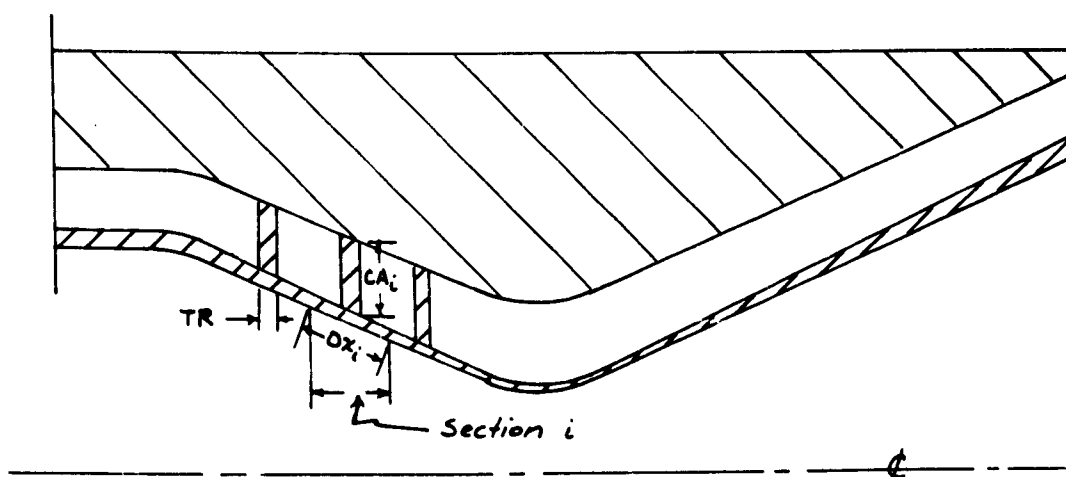
PB	T2	T1	T1	TB	DR
0.000	.150	.035	972.263	218.333	.172
S1PC1	S1PC2	S2PC1	S2PC2		

-58081.400	-28939.460	-145401.580	58380.745		
SPL1	SPL2	SR12	SSC22	SLS	
-117966.190	24331.083	-27498.272	14744.236	6825.731	
S1M1	S1M2	S2M1	S2M2		
47553.453	24779.245	62362.976	23943.656		
LONGITUDINAL RIB NOZZLE					
PB	T2	T1	T1	TB	DR
0.000	.150	.040	1078.475	218.333	.185
S1PC1	S1PC2	S2PC1	S2PC2		
-70692.100	-26029.401	-161219.540	64498.063		
SPL1	SPL2	SR12	SSC22	SLS	
-130190.720	31067.130	-34028.284	18469.955	6160.367	
S1M1	S1M2	S2M1	S2M2		
52587.393	29163.806	69149.126	26336.911		
LONGITUDINAL RIB NOZZLE					
PB	T2	T1	T1	TB	DR
0.000	.150	.040	1184.274	218.333	.198
S1PC1	S1PC2	S2PC1	S2PC2		
-82769.360	-22932.020	-176559.600	70858.231		
SPL1	SPL2	SR12	SSC22	SLS	
-142112.050	37840.264	-42563.592	22486.049	9541.845	
S1M1	S1M2	S2M1	S2M2		
57636.750	34227.086	75721.023	28950.064		

RIB STRESS PROGRAM

This program is written in the Fortran II language and may be run on any digital computer designed to use this compilation language.

A sketch of the nozzle liner and sleeve with circumferential ribs is shown below. A typical section is labelled according to the program naming of variables.



INPUT DATA

The input data, in order of read-in are:

First Card

Title card, which may contain up to 50 letters and/or numbers to identify the case.

Second Card

This card is divided into three 10-space columns and one 3-space column according to the Fortran FORMAT form (E10.1, E10.1, E10.1, I3). It contains in order:

TR - The rib axial thickness in inches, same for all ribs.

EL - The liner modulus of elasticity, lb/in².

TEST 1 - The convergence criterion for each iteration for stress distribution. A reasonable value is from 1 to 100. Since this number is compared with the residual in the force balance equation it is of the order of the forces involved, which, for each section is several hundred pounds.

N - The number of sections, including Number 1 as a dummy section at the exit end, Number 2 the first section at the exit end, and Number N the last section at the entrance end. Sections Number 2 and N do not have ribs, and are only half as long as their neighboring sections. Up to and including 99 sections may be used.

Cards 3 through (N + 2)

These cards each contain in order the following values for sections 1 through N according to FORMAT (E10.1, E10.1, E10.1, E10.1, E10.1):

PA - The airside pressure on the section in lb/in^2 .
 PC - The coolant side pressure on the section in lb/in^2 .
 DL - The liner diameter at the entrance end of the section in inches.
 CA - The radial width of the rib for the section, inches.
 DX - The length along the liner of the section, inches.

Cards (N + 3) through (2N + 2)

These cards each contain in order the following values for the sections 1 through N according to FORMAT (E10.1, E10.1, E10.1, E10.1):

TH - The angle between the liner and the nozzle axis, taken at the middle of the section in radians. Note that for sections on the exit side of the throat this angle is given a negative value so the force of the air pressure on these sections will be negative.
 THCK - The thickness of the liner at the entrance end of the section, inches.
 ER - The modulus of elasticity of the rib in the section. This value is made 0.0 for a section with no rib. It will usually be the same for other sections. Units are lb/in^2 .
 S - The initial stress value inserted for the section. Any value may be used, but good original estimating will shorten convergence time slightly.

PROGRAM OPERATION

After the data are entered the computation will proceed automatically until the convergence criterion for the residuals is satisfied for all sections, at which time the exit end liner displacement will be printed out. The computer will then pause. The operator may examine this displacement. If it is positive he prepares a single card for a new value of S_1 , the exit end stress, which is less than the original value. The FORMAT is (E10.1). He places this card in the machine and starts the computer. It reads the new S_1 value and again calculates the stresses. If the displacement as calculated is negative the operator increases S_1 for the next iteration. The end displacement is thus made to approach zero as closely as desired.

If a readout of rib number, residual, and stress is desired during the relaxation of residuals SENSE SWITCH 3 is turned on. When the end displacement is close enough to zero the operator turns on SENSE SWITCH 2. This causes a print out of rib number, residual, stress, section displacement, and force (in pounds) on the rib.

The FORTRAN program, entitled H. C. Roland, RIB STRESS PROGRAM, follows on pages 124 through 126. Sample data are given on page 127, and the final print out on page 128.

```

C C H. C. ROLAND ** RIB STRESS PROGRAM
C SENSE SWITCH 3 ON GIVES READ OUT OF RIB NO., RESIDUAL, AND STRESS
C INPUTS * TR-RIB THCK, TL-LINR THCK, EL-LINER MOD OF FLAST.
C TEST1-1ST CONV CRIT, TEST2-2ND CONV CRIT, N-NO OF STRESSES
C PA(1)-AIR PRESS., PC(1)-COOL. PRESS., DL(1)-DIA. LINER.
C CA(1)-COOL. ANNULUS, DX(1)-SECT. LGTH ON LINER, S(1)-STRESS
C TH(1)-SECT. ANG., THCK(1)-LINER THCK, ER(1)-RIB ELAST MOD.
C GIVE TH NEG. ON OUTLET SIDE OF THROAT
C GIVE ER(1)=0. FOR SECTS. U,2, N
100 FORMAT (50H
101 FORMAT (10HINPUT DATA)
102 FORMAT (E10.1,E10.1,E10.1,E10.1,E10.1,E10.1)
103 FORMAT (E10.1,E10.1,E10.1,E10.1,E10.1,E10.1)
104 FORMAT (E10.1,E10.1,E10.1,E10.1,E10.1,E10.1)
105 FORMAT (13HITERATION NO.)
106 FORMAT (8HLOOP NO.)
107 FORMAT (16)
108 FORMAT (7HRIB NO.,4X,8HRESIDUAL,6X,6HSTRESS,7X,5HDELTA,
17X,5HFORCE)
109 FORMAT (14,3X,F12.1,F12.1,F12.1,F12.1,F12.1)
110 FORMAT (17HPROBLEM COMPLETED)
111 FORMAT (2X,1H1,15X,F12.1)
112 FORMAT (17HEND DISPLACEMENT-,F12.8)
    DIMENSION PA(20),PC(20),DL(20),CA(20),DX(20),TH(20),THCK(20),
    1ER(20),S(20),DM(20),A(20),COS(20),COSR(20),W(20),C(20),D(20),
    2Y(20),SUM(20),SUM1(20),DEL(20),P(20),F(20)
    LF=0
    READ 100
    PUNCH 100
    PUNCH 101
    READ 102, TR, EL,TEST1, N
    PUNCH 102, TR, EL, TEST1, N
    DO 5 I=1,N
    READ 103, PA(I), PC(I), DL(I), CA(I), DX(I)
    5 PUNCH 103, PA(I), PC(I), DL(I), CA(I), DX(I)
    DO 10 IX=1,N
    READ 104, TH(IX), THCK(IX), ER(IX), S(IX)
    10 PUNCH 104, TH(IX), THCK(IX), ER(IX), S(IX)
    NO=N-1
    DO 15 J=1,N
    IF (J-1)9,9,11
    9 DM(J)=3.142*(DL(J)+CA(J))
    A(J)=3.142*DX(J)*DL(J)
    GO TO 3
    11 DX(J)=1.57*(DL(J)+DL(J-1))+2.*CA(J)
    A(J)=1.571*DX(J)*(DL(J)+DL(J-1))
    3 IF (J-N)6,7,7
    6 COS(J)=COSF((TH(J)+TH(J+1))/2.)
    GO TO 8
    7 COS(J)=COSF(TH(J))
    8 COSR(J)=EL*COSF(TH(J))
    W(J)=3.142*DL(J)
    C(J)=(PA(J)-PC(J))*A(J)*SINF(TH(J))
    D(J)=W(J)*THCK(J)*COS(J)
    Y(J)=DM(J)*(TR**3)*ER(J)/(CA(J)**3)
    15 CONTINUE

```

```

16  LP=LP+1
    IT=0
19  CONTINUE
    DO 18 NA=2,N
    ADD=0.
    IF (NA-N) 45,47,18
45  DO 20 L=NA,N
20  ADD=ADD+.5*(S(L)+S(L+1))*DX(L+1)/COSR(L+1)
47  SUM(NA)=ADD
18  CONTINUE
    DO 55 MF=2,N
    SUM1(MF)=DX(MF)*.25*(S(MF)+S(MF-1))/COSR(MF)
55  CONTINUE
    DO 25 M=2,N
25  R(M)=Y(M)*(SUM1(M)+SUM(M))+D(M)*S(M)-D(M-1)*S(M-1)-C(M)
    IT=IT+1
    IF (SENSE SWITCH 3) 26,27
26  PUNCH 106
    PUNCH 107, LP
    PUNCH 105
    PUNCH 107, IT
    PUNCH 108
    PUNCH 111, S(1)
    DO 35 MP=2,N
35  PUNCH 109, MP, R(MP), S(MP)
27  DO 28 MC=2,N
    IF (ABS(R(MC))-TEST1) 28,28,29
28  CONTINUE
    GO TO 40
29  MX=2
    DO 30 MA=3,N
    IF (ABS(R(MA))-A*S(R(MX))) 30,30,32
32  MX=MA
30  CONTINUE
    S(MX)=R(MX)-R(MX)/(2.+(Y(MX)*3.+DX(MX)/COSR(MX)+D(MX)))
    GO TO 10
50  CONTINUE
51  DO 54 MY=2,N
    DEL(MY)=SUM1(MY)+SUM(MY)
    F(MY)=Y(MY)*DEL(MY)
54  CONTINUE
    DT=DEL(2)+.25*(S(2)+S(1))*DX(2)/COSR(2)
    PUNCH 112, DT
    PAUSE
    IF (SENSE SWITCH 2) 64,65
C   SENSE SWITCH 2 ON IF PROBLEM COMPLETE. PRESS START
C   SWITCH 2 OFF--CHANGE S(1) OPP. SIGN TO END DISP.B PRESS START
64  GO TO 66
65  READ 104, S(1)
    GO TO 16
66  PUNCH 110
    PUNCH 106
    PUNCH 107, LP
    PUNCH 105
    PUNCH 107, IT
    PUNCH 108

```

AEDC-TDR-63-58

```
PUNCH 111, S(1)
DO 60 MD=2,N
60 PUNCH 109,MD,R(MD),S(MD),DEL(MD),F(MD)
END
```

```

H C ROLAND RIB STRESS ** MO-TI 200 ATM .2401A
INPUT DATA
250.0E-04 450.0E+05 400.0E-01 20
500.0E-02 600.0E-01 132.0E-02 100.0E-03 130.0E-04
100.0E-00 600.0E-01 124.0E-02 100.0E-03 126.0E-03
200.0E-00 700.0E-01 116.0E-02 100.0E-03 252.0E-03
300.0E-00 700.0E-01 108.0E-02 100.0E-03 252.0E-03
400.0E-00 800.0E-01 100.0E-02 100.0E-03 252.0E-03
500.0E-00 800.0E-01 920.0E-03 100.0E-03 252.0E-03
600.0E-00 800.0E-01 840.0E-03 100.0E-03 252.0E-03
700.0E-00 900.0E-01 760.0E-03 100.0E-03 252.0E-03
800.0E-00 900.0E-01 680.0E-03 100.0E-03 252.0E-03
900.0E-00 100.0E-00 600.0E-03 100.0E-03 252.0E-03
100.0E+01 100.0E-00 520.0E-03 100.0E-03 252.0E-03
110.0E+01 110.0E-00 440.0E-03 100.0E-03 252.0E-03
120.0E+01 110.0E-00 360.0E-03 100.0E-03 252.0E-03
150.0E+01 120.0E-00 280.0E-03 100.0E-03 252.0E-03
140.0E+01 120.0E-00 240.0E-03 100.0E-03 252.0E-03
280.0E+01 140.0E-00 600.0E-03 100.0E-03 350.0E-04
280.0E+01 140.0E-00 104.0E-02 100.0E-03 350.0E-04
280.0E+01 140.0E-00 141.0E-02 100.0E-03 290.0E-03
280.0E+01 140.0E-00 150.0E-02 100.0E-03 250.0E-03
280.0E+01 140.0E-00 150.0E-02 100.0E-03 125.0E-03
-140.0E-03 340.0E-04 000.0E-99-200.0E+01
-140.0E-03 330.0E-04 000.0E-99-190.0E+01
-140.0E-03 320.0E-04 450.0E+05-120.0E+01
-140.0E-03 310.0E-04 450.0E+05-650.0E-00
-140.0E-03 300.0E-04 450.0E+05-500.0E-00
-140.0E-03 290.0E-04 450.0E+05-490.0E-00
-140.0E-03 280.0E-04 450.0E+05-500.0E-00
-140.0E-03 280.0E-04 450.0E+05-550.0E-00
-140.0E-03 270.0E-04 450.0E+05-300.0E-00
-140.0E-03 260.0E-04 450.0E+05-440.0E-00
-140.0E-03 250.0E-04 450.0E+05-400.0E-00
-140.0E-03 240.0E-04 450.0E+05-300.0E+01
-140.0E-03 230.0E-04 450.0E+05-470.0E+01
-140.0E-03 220.0E-04 450.0E+05-750.0E+01
500.0E-03 250.0E-04 450.0E+05-890.0E+01
845.0E-03 280.0E-04 450.0E+05-410.0E+01
845.0E-03 310.0E-04 450.0E+05-210.0E+01
670.0E-03 330.0E-04 450.0E+05 113.0E+02
000.0E-99 340.0E-04 450.0E+05 830.0E+01
000.0E-99 350.0E-04 000.0E-99 700.0E+01

```


PROBLEM COMPLETED

LOOP NO.

9

ITERATION NO.

1

RIB NO.	RESIDUAL	STRESS	DELTA	FORCE
1		200.0		
2	39.8	509.8	.00000298	0.0
3	35.0	696.9	.00000078	2.2
4	32.6	894.6	-.00000317	-8.5
5	36.4	1221.7	-.00000841	-21.1
6	-21.1	991.8	-.00001453	-34.0
7	-29.0	626.7	-.00001995	-43.1
8	-35.0	44.5	-.00002319	-46.0
9	-6.6	-300.0	-.00002378	-43.0
10	15.7	-440.0	-.00002237	-36.5
11	31.5	-400.0	-.00002014	-29.3
12	-33.7	-2541.1	-.00001479	-18.9
13	10.1	-4700.0	-.00000039	-.4
14	32.3	-8218.9	.00002810	26.0
15	-29.6	-7942.0	.00007215	57.3
16	-1.9	-4100.0	.00010145	116.4
17	26.6	-2100.0	.00010680	216.9
18	24.1	10472.8	.00009141	267.4
19	31.0	8182.9	.00004828	165.7
20	-3.1	7930.0	.00001118	0.0

APPENDIX B

FORTRAN PROGRAMS

FOR

BACKSIDE COOLING CALCULATIONS

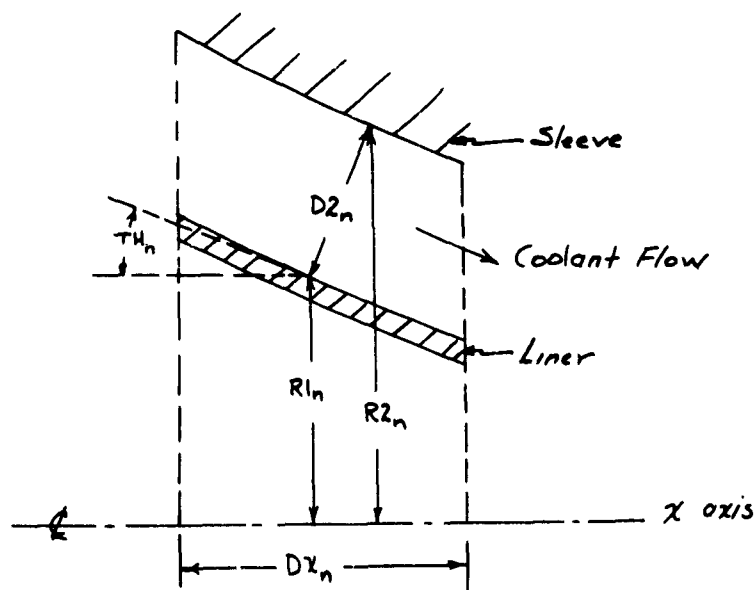
LINER BACKSIDE COOLING COMPUTER PROGRAM

The program described below is written in Fortran II language. It is designed to calculate the bulk temperature, static pressure, convection heat transfer coefficient, surface temperature, boiling heat transfer coefficient and boiling burnout heat load along a nozzle liner coolant annulus with longitudinal ribs. The program proper is preceded by a brief discussion of the equations used for calculation. In this discussion the notation used is the same as that used in the computer program.

COOLANT ANNULUS DESCRIPTION

The coolant flows axially in an annulus around the nozzle liner. The coolant side surface of the liner is a surface of revolution about the nozzle centerline which is designated the x-axis. For calculation of the required variables in a stepwise fashion, the liner is divided axially into small finite sections. A description of each section as to length, radius, angle of the liner surface with the x-axis and distance across the coolant annulus perpendicular to the liner surface, provides the necessary liner and annulus description. Using these variables, the liner heated area, coolant annulus flow area and flow path length along the liner, are calculated.

A cross-sectional view of a typical liner and annulus section is shown below with the necessary variables identified.



If the section length Dx_n is made small compared to the radius of curvature of the liner, the heated area of the section is

$$A_{HOT_n} = \frac{2\pi R_{1n} Dx_n}{\cos(\theta_n)} \quad (1)$$

The coolant annulus flow area is

$$A_{COOL_n} = \pi(R_{1n} + R_{2n}) D_{2n} \quad (2)$$

Now

$$R_{2n} = R_{1n} + D_{2n} \cos(\theta_n) \quad (3)$$

So

$$A_{COOL_n} = 2\pi R_{1n} D_{2n} + \pi \cos(\theta_n) D_{2n}^2 \quad (4)$$

The above equation for the coolant flow area applies only in sections where there are no ribs. If there are RN ribs of thickness RT , the coolant flow area is

$$A_{COOL_n} = 2\pi R_{1n} D_{2n} + \pi \cos(\theta_n) D_{2n}^2 - RN RT D_{2n} \quad (5)$$

If a constant flow area is desired let $A_{COOL_n} = D_{COOL} = \text{constant}$.

Then

$$\pi \cos(\theta_n) D_{2n}^2 + (2\pi R_{1n} - RN RT) D_{2n} - D_{COOL} = 0 \quad (6)$$

$$\text{and } D_{2n} = \frac{-(2\pi R_{1n} - RN RT) + \sqrt{(2\pi R_{1n} - RN RT)^2 + 4\pi \cos(\theta_n) D_{COOL}}}{2\pi \cos(\theta_n)} \quad (7)$$

BULK TEMPERATURE, VELOCITY AND PRESSURE CALCULATIONS

Given a coolant water flow rate and a heat load distribution along the liner, the bulk temperature at the n^{th} section is calculated from

$$TB_n = TB_{n-1} + \frac{Q_{n-1} ANOT_{n-1}}{2 \cdot CP \cdot FLR} + \frac{Q_n ANOT_n}{2 \cdot CP \cdot FLR} \quad (8)$$

where TB_n = bulk temperature at section n , °F
 Q_n = heat load on liner at section n , B/hr ft²
 $ANOT_n$ = liner section area at section n , ft²
 CP = coolant heat capacity, B/lbm °F
 FLR = coolant flow rate, lbm/hr.

The velocity at each section is calculated from

$$V_n = \frac{FLR}{AC_{COOL_n} RHO_n} \quad (9)$$

where V_n = velocity, ft/sec
 RHO_n = density, lbm/ft³
 FLR = coolant flow rate, lbm/sec
 AC_{COOL_n} = coolant flow area, ft².

The static pressure is calculated from

$$PRESS_n = PRESS_{n-1} - DPS_{n-1} - DPS_n - DPV_{(n-1) \rightarrow n} \quad (10)$$

where $PRESS_n$ = static pressure at section n , psia
 $PRESS_{n-1}$ = static pressure at section $n-1$, psia
 DPS_{n-1} = frictional pressure loss in exit half of section $(n-1)$, psia
 DPS_n = frictional pressure loss in entrance half of section n , psia
 $DPV_{(n-1) \rightarrow n}$ = pressure loss due to acceleration from $(n-1)$ to n , psia.

The pressure loss terms in equation (10) are calculated as follows:

For DPS

$$DPS_n = \frac{9.15 \times 10^{-5} DX_n}{DH_n} \left(\frac{RHO_n V_n^2}{2g_c} \right) RE_n^{-0.25} \quad (11)$$

where DPS_n = frictional pressure drop in half of section n, psia
 DX_n = section length, inches
 DH_n = coolant annulus hydraulic diameter, ft
 RE_n = Reynolds number at section n.

For DPV

$$DPV_{(n-1) \rightarrow n} = \left(\frac{RHO_n V_n^2}{2g_c} - \frac{RHO_{n-1} V_{n-1}^2}{2g_c} \right) / 144 \quad (12)$$

where DPV = acceleration pressure drop from (n-1) to n, psia
 RHO_n = coolant density at section n, lbm/ft³
 V_n = coolant velocity at section n, ft/sec
 $g_c = 32.2 \frac{\text{lbm ft}}{\text{lbf sec}^2}$

FORCED CONVECTION AND SURFACE BOILING HEAT TRANSFER

The forced convection heat transfer coefficient is calculated from

$$BARH_n = 5134 \cdot V_n^{-.02} RE_n^{-.667} PR_n \quad (13)$$

where PR_n = Prandtl's number at section n.

For evaluating RE_n the viscosity is calculated from the following empirical equation

$$FMU_n = \frac{0.045}{TC_n} - (4.5 \times 10^{-8}) TC_n + (2 \times 10^{-11}) TC_n^2 \quad (14)$$

where FMU_n = viscosity at section n, lbm/ft sec
 TC_n = film temperature at section n, °F

For calculating PR_n the following empirical equation is used

$$PR_n = \frac{480}{TC_n} - 0.002 TC_n + (7 \times 10^{-9}) TC_n^3 \quad (15)$$

Equations (14) and (15) are plotted with experimental values for comparison in Figures 1 and 2 respectively.

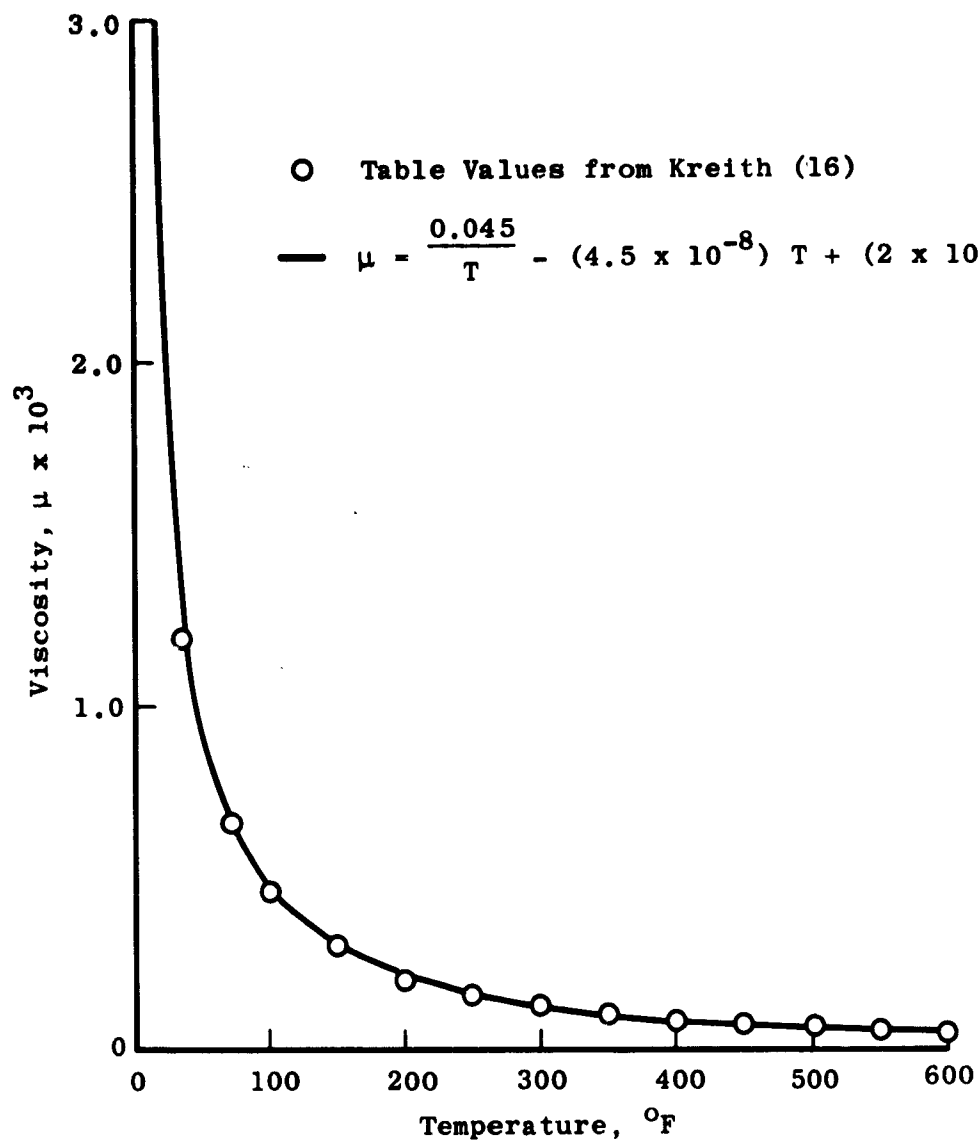


Fig. 44 Viscosity of Water

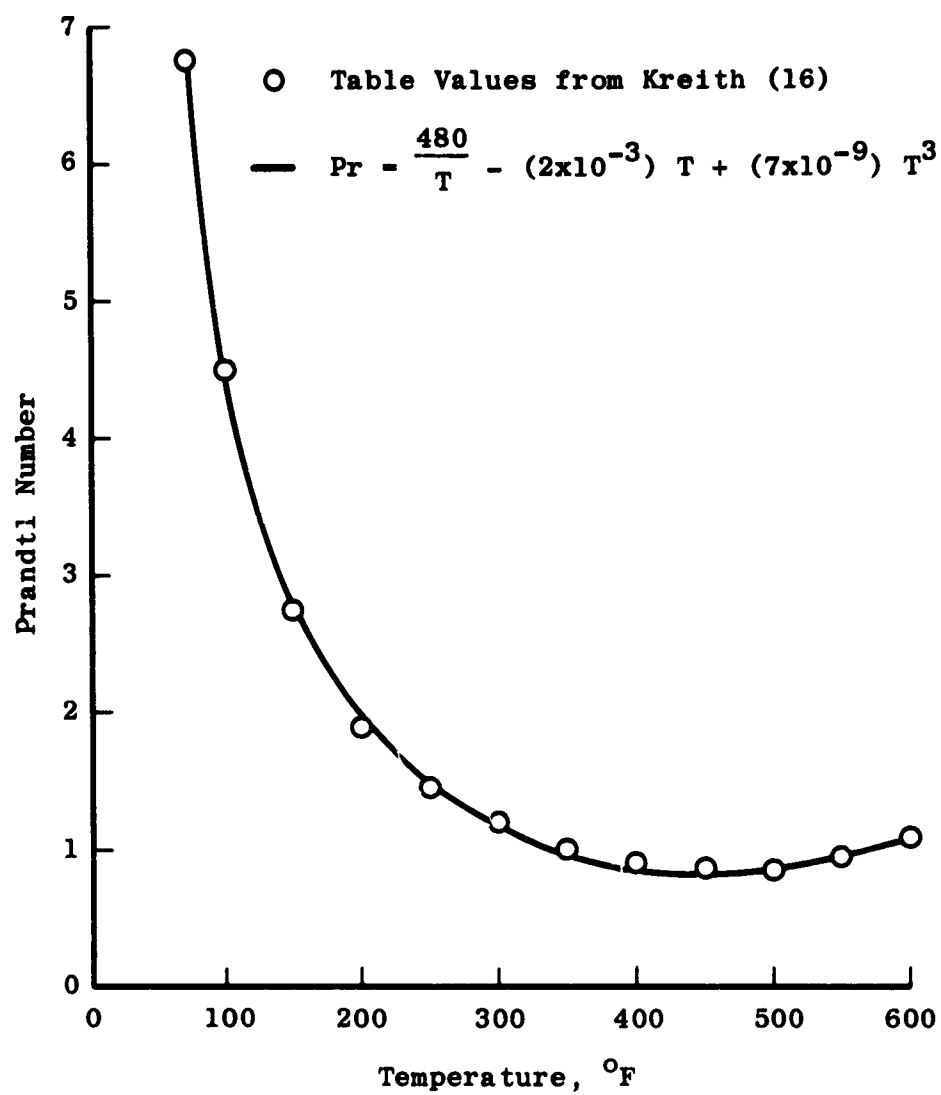


Fig. 45 Prandtl Number for Water

The liner coolant side surface temperature in forced convection is calculated from

$$TS_n = TB_n + \frac{Q_n}{BARH_n} \quad (16)$$

where TS_n = surface temperature, °F
 TB_n = bulk coolant temperature, °F
 Q_n = heat load at section n, B/hr ft²
 $BARH_n$ = heat transfer coefficient.

Since RE_n and PR_n are functions of the film temperature TC_n , and TC_n varies with TS_n , equations (13), (14), (15), and (16) are used to solve for TS_n by successive approximation.

At each section the saturation temperature is first calculated based on the static pressure. For pressures to 400 psia the saturation temperature is calculated from

$$TSAT_n = 240 + PRESS_n - 1.25 \times 10^{-3} PRESS_n^2 - \frac{660}{2.75 + PRESS_n} \quad (17)$$

For pressures from 400 psia to 1000 psia the following equation is used

$$TSAT_n = 390 + 0.16 PRESS_n \quad (18)$$

For pressures above 1000 psia the saturation temperature is calculated from

$$TSAT_n = 470 + 0.082 PRESS_n \quad (19)$$

Equations (17), (18), and (19) are plotted with experimental values of the saturation temperature in Figure 3.

If the required surface temperature exceeds the saturation temperature at any section by more than 10°F a boiling heat transfer calculation is made. The convection heat load is first calculated by assuming a value

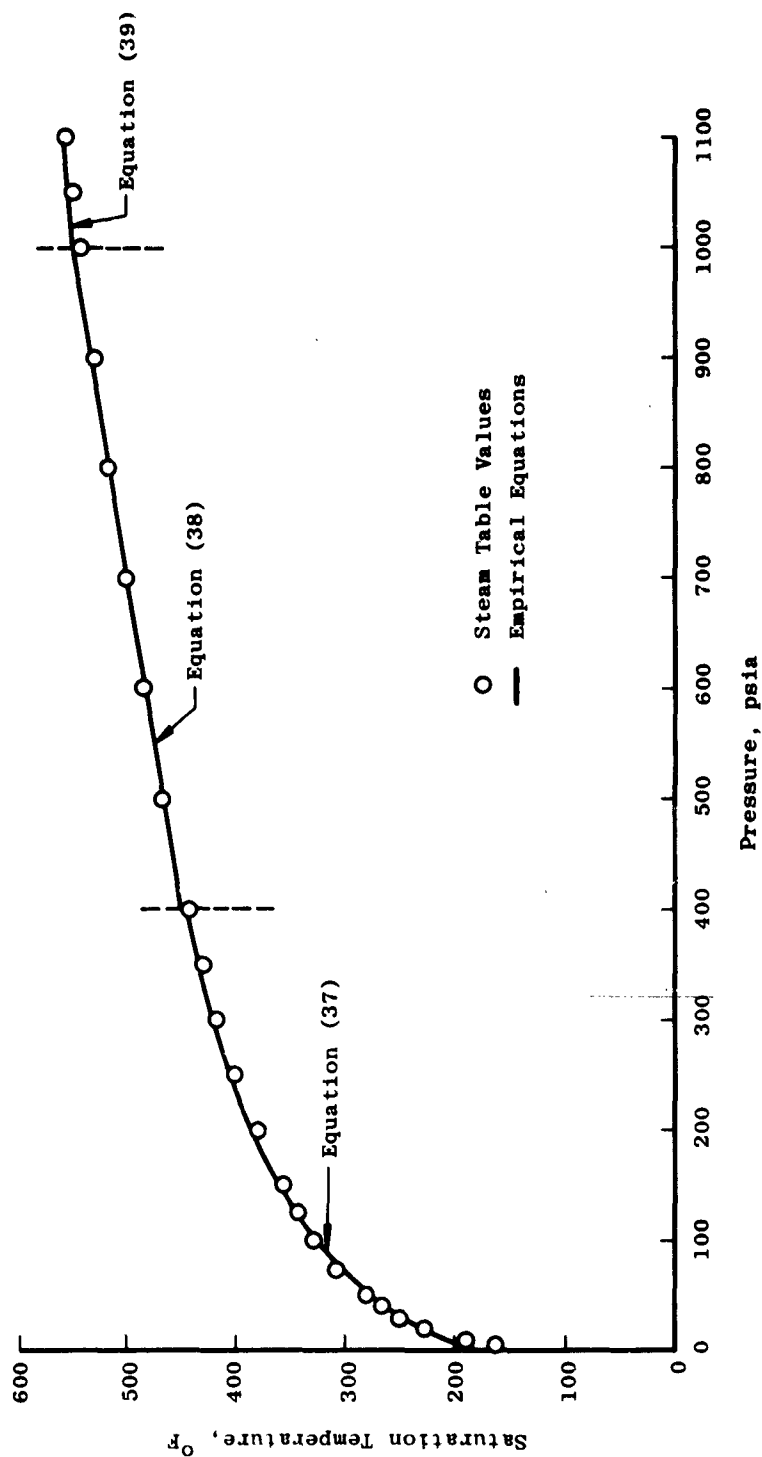


Fig. 46 Pressure-Temperature Relationships for Water

for TS_n and using

$$Q_{n\text{convection}} = BARH_n(TS_n - TB_n) \quad (20)$$

The boiling heat transfer load is then calculated from

$$Q_{n\text{boiling}} = 0.2 [TS_n - (TSAT_n + 10)]^{3.86} \quad (21)$$

If $(Q_n)_{\text{convection}} + (Q_n)_{\text{boiling}} \neq Q$ another value of TS_n is chosen and the process repeated until the proper value of TS_n is reached.

The burn-out heat flux is evaluated using each of the following three equations

$$QB0_n = (4 \times 10^5) \left(1 + 0.0217 DTSUB_n \right) \left[1 + 30 \left(\frac{PRESS_n}{3200} \right) - 31 \left(\frac{PRESS_n}{3200} \right)^{1.33} \right] V_n^{0.333} \quad (22)$$

$$QB2_n = 7000 (DTSUB_n) V_n^{0.5} \quad (23)$$

$$QB3_n = (4 \times 10^5) (1 + 0.02 DTSUB_n) V_n^{0.333} \quad (24)$$

where

$$DTSUB_n = TSAT_n - TB_n$$

At sections where there is no boiling, the burn-out heat flux is set equal to 0.0.

PROGRAM SWITCH SETTINGS

If the program is executed with Sense Switch 1 off, the pressure distribution is first calculated, then the inlet pressure is automatically set to give a static pressure of 10 psia at the last section. This automatic inlet pressure adjustment does not occur if the program is run with Sense Switch 1 on.

If the input data is read in with Sense Switch 3 off the coolant annulus widths input as data are used for all calculations. If Sense Switch 3 is on when the data is entered, the coolant annulus widths are automatically calculated to give a flow area equal to DC001 at each section.

INPUT DATA CARDS

First data card - FORMAT (50H - 50 spaces -)

This card provides for input and output of up to 50 alphabetic characters to provide a title for each case.

Second data card - FORMAT (15, F10.5, F10.5, F10.3, F10.5, F10.5)

This card contains data in order as follows:

N - Number of liner sections.
 FLR - Coolant flow rate, lbm/sec.
 TCOOL- Inlet coolant bulk temperature, °F.
 PRIN - Inlet static pressure (plenum), psia.
 AIN - Inlet area at the bend, in².
 DHIN - Inlet hydraulic diameter at the bend, inches.

Third data card - FORMAT (15, 5X, F10.5, F10.5, F10.5)

This card contains data in order as follows:

NRS - Number of sections from entrance having ribs.
 RN - Number of longitudinal ribs around liner.
 RT - Rib circumferential thickness, inches.
 DC00L- Coolant flow area for automatic annulus width calculations, in².

Fourth card through (3 + n)th card - FORMAT (F10.5, F10.5, F10.5, F10.5, F10.0)

These n cards contain the following data in order for the n liner sections:

Fl_n = Liner outside radius at n^{th} section, inches.
 $D2_n$ = Coolant annulus width at n^{th} section, inches.
 TH_n = Liner angle with axis at n^{th} section, radians.
 DX_n = Length of n^{th} section, inches.
 Q_n = Liner heat load at n^{th} section, B/hr ft².

All input is punched out as a check on the input data.

OUTPUT NOTATION

Output values are labeled according to the following notation:

N - Same as input.
 FL.RATE - Coolant flow rate, lbm/sec.
 TCOOL - Same as input.
 PRIN - Same as input (may be different value).
 AIN - Same as input.
 DHIN - Same as input.
 SEC. - Section number
 T-BULK - Bulk coolant temperature, °F.
 T-SURF - Liner coolant side surface temperature, °F.
 T-SAT - Coolant saturation temperature, °F.
 VEL. - Coolant mean velocity, ft/sec.
 PRESS - Coolant static pressure, psia.
 Q - Liner heat load, B/hr ft².
 H - Surface heat transfer coefficient, B/hr ft² °F.
 QB01 - Burnout heat flux from equation (22), B/hr ft².
 QB02 - Burnout heat flux from equation (23), B/hr ft².
 QB03 - Burnout heat flux from equation (24), B/hr ft².

Note: If QB01 = QB02 = QB03 = 0.0 at a section, it shows there is no boiling at the section.

The program follows on pages 141, 142, and 143, and sample data and output on pages 144 through 155.

```

C C H C ROLAND ** BACKSIDE COOLING PROGRAM
C SENSE SWITCH 1 ON BYPASSES AUTO PRESS SETTING
C SENSE SWITCH 3 ON CAUSES EQUALIZATION OF ALL FLOW AREAS
C DIMENSION R1(50),D2(50),TH(50),Q(50),COS(50),ACCOOL(50),DH(50),
1AHOT(50),G(50),V(50),DTB(50),TB(50),TF(50),FMU(50),PR(50),
2BARH(50),DTS(50),TS(50),RE(50),DPS(50),DPV(50),VH(50),RHU(50),
3PRESS(50),TSAT(50),DX(50),TSB(50),TC(50),QBO(50),QB2(50),QB3(50)
100 FORMAT (50H
101 FORMAT (10HINPUT DATA)
102 FORMAT (4X,1HN,3X,7HFL.RATE,3X,5HTCOOL,6X,4HPRIN,
18X,3HAIN,6X,4HDMIN)
103 FORMAT (15,F10.5,F10.5,F10.3,F10.5,F10.5)
104 FORMAT (2X,3HSEC,6X,2HR),8X,2HD2,6X,2HTH,8X,2HDX,6X,1HQ)
105 FORMAT (F10.5,F10.5,F10.5,F10.5,F10.0)
106 FORMAT (15,F10.5,F10.5,F10.5,F10.5,F10.5,F10.0)
107 FORMAT (6HOUTPUT)
108 FORMAT (3HSEC,3X,6HT-BULK,4X,6HT-SURF,5X,5HT-SAT,6X,4HVEL,
15X,5HPRESS)
109 FORMAT (12,F10.1,F10.1,F10.1,F10.1,F10.1)
110 FORMAT (12,F10.0,F10.1,F12.0,F12.0,F12.0)
111 FORMAT (3HSEC,4X,1HQ,9X,1HH,9X,4HQBO1,8X,4HQBO2,8X,4HQBO3)
112 FORMAT (8HRIB,SECS,3X,8HNO, RIBS,2X,10HRIB THCKNS,4X,5HDCOOL)
113 FORMAT (15,5X,F10.5,F10.5,F10.5)
80 DO 40 L=1,20
READ 100
PUNCH 100
PUNCH 101
PUNCH 102
READ 103, N, FLR, TCOOL, PRIN, AIN, DHIN
READ 113, NRS, RN, RT, DCCOOL
PUNCH 103, N, FLR, TCOOL, PRIN, AIN, DHIN
PUNCH 112
PUNCH 113, NRS, RN, RT, DCCOOL
PUNCH 104
LV=0
DO 20 IX=1,N
READ 105, R1(IX), D2(IX), TH(IX), DX(IX), Q(IX)
COS(IX)=COSF(TH(IX))
42 IF (SENSE SWITCH 3) 45,20
45 A=3.14*COS(IX)
B=6.28*R1(IX)-RN*RT
B1=6.28*R1(IX)
C=-DCCOOL
IF (IX-NRS)180,180,181
180 D2(IX)=(-B+SQRTF((B**2)-4.*A*C))/(2.*A)
GO TO 20
181 D2(IX)=(-B1+SQRTF((B1**2)-4.*A*C))/(2.*A)
20 PUNCH 106, IX, R1(IX), D2(IX), TH(IX), DX(IX), Q(IX)
8 VIN=144.*FLR/(AIN*62.4)
VHIN=62.4*(VIN**2)/64.4
VO=144.*FLR/(62.4*(DCCOOL+RN*RT*D2(1)))
VHO=62.4*(VO**2)/64.4
66 DO 7 I=1,N
IF (I-NRS) 47,47,150
47 ACCOOL(I)=D2(I)*(6.28*R1(I)+3.14*COS(I)*D2(I)-RN*RT)/144.
DH(I)=24.*ACCOOL(I)/(6.28*R1(I)+3.14*COS(I)*D2(I)+RN*(D2(I)-RT))

```

```

      GO TO 151
150  AC00L(1)=D2(1)*(6.28*R1(1)+3.14*COS(1)*D2(1))/144.
151  DH(1)=48.*AC00L(1)/(12.56*R1(1)+6.28*D2(1)*COS(1))
      AHOT(1)=6.283*DX(1)*R1(1)/COS(1)
      G(1)=FLR/AC00L(1)
      DTB(1)=Q(1)*AHOT(1)/(7200.*FLR*144.)
      IF (I-1) 1,1,2
1    TB(1)=TC00L+DTB(1)
      GO TO 3
2    TB(1)=TB(I-1)+DTB(I-1)+DTB(1)
3    RHO(1)=62.6-(1.5E-03)* TB(1)-(5.3E-05)*( TB(1)**2)
      V(1)=G(1)/RHO(1)
      VH(1)=RHO(1)*(V(1)**2)/64.4
      FMU(1)=.045/TB(1)-(4.5E-08)*TB(1)+(2.E-11)*(TB(1)**2)
50   REIN=62.4*VIN*DHIN/(12.*FMU(1))
      DPINS=.1*VHIN/(REIN**.25)
      DPINV=VH0/144.
      RE(1)=RHO(1)*V(1)*DH(1)/FMU(1)
      DPS(1)=(9.15E-05)*VH(1)*DX(1)/(DH(1)*COS(1)*(RE(1)**.25))
      IF (I-1) 5,5,6
5    DPV(1)=(VH(1)-VH0)/144.
      PRESS(1)=PRIN-DPS(1)-DPV(1)-DPINS-DPINV
      GO TO 7
6    DPV(1)=(VH(1)-VH(I-1))/144.
      PRESS(1)=PRESS(I-1)-DPS(1)-DPV(1)-DPS(I-1)
7    CONTINUE
      LV=LV+1
      IF (LV-1) 81,81,65
81   IF (SENSE SWITCH 1) 65,82
82   PRIN=PRIN-PRESS(N)+10.
      GO TO 8
65   PUNCH 107
      PUNCH 102
      PUNCH 103, N, FLR, TC00L, PRIN, AIN, DHIN
      DO 25 K=1,N
      IF (PRESS(K)-400.) 70,70,71
70   TSAT(K)=240.*PRESS(K)-.001250*(PRESS(K)**2)-660./(2.75+PRESS(K))
      GO TO 79
71   IF (PRESS(K)-1000.) 72,72,73
72   TSAT(K)=390.*.16*PRESS(K)
      GO TO 79
73   TSAT(K)=470.*.082*PRESS(K)
79   CONTINUE
      LOP=1
      LOT=2
      LZ=0
      TSB(K)=TSAT(K)+10.
93   TC(K)=(TSB(K)+TB(K))/2.
      FMU(K)=.045/TC(K)-(4.5E-08)*TC(K)+(2.E-11)*(TC(K)**2)
      PR(K)=480./TC(K)-(2.E-03)*TC(K)+(7.E-09)*(TC(K)**3)
      BARH(K)=5134.*V(K)*((FMU(K)/(DH(K)*RHO(K)*V(K))**.2)/(PR(K)
1**0.667)
      QC=BARH(K)*(TSB(K)-TB(K))
      LZ=LZ+1
      IF (QC-Q(K)) 30,95,48
48   IF (LOT-LOP) 49,95,49

```

```

49  TSB(K)=TSB(K)-20.
    GO TO 93
30  IF (LZ-1)51,51,27
27  TSB(K)=TSB(K)+5.
    LOP=LOT
    GO TO 93
95  BARH(K)=Q(K)/(TSB(K)-TB(K))
    TS(K)=TSB(K)
    QB0(K)=0.
    QB2(K)=0.
    QB3(K)=0.
    GO TO 25
51  TSB(K)=((5.*Q(K))**.259)+TSAT(K)+10.
120 TF(K)=(TSB(K)+TB(K))/2.
    FMU(K)=.045/TF(K)-(4.5E-08)*TF(K)+(2.E-11)*(TF(K)**2)
    PR(K)=480./TF(K)-(2.E-03)*TF(K)+(7.E-09)*(TF(K)**3)
    BARH(K)=5134.*V(K)*((FMU(K)/(DH(K)*62.*V(K))**.2)/(PR(K)**.667)
    QTEST=BARH(K)*(TSB(K)-TB(K))+.2*((TSB(K)-TSAT(K)-10.))**.86)
    IF (QTEST-Q(K)) 29,29,91
91  IF (LOT-LOP) 92,99,92
92  TSB(K)=TSB(K)-20.
    GO TO 120
29  TSB(K)=TSB(K)+5.
    LOP=LOT
    GO TO 120
99  BARH(K)=Q(K)/(TSB(K)-TB(K))
    DTSUB=TSAT(K)-TB(K)
    QB0(K)=(4.E+05)*(1.+.0217*DTSUB)*(1.+30.*
1 (PRESS(K)/3200.)-31.0*((PRESS(K)/3200.))**.33))*(V(K)**.333)
    QB2(K)=7000.*(SQRTF(V(K)))*DTSUB
    QB3(K)=(4.E+05)*(1.+.02*DTSUB)*(V(K)**.333)
    TS(K)=TSB(K)
25  CONTINUE
    PUNCH 108
    DO 10 IL=1,N
10  PUNCH 109, IL, TB(IL), TS(IL), TSAT(IL), V(IL), PRESS(IL)
    PUNCH 107
    PUNCH 111
    DO 35 IK=1,N
35  PUNCH 110, IK, Q(IK), BARH(IK), QB0(IK), QB2(IK), QB3(IK)
40  CONTINUE
    END

```


H C ROLAND * FILM COEFF - .30DIA - 60 B/IN2SEC

INPUT DATA

N	FL.RATE	TCOOL	PRIN	AIN	DHIN
20	20.00000	85.00000	2000.000	.57500	.25000
RIB.SEC	NO.	RIBS	RIB THCKNS	DCOOL	
6	20.00000		.02000	.20000	
SEC	R1	D2	TH	DX	Q
1	.70000	.04874	.80000	.10000	30000000.
2	.60000	.05725	.80000	.10000	30000000.
3	.50000	.06917	.80000	.10000	30000000.
4	.40000	.08687	.80000	.10000	30000000.
5	.30000	.11520	.80000	.10000	30000000.
6	.20000	.16449	.80000	.10000	30000000.
7	.15000	.14812	.50000	.05000	30000000.
8	.12500	.15685	.10000	.05000	30000000.
9	.12500	.15685	.10000	.05000	30000000.
10	.16250	.13797	.14000	.50000	25000000.
11	.22500	.11329	.14000	.50000	20000000.
12	.28750	.09517	.14000	.50000	18000000.
13	.35000	.08157	.14000	.50000	16000000.
14	.41250	.07113	.14000	.50000	14000000.
15	.47500	.06292	.14000	.50000	12000000.
16	.53750	.05632	.14000	.50000	10000000.
17	.60000	.05093	.14000	.50000	8000000.
18	.66250	.04645	.14000	.50000	7000000.
19	.72500	.04268	.14000	.50000	6000000.
20	.78750	.03946	.14000	.50000	6000000.

OUTPUT						
	N	FL.RATE	TCOOL	PRIN	AIN	DHIN
	20	20.00000	85.00000	632.665	.57500	.25000
SEC	T-BULK	T-SURF	T-SAT	VEL.	PRESS	
1	85.9	485.8	404.7	231.9	238.6	
2	87.6	487.4	401.3	232.0	230.6	
3	89.0	489.4	398.3	232.0	224.0	
4	90.2	492.0	395.9	232.1	218.8	
5	91.1	495.2	394.1	232.1	214.8	
6	91.7	493.8	392.7	232.1	211.9	
7	92.1	498.0	391.9	232.2	210.3	
8	92.2	497.7	391.6	232.2	209.6	
9	92.3	497.4	391.3	232.2	209.0	
10	93.0	479.3	389.3	232.2	205.0	
11	94.3	448.0	385.0	232.3	196.7	
12	95.8	424.2	379.4	232.3	186.3	
13	97.4	393.5	372.1	232.4	173.5	
14	99.2	362.9	362.9	232.5	158.3	
15	100.9	331.3	351.3	232.6	140.6	
16	102.6	301.7	336.7	232.6	120.2	
17	104.2	268.6	318.6	232.7	97.0	
18	105.6	250.7	295.7	232.8	70.9	
19	107.0	235.0	265.0	232.8	41.9	
20	108.4	229.5	198.0	232.9	9.9	

OUTPUT

SEC	Q	H	QB01	QB02	QB03
1	30000000.	75015.8	43819626.	33989235.	18095875.
2	30000000.	75035.4	42606443.	33449912.	17847155.
3	30000000.	74914.7	41597287.	32989585.	17634880.
4	30000000.	74649.6	40785714.	32611449.	17460517.
5	30000000.	74242.7	40161026.	32315738.	17324169.
6	30000000.	74620.9	39706804.	32099183.	17224327.
7	30000000.	73905.3	39461055.	31982089.	17170344.
8	30000000.	73991.5	39354934.	31932026.	17147269.
9	30000000.	74068.2	39260061.	31887560.	17126774.
10	25000000.	64711.3	38658761.	31606412.	16997208.
11	20000000.	56541.2	37403280.	31014405.	16724433.
12	18000000.	54803.4	35832543.	30261063.	16377399.
13	16000000.	54037.8	33912359.	29315211.	15941776.
14	14000000.	53089.2	0.	0.	0.
15	12000000.	52100.7	0.	0.	0.
16	10000000.	50227.9	0.	0.	0.
17	8000000.	48665.2	0.	0.	0.
18	7000000.	48267.0	0.	0.	0.
19	6000000.	46888.9	0.	0.	0.
20	6000000.	49560.9	7809965.	9578363.	6861783.

H C ROLAND * FILM COEFF - .30DIA - 60 B/IN2SEC
INPUT DATA

N	FL.RATE	TCOOL	PRIN	AIN	DHIN
20	20.00000	85.00000	2000.000	.57500	.25000
RIB.SEC	NO.	RIBS	RIB THCKNS	DCOOL	
6	20.00000		.02000	.20000	
SEC	R1	D2	TH	DX	Q
1	.70000	.04874	.80000	.10000	30000000.
2	.60000	.05725	.80000	.10000	30000000.
3	.50000	.06917	.80000	.10000	30000000.
4	.40000	.08687	.80000	.10000	30000000.
5	.30000	.11520	.80000	.10000	30000000.
6	.20000	.16449	.80000	.10000	30000000.
7	.15000	.14812	.50000	.05000	30000000.
8	.12500	.15685	.10000	.05000	30000000.
9	.12500	.15685	.10000	.05000	30000000.
10	.16250	.13797	.14000	.50000	25000000.
11	.22500	.11329	.14000	.50000	20000000.
12	.28750	.09517	.14000	.50000	18000000.
13	.35000	.08157	.14000	.50000	16000000.
14	.41250	.07113	.14000	.50000	14000000.
15	.47500	.06292	.14000	.50000	12000000.
16	.53750	.05632	.14000	.50000	10000000.
17	.60000	.05093	.14000	.50000	8000000.
18	.66250	.04645	.14000	.50000	7000000.
19	.72500	.04268	.14000	.50000	6000000.
20	.78750	.03946	.14000	.50000	6000000.

OUTPUT						
	N	FL.RATE	TCOOL	PRIN	AIN	DHIN
	20	20.00000	85.00000	632.665	.57500	.25000
SEC	T-BULK	T-SURF	T-SAT	VEL.	PRESS	
1	85.9	485.8	404.7	231.9	238.6	
2	87.6	487.4	401.3	232.0	230.6	
3	89.0	489.4	398.3	232.0	224.0	
4	90.2	492.0	395.9	232.1	218.8	
5	91.1	495.2	394.1	232.1	214.8	
6	91.7	493.8	392.7	232.1	211.9	
7	92.1	498.0	391.9	232.2	210.3	
8	92.2	497.7	391.6	232.2	209.6	
9	92.3	497.4	391.3	232.2	209.0	
10	93.0	479.3	389.3	232.2	205.0	
11	94.3	448.0	385.0	232.3	196.7	
12	95.8	424.2	379.4	232.3	186.3	
13	97.4	393.5	372.1	232.4	173.5	
14	99.2	362.9	362.9	232.5	158.3	
15	100.9	331.3	351.3	232.6	140.6	
16	102.6	301.7	336.7	232.6	120.2	
17	104.2	268.6	318.6	232.7	97.0	
18	105.6	250.7	295.7	232.8	70.9	
19	107.0	235.0	265.0	232.8	41.9	
20	108.4	229.5	198.0	232.9	9.9	

OUTPUT

SEC	Q	H	QB01	QB02	QB03
1	30000000.	75015.6	43819626.	33989235.	18095875.
2	30000000.	75035.4	42606443.	33449912.	17847155.
3	30000000.	74914.7	41597287.	32989585.	17634880.
4	30000000.	74649.6	40785714.	32611449.	17460517.
5	30000000.	74242.7	40161026.	32315738.	17324169.
6	30000000.	74620.9	39706804.	32099183.	17224327.
7	30000000.	73905.3	39461055.	31982089.	17170344.
8	30000000.	73991.5	39354934.	31932026.	17147269.
9	30000000.	74068.2	39260061.	31887560.	17126774.
10	25000000.	64711.3	38658761.	31606412.	16997208.
11	20000000.	56541.2	37403280.	31014405.	16724433.
12	18000000.	54803.4	35832543.	30261063.	16377399.
13	16000000.	54037.8	33912359.	29315211.	15941776.
14	14000000.	53089.2	0.	0.	0.
15	12000000.	52100.7	0.	0.	0.
16	10000000.	50227.9	0.	0.	0.
17	8000000.	48665.2	0.	0.	0.
18	7000000.	48267.0	0.	0.	0.
19	6000000.	46888.9	0.	0.	0.
20	6000000.	49560.9	7809965.	9578363.	6861783.

H C ROLAND * FILM COEFF - .30DIA - 60 B/IN2SEC

INPUT DATA

N	FL.RATE	TCOOL	PRIN	AIN	DHIN
20	20.00000	85.00000	310.000	.57500	.25000
RIB.SEC	NO. RIBS	RIB THCKNS	DCOOL		
6	20.00000	.02000	.35000		
SEC	R1	D2	TH	DX	Q
1	.70000	.08374	.80000	.10000	30000000.
2	.60000	.09771	.80000	.10000	30000000.
3	.50000	.11683	.80000	.10000	30000000.
4	.40000	.14418	.80000	.10000	30000000.
5	.30000	.18525	.80000	.10000	30000000.
6	.20000	.24962	.80000	.10000	30000000.
7	.15000	.22433	.50000	.05000	30000000.
8	.12500	.23187	.10000	.05000	30000000.
9	.12500	.23187	.10000	.05000	30000000.
10	.16250	.20938	.14000	.50000	25000000.
11	.22500	.17798	.14000	.50000	20000000.
12	.28750	.15335	.14000	.50000	18000000.
13	.35000	.13388	.14000	.50000	16000000.
14	.41250	.11830	.14000	.50000	14000000.
15	.47500	.10568	.14000	.50000	12000000.
16	.53750	.09531	.14000	.50000	10000000.
17	.60000	.08668	.14000	.50000	8000000.
18	.66250	.07941	.14000	.50000	7000000.
19	.72500	.07321	.14000	.50000	6000000.
20	.78750	.06787	.14000	.50000	6000000.

OUTPUT

	N	FL.RATE	TCOOL	PRIN	AIN	DHIN
	20	20.00000	85.0C000	310.000	.57500	.25000
SEC	T-BULK	T-SURF	T-SAT	VEL.	PRESS	
1	85.9	486.3	365.2	132.5	162.0	
2	87.6	485.3	364.2	132.5	160.5	
3	89.0	484.5	363.4	132.6	159.2	
4	90.2	488.9	362.8	132.6	158.2	
5	91.1	488.4	362.3	132.6	157.4	
6	91.7	488.0	361.9	132.6	156.7	
7	92.1	487.8	361.7	132.6	156.4	
8	92.2	487.7	361.6	132.6	156.2	
9	92.3	487.6	361.5	132.6	156.1	
10	93.0	481.0	360.9	132.7	155.2	
11	94.3	467.8	359.7	132.7	153.4	
12	95.8	458.2	358.3	132.7	151.2	
13	97.4	448.0	356.6	132.8	148.6	
14	99.2	437.2	354.6	132.8	145.5	
15	100.9	420.6	352.2	132.9	142.0	
16	102.6	393.1	349.5	132.9	138.0	
17	104.2	351.3	346.3	133.0	133.5	
18	105.6	327.8	342.8	133.0	128.4	
19	107.0	298.7	338.7	133.0	122.9	
20	108.4	299.2	334.2	133.1	116.7	

OUTPUT

SEC	Q	H	QB01	QB02	QB03
1	30000000.	74921.4	27787656.	22510394.	13410820.
2	30000000.	75422.0	27462622.	22299496.	13303899.
3	30000000.	75848.3	27191553.	22122063.	13213947.
4	30000000.	75244.0	26971956.	21977581.	13140600.
5	30000000.	75513.3	26800979.	21864498.	13083375.
6	30000000.	75711.1	26675194.	21782134.	13041625.
7	30000000.	75817.6	26606641.	21737909.	13019211.
8	30000000.	75862.6	26576934.	21719244.	13009752.
9	30000000.	75902.1	26550506.	21702876.	13001460.
10	25000000.	64441.0	26389280.	21603645.	12951186.
11	20000000.	53554.4	26066900.	21406474.	12851301.
12	18000000.	49672.8	25686454.	21175238.	12734180.
13	16000000.	45640.9	25244280.	20907643.	12598662.
14	14000000.	41418.7	24743665.	20607438.	12446666.
15	12000000.	37537.7	24188255.	20278402.	12280115.
16	10000000.	34425.8	23581916.	19924250.	12100904.
17	8000000.	32368.8	0.	0.	0.
18	7000000.	31512.0	0.	0.	0.
19	6000000.	31295.6	0.	0.	0.
20	6000000.	31450.6	0.	0.	0.

H C ROLAND * FILM COEFF - .30DIA - 60 B/IN2SEC
INPUT DATA

N	FL.RATE	TCOOL	PRIN	AIN	DHIN
20	25.00000	85.00000	3000.000	.57500	.25000
RIB.SEC	NO. RIBS	RIB THCKNS	DCOOL		
6	20.00000	.02000	.16000		
SEC	R1	D2	TH	DX	Q
1	.70000	.03919	.80000	.10000	30000000.
2	.60000	.04612	.80000	.10000	30000000.
3	.50000	.05589	.80000	.10000	30000000.
4	.40000	.07059	.80000	.10000	30000000.
5	.30000	.09461	.80000	.10000	30000000.
6	.20000	.13814	.80000	.10000	30000000.
7	.15000	.12450	.50000	.05000	30000000.
8	.12500	.13320	.10000	.05000	30000000.
9	.12500	.13320	.10000	.05000	30000000.
10	.16250	.11587	.14000	.50000	25000000.
11	.22500	.09385	.14000	.50000	20000000.
12	.28750	.07811	.14000	.50000	18000000.
13	.35000	.06653	.14000	.50000	16000000.
14	.41250	.05775	.14000	.50000	14000000.
15	.47500	.05093	.14000	.50000	12000000.
16	.53750	.04549	.14000	.50000	10000000.
17	.60000	.04107	.14000	.50000	8000000.
18	.66250	.03741	.14000	.50000	7000000.
19	.72500	.03433	.14000	.50000	6000000.
20	.78750	.03172	.14000	.50000	6000000.

OUTPUT						
	N	FL.RATE	TCOOL	PRIN	AIN	DHIN
	20	25.00000	85.00000	3000.000	.57500	.25000
SEC	T-BULK	T-SURF	T-SAT	VEL.	PRESS	
1	85.7	414.3	639.3	362.4	2064.6	
2	87.0	422.4	637.4	362.5	2041.7	
3	88.2	430.8	635.8	362.5	2022.9	
4	89.1	439.6	634.6	362.6	2008.1	
5	89.9	448.7	633.7	362.6	1996.8	
6	90.4	463.0	633.0	362.7	1988.7	
7	90.6	472.7	632.7	362.7	1984.4	
8	90.8	477.5	632.5	362.7	1982.5	
9	90.8	477.4	632.4	362.7	1980.8	
10	91.4	426.5	631.5	362.7	1970.1	
11	92.4	369.6	629.6	362.8	1947.2	
12	93.6	347.2	627.2	362.9	1918.1	
13	94.9	319.3	624.3	363.0	1882.3	
14	96.3	295.8	620.8	363.1	1839.2	
15	97.7	271.6	616.6	363.2	1788.5	
16	99.1	246.8	611.8	363.3	1730.0	
17	100.3	221.3	606.3	363.4	1663.3	
18	101.5	205.2	600.2	363.4	1588.2	
19	102.6	193.3	593.3	363.5	1504.5	
20	103.7	195.7	585.7	363.6	1412.0	

OUTPUT

SEC	Q	H	QB01	QB02	QB03
1	30000000.	91304.7	0.	0.	0.
2	30000000.	89462.9	0.	0.	0.
3	30000000.	87553.3	0.	0.	0.
4	30000000.	85594.3	0.	0.	0.
5	30000000.	83603.8	0.	0.	0.
6	30000000.	80504.4	0.	0.	0.
7	30000000.	78529.1	0.	0.	0.
8	30000000.	77566.8	0.	0.	0.
9	30000000.	77612.6	0.	0.	0.
10	25000000.	74602.8	0.	0.	0.
11	20000000.	72153.7	0.	0.	0.
12	18000000.	70973.0	0.	0.	0.
13	16000000.	71314.5	0.	0.	0.
14	14000000.	70198.9	0.	0.	0.
15	12000000.	69015.4	0.	0.	0.
16	10000000.	67696.4	0.	0.	0.
17	8000000.	66113.3	0.	0.	0.
18	7000000.	67507.4	0.	0.	0.
19	6000000.	66131.4	0.	0.	0.
20	6000000.	65196.0	0.	0.	0.

<p>Arnold Engineering Development Center Arnold Air Force Station, Tennessee Rpt. No. AEDC-TDR-63-58, ANALYTICAL STUDIES ON NOZZLE THROAT COOLING. April 1963, 163 p. incl 20 refs., illus., tables. Unclassified Report</p> <p>Analytical studies have been made concerning many of the problems associated with the expansion of extremely high temperature and pressure plasmas through the converging section of a hypersonic wind tunnel nozzle. The problems in this study relate to the establishment of heat fluxes to the nozzle wall, methods of removing the heat load or protecting the nozzle wall, determining the stress levels in the nozzle liner, analyzing various materials for strength and thermal properties. In all cases parametric studies have been made resulting in design criteria which can be used for specific conditions. The conditions are established from the performance envelope for a typical low density</p>	<ol style="list-style-type: none">1. Hypersonic nozzles2. Film cooling3. Heat transfer4. Thermal stresses5. Evapotranspiration6. Laminar boundary layer7. Turbulent boundary layer8. Design9. Materials10. Boundary layer transition11. Analysis <ol style="list-style-type: none">I. AFSC Program Area 750E, Project 6951, Task 695101II. Contract AF 40(600)-981III. University of Tennessee, Knoxville, Tenn.IV. P. F. Pasqua, P. N. Stevens, J. E. Mott, et al.V. Available from OTSVI. In ASTIA Collection	<p>Arnold Engineering Development Center Arnold Air Force Station, Tennessee Rpt. No. AEDC-TDR-63-58, ANALYTICAL STUDIES ON NOZZLE THROAT COOLING. April 1963, 163 p. incl 20 refs., illus., tables. Unclassified Report</p> <p>Analytical studies have been made concerning many of the problems associated with the expansion of extremely high temperature and pressure plasmas through the converging section of a hypersonic wind tunnel nozzle. The problems in this study relate to the establishment of heat fluxes to the nozzle wall, methods of removing the heat load or protecting the nozzle wall, determining the stress levels in the nozzle liner, analyzing various materials for strength and thermal properties. In all cases parametric studies have been made resulting in design criteria which can be used for specific conditions. The conditions are established from the performance envelope for a typical low density</p>	<ol style="list-style-type: none">1. Hypersonic nozzles2. Film cooling3. Heat transfer4. Thermal stresses5. Evapotranspiration6. Laminar boundary layer7. Turbulent boundary layer8. Design9. Materials10. Boundary layer transition11. Analysis <ol style="list-style-type: none">I. AFSC Program Area 750E, Project 6951, Task 695101II. Contract AF 40(600)-981III. University of Tennessee, Knoxville, Tenn.IV. P. F. Pasqua, P. N. Stevens, J. E. Mott, et al.V. Available from OTSVI. In ASTIA Collection
<p>hypersonic wind tunnel. Throughout the report the performance envelope is plotted on stagnation pressure and temperature coordinates which correspond to free stream velocities and altitudes up to 25 kilofeet/sec and 350 kilofeet respectively. Ultimate use of the information will depend upon the reliability of the assumptions made which in many cases must be determined by new experiments.</p>		<p>hypersonic wind tunnel. Throughout the report the performance envelope is plotted on stagnation pressure and temperature coordinates which correspond to free stream velocities and altitudes up to 25 kilofeet/sec and 350 kilofeet respectively. Ultimate use of the information will depend upon the reliability of the assumptions made which in many cases must be determined by new experiments.</p>	